Scholars' Mine

Doctoral Dissertations | Student Theses and Dissertations

Fall 2020

Fully differential study of higher-order contributions to the few-body dynamics of simple atomic systems

Madhav Dhital

FULLY DIFFERENTIAL STUDY OF HIGHER-ORDER CONTRIBUTIONS TO THE

FEW-BODY DYNAMICS OF SIMPLE ATOMIC SYSTEMS

by

MADHAV DHITAL

A DISSERTATION

Presented to the Graduate Faculty of the

MISSOURI UNIVERSITY OF SCIENCE AND TECHNOLOGY

In Partial Fulfillment of the Requirements for the Degree

DOCTOR OF PHILOSOPHY

in

PHYSICS

2020

Approved by:

Michael Schulz, Advisor
Don H. Madison
Paul E. Parris
Daniel Fischer
Sanjay Madria

PUBLICATION DISSERTATION OPTION

This dissertation consists of the following three articles, formatted in the style used by the Missouri University of Science and Technology:

Paper I, found on pages 16–39, has been published in Physical Review A.

Paper II, found on pages 40–67, has been published in Physical Review A.

Paper III, found on pages 68–103, has been published in Physical Review A.

ABSTRACT

Advancing our understanding of the few-body dynamics in simple atomic systems is one of the most important goals of atomic scattering research. In perturbation theory, this goal entails accurately describing the relative contributions from first versus higher-order mechanisms. One higher-order mechanism that is particularly important for target ionization by a charged-particle impact is known as post-collision interaction (PCI). There, the projectile and the ejected electron interact with each other at least twice. In the first interaction, the projectile transfers sufficient energy for the electron to be lifted to the continuum. The second interaction occurs in the outgoing part of the collision, where the projectile and the electron attract each other towards the initial beam axis. It is well known that PCI maximizes when the electrons are ejected with a speed close to that of the projectiles. However, a systematic study on a fully differential level of ionization by ion impact was lacking for this kinematic regime. Kinematically complete experiments on ionization of H_2 and He by 75 keV proton impact were performed. Fully differential cross sections (FDCS) were extracted for a broad range of fixed electron energies for each of the targets. Pronounced post-collisional effects between the projectile and the ejected electrons were observed. The results were compared with two conceptually similar calculations, both based on distorted wave approaches. Surprising discrepancies were observed between the experimental data and theory, and also between conceptually similar theoretical models. This shows that the FDCS are very sensitive to the details of the underlying few-body dynamics in this region. Data also indicated the limitations of perturbative methods and the need for non-perturbative approaches.

ACKNOWLEDGMENTS

I would like to thank my research advisor, Dr. Michael Schulz, for the opportunity to learn exciting physics and scientific diplomacy. I would never have achieved this without your continuous support and guidance. I would also like to thank the other members of my advisory committee: Dr. Don Madison, Dr. Paul Parris, Dr. Daniel Fischer, and Dr. Sanjay Madria for their efforts, discussions, and suggestions.

I offer sincere gratitude to the visiting scholars: Dr. Ahmad Hasan and Dr. Ramaz Lomsadze for their fruitful discussions and help with performing experiments and data analysis. I would like to commemorate the valuable contributions from the theoretical collaborators: Dr. Madison, Dr. Ciappina, and their groups. I greatly appreciate the hard work from my lab colleagues: Sujan, Aaron, Basu, Thusitha, Trevor, Krishna, Brendon, Deni, and Jake. I would like to acknowledge the physics department chair, Dr. Thomas Vojta, and academic advisor, Dr. Jerry Peacher. I would also like to thank the department staff: Andy, Pam, Jan, and Ron. I am very grateful to the Nepali community in Rolla, who made my stay very enjoyable. I would like to thank all my mentors, teachers, friends, and well-wishers associated with the journey.

In the end, I would like to thank my loving wife, Shirish Pathak, for her continuous love, care, and support. I sincerely acknowledge the sacrifices made by my parents, Krishna Prasad Dhital and Sabitri Devi Dhital, to help me reach this point. Without your continuous inspiration, it would have been simply impossible. I would also like to thank my sister, Sumitra, brothers, Bhabani and Madhu, and my extended family for their support. I am forever indebted to you all.

TABLE OF CONTENTS

LIST OF ILLUSTRATIONS

1. INTRODUCTION

Fundamental research is crucially important because at the beginning of any scientific and technological development is the need to understand nature. This raises the question, what does it take to understand nature on a fundamental level? The answer to this question can be summarized, perhaps somewhat crudely, in two points. The first one, and the most basic step, is to obtain a complete understanding of the fundamental forces acting in nature, namely the gravitational, weak, electromagnetic, and strong forces. One important common feature of all these forces is that they are mediated by the exchange of particles called gauge bosons.

Repulsive force due to particle exchange

(a)   (b)
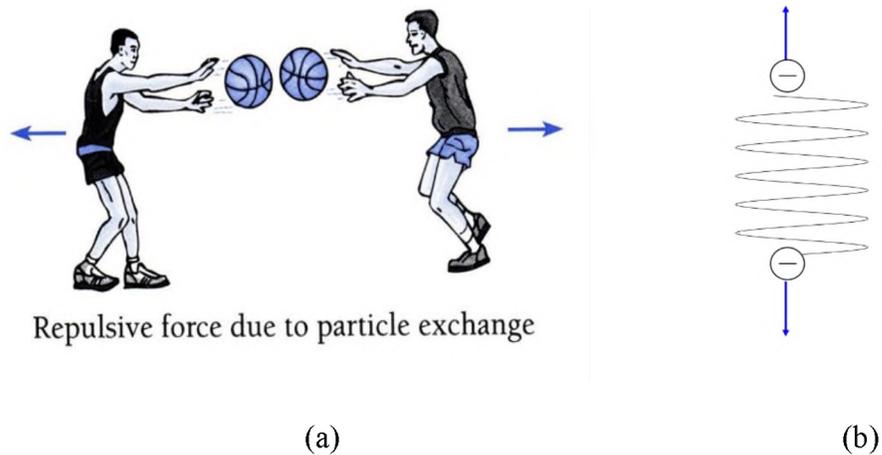
Figure 1.1. Illustration of mediation of force by particle exchange. (a) classical (adapted from source), and (b) quantum mechanical case

The mediation of a force between two objects through the exchange of another particle can be illustrated with simple examples. Let us start with a classical example with two basketball players as in Figure 1.1 (a) [1]. When one of the players throws a ball to another player, then the throwing player suffers some recoil opposite to the direction of the motion of the ball. Once the ball is received by the second player, the catching player also feels some recoiling effect in the direction of the ball. Thus, a repulsive force is mediated between these two players through the exchange of the ball. Moving to a quantum mechanical case, for example, the mediation of a force between two electrons, as in Figure 1.1 (b), works to some degree the same way as in the classical example. These electrons obviously do not throw basketballs onto each other, but they can exchange virtual photons between them. If one of the electrons emits a virtual photon, it suffers recoil, and once another electron absorbs the virtual photon, it also suffers some recoil. Thus, a force is mediated by the exchange of a virtual photon between these electrons.

This is a somewhat simplified picture because in quantum mechanics there are no well-defined trajectories. As a result, the classical analogy assuming such trajectories is not able, for example, to explain an attractive force. Nevertheless, this classical picture illustrates one important feature, which is common to all fundamental forces; the mediation of a force is fundamentally a two-body process, not counting virtual particles, because the gauge boson can only be emitted and absorbed by one particle at a time.

This directly leads to the second point we need to address in order to understand nature at a fundamental level, that is, how do systems with more than two particles develop in space and time under the influence of these pairwise acting forces? The basic problem is that the Schrödinger wave equation, in general, is not analytically solvable for more than

two mutually interacting particles even when the underlying forces are precisely known. This is known as the quantum-mechanical few-body problem (FBP), one of the most fundamentally important and yet unsolved problems in physics [2]. Theory has to resort to numeric models using approximations because a general analytic solution is not possible. This kind of modeling is very challenging as a large manifold of forces acting between all particle pairs has to be considered. These models need to be tested by detailed experimental results. In the case of stationary atomic systems, accurate solutions are nevertheless often obtained by using different numerical models e.g. the multi-configuration Hartree-Fock model [3]. However, dynamic few-body systems, like atomic fragmentation processes, are still very challenging and often understanding is rather incomplete.

Research on atomic collisions has played an important role to advance our understanding of dynamic atomic systems since the famous Rutherford scattering experiment [4]. To study the few-body dynamics, atomic fragmentation processes are particularly suitable for two important reasons [7]. First, in atomic systems, the underlying interaction is the electromagnetic force, which is essentially completely understood. This is an important point because it means that the experiment directly tests the theoretical description of the few-body dynamics because the underlying force is under control. In constrast, in nuclear systems, the underlying interaction is the strong force that is not nearly as well understood as the electromagnetic interaction. Therefore, in this case, we do not know which part of the theory the experiment is testing; either the description of the underlying force or the few-body dynamics.

Second, in atomic collision experiments, systems with small particle numbers (≈ 3-5) can be selected. For such simple systems, after the development of cold target recoil ion

momentum spectroscopy (COLTRIMS) [38], the complete momentum vectors of each particle can be obtained, and the experiments are kinematically complete. Such a kinematically complete experiment offers the most sensitive tests of theoretical models. In contrast, in solid-state systems, we have to deal with a huge particle number, the order of the Avogadro number (10^{23} particles). In such a large particle number system, a kinematically complete experiment is obviously not feasible. As a result, only statistically averaged quantities are obtained, which could not provide sensitive test to the theoretical models.
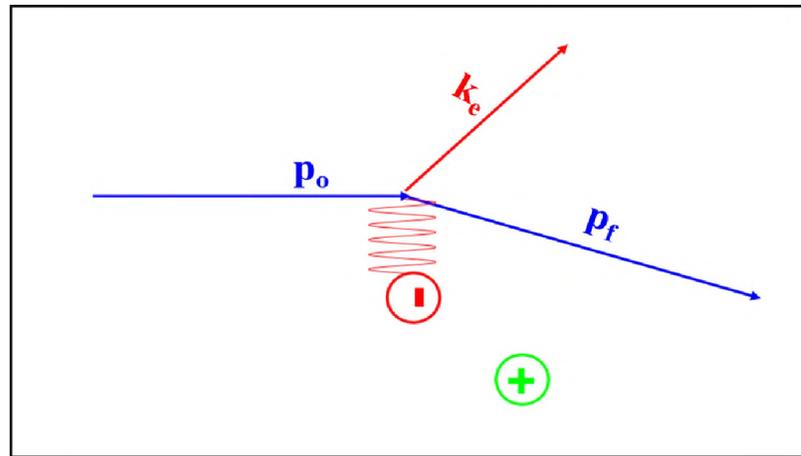
Figure 1.2. Schematic representation of ionization

The most basic inelastic processes during atomic collisions are electron capture, ionization, and excitation. In (single) ionization, an electron from the target is ejected because of the impact of the incoming projectile beam, as shown in Figure 1.2, where P_0

and P_f are the initial and final projectile momenta and K_f is the momentum of the ejected electron. In this case, there are at least three unbound particles in the final state, which are the scattered projectile, the ejected electron, and the recoiling target ion. In contrast, capture and excitation lead to only two independently moving particles in the final state. Therefore, ionization is particularly well suited to study the few-body dynamics. Hence, our interest was focused on the single ionization of simple target atoms and molecules by charged particle impact.

The theoretical models being used to describe few-body dynamics in charged particle interaction can be grouped into two broad categories; perturbative and non-perturbative models. The non-perturbative approach is conceptually and numerically more complete because a large number of basis sets can be included, which enables us to account for the influence of reaction channels other than the process of interest on the cross-section [8]. On the other hand, perturbative models effectively represent two-state approximations, which are the well-defined initial state and the final state observed in the experiment.

As in the case of other atomic processes, ionization of simple targets by electron impact is often well described by non-perturbative models [8,9]. Kinematically complete studies have been performed extensively for target ionization by electron impact and very good agreement between experiment and theory is routinely observed even close to the threshold (equal to ionization potential of the target), which was considered a particularly challenging regime [5]. This is because the electronic mass is much smaller than that of ionic projectiles, which corresponds to a larger de-Broglie wavelength. In such cases, two electrons (light particles) and only one heavy particle (the residual target ion) are involved, and the heavy particle practically acts as the center of mass of the system. Hence, just a

small number of partial waves representing angular momentum states are needed to describe the process.

However, research about the few-body dynamics in the ionization of targets by ion impact is not as advanced as for electron impact. Fully differential studies of ionization by ion impact are much more challenging for both experimental and theoretical studies because of the much larger mass of the projectile. Experimentally, the large projectile mass results in very small scattering angles, which are typically only a fraction of a mrad. Scattering angles are even smaller, a fraction of a μrad, for fast heavy ions, and the projectile energy loss is usually only a tiny fraction of the initial energy, which makes it difficult to measure the energy loss even with sophisticated techniques. Another difficulty in the experiment is to measure fast ejected electrons. Slow electrons can be easily confined to the solid angle covered by the detector with the use of small electric and magnetic fields in the recoil-ion momentum spectrometer. To collect fast electrons, both of these fields need to be large, which will compromise the momentum resolution.

The larger projectile mass leads to theoretical difficulties as well. Non-perturbative calculations are especially more challenging for ion impact. This is because an enormous number of angular momentum states (which require the inclusion of a very large number of partial waves) must be considered to accurately describe the scattered projectiles. Furthermore, the positive charge of the projectile necessitates the inclusion of projectile states in the basis sets if the effect of the capture channel is to be considered. Several non-perturbative methods on ionization have been developed, however, because of these challenges the literature on non-perturbative calculations for ion impact is not as extensive as for electron impact. As a result, the comparison between fully differential cross-section

(FDCS) calculated with these approaches with experimental data is still rather limited [10, 11], and the agreement is not as satisfactory as it is for electron impact.

The theory on ionization by ion impact relies, to a large extent, on perturbative models. One approach in perturbative theory is given by the Born Series [12], where the projectile is treated as a perturbation to the target Hamiltonian, and the few-body dynamics is described by expanding the transition amplitude (the square of which gives the cross-section of the reaction) in powers of the perturbation. Hence, the transition amplitude (T) can be expressed as a power series expansion of the interaction potential (V) as follows,

$$T = <e^{ik_f r} \varphi_f |V| e^{ik_i r} \varphi_i> + <e^{ik_f r} \varphi_f |VG_0V| e^{ik_i r} \varphi_i> + < e^{ik_f r} \varphi_f |VG_0VG_0V| e^{ik_i r} \varphi_i>$$

$$+ ....$$

Here, the plane waves describe the projectile in the initial and final states, φ_i and φ_f are the initial and final eigenstates of the target atom, and G_0 is the Green's function, which describes the propagation of the system between successive interactions.

In this expression, the first term describes a single interaction of the projectile with the target, and therefore it represents first order processes. The second term describes two interactions between the projectile and the target, and therefore represents second order processes, and so on. As an advantage, this approach is more transparent in terms of describing the reaction process of interest compared to the non-perturbative approaches. The disadvantage of this method is, apart from being a two-state approximation, this infinite power series expansion must be truncated after some term. So far, calculations only up to the second order are available for most of the reactions. By comparing experimental results with the theory, the relative importance of the various interaction sequences in the collision dynamics can be evaluated. For collision systems with a relatively small (much

less than 1) perturbation parameter η (charge to speed ratio of the projectile), second-order calculation and even first-order calculations, are sufficient to accurately describe the cross-section for many processes. However, for larger η, higher-order contributions are more important, and eventually, the expansion series may not converge at all [10, 13].

In perturbation theory, an alternative approach to describing ion-atom collisions with the inclusion of higher-order contributions is provided by distorted wave methods [14, 15]. In contrast to the power series expansion in the interaction potential of the Born Series, in distorted wave approaches higher-order contributions are treated mainly in the final state wave function of the system. Here, the convergence problem of the Born series does not occur directly because any interaction contained in the wave function is conceptually included to all orders. However, the challenge of distorted wave methods is to find a sufficiently accurate final-state wave function.
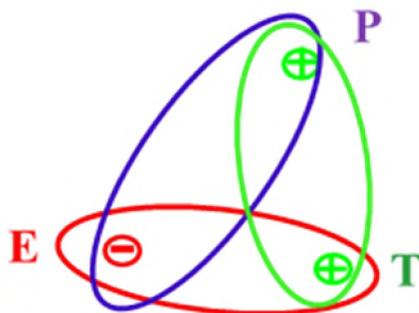
Figure 1.3. Three-body system broken into three two-body subsystems

In distorted wave methods, the three-body system consisting of the target-nucleus (T), the target-electron (E), and the projectile (P) are broken into three two-body

subsystems, which are target-nucleus and electron, target-nucleus and projectile, and target-electron and projectile (as represented by different colored ovals in Figure 1.3). For each of these two-body subsystems, the continuum eigenstate is a (distorted, in case of multi-electron target) Coulomb-wave. The approximation used here is that the total final state wave function of the system (Ψ_f) is described as a product of these three Coulomb-interactions i.e. $\Psi_f = C_{PE} * C_{PT} * C_{TE}$; where, C_{XY} represents the Coulomb interaction between the particle pair X and Y. The disadvantage of this product wave function is that it ignores the correlations between the three particle-pairs. As a result, it is only accurate if at least one of the particles is far from the other two [16].

The theoretical calculations which were used to compare with the experimental results are summarized below [17]. These are two different calculations based on different versions of the distorted wave approximation carrying essentially the same physics.

The CDW-EIS, continuum-distorted wave eikonal initial state, model was employed by our collaborator Dr. Marcelo Ciappina and his group. It is a single active electron approach in which it is assumed that in the final state the ejected electron moves in the combined Coulomb field of the incident proton and the residual target core. Partial screening of the active electron-target interaction due to the 'passive' target electron is modeled by means of a Hartree-Fock scheme. The distortion of the final electronic state by the projectile is represented by a pure Coulomb function, and by an eikonal phase in the entrance channel. The projectile and residual target ion (PT) interaction is treated as a pure Coulomb interaction between the projectile and the target core. This interaction is then included in the transition amplitude, by invoking the eikonal approximation, through its multiplication by a phase factor.

The 3DW-EIS, three-body-distorted wave eikonal initial state, model was developed and calculated by our collaborator Dr. Don Madison and his group. The incident projectile is treated as a plane wave with an eikonal phase approximating the initial state PT interaction. The final state wave function for the projectile is a Coulomb wave in the field of the target ion with a net charge of +1. The ejected electron wave function is a distorted wave which is a solution of the Schrödinger equation using a numerical potential whose radial dependence includes the screening of the nucleus by the electron cloud. For small radii, this potential has a net charge equal to that of the nucleus. For increasing radii, the net charge reduces to that of the ion for radii larger than the size of the ion.

PE – ET – PE collision sequence

PE – PT – PE collision sequence

(a)

(b)
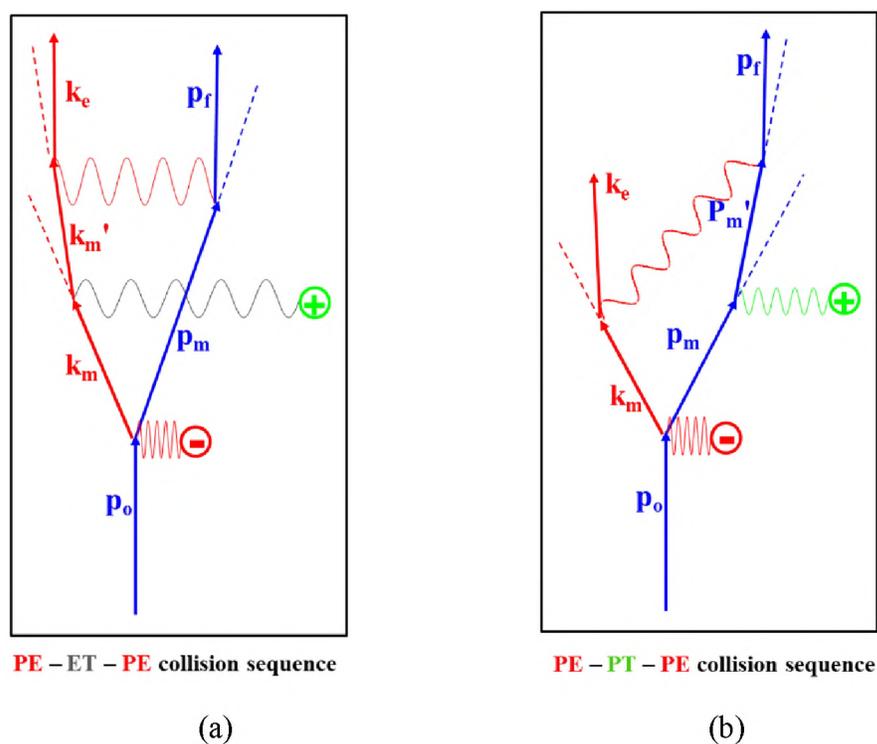
Figure 1.4. Schematic diagram of two classical PCI sequences

Generally, in perturbation theory, understanding the few-body dynamics means accurately describing the relative contributions of higher vs first-order mechanisms. One higher-order mechanism that is particularly important in ionization by low- or intermediate-energy ion and/or highly charged ion impact is known as post-collision interaction (PCI) [20, 21]. In PCI, the projectile interacts with a target electron at least twice. In the first interaction, the projectile transfers sufficient energy to the electron to be lifted to the continuum; in the second interaction in the outgoing part of the collision, the scattered projectile and the ejected electron are attracted towards the original projectile beam direction so that both particles are focused to a smaller angle as shown in Figure 1.4 (a) and (b) [37]. However, because of energy and momentum conversation, there must be a third interaction with the target nucleus for a second interaction between the projectile and the ejected electron to happen. This interaction can occur between the target nucleus and either the electron or the projectile. Hence, PE-TE-PE and PE-TP-PE, where P, E, and T stand for the projectile, the electron, and the target, are the two leading-order interaction sequences that lead to PCI [22]. Contributions from even higher orders are also possible and are included in distorted wave approaches.

The electrons are ejected with different velocities during ionization. The regime where electrons are ejected with the velocity close to that of the projectiles, known as the velocity matching region, is of great importance. In the velocity matching region, there is a higher chance of multiple interactions between the scattered projectile and the ejected electron due to the increased time that both particles are close to each other. As a result, they effectively attract each other and both particles are focused on the initial projectile

beam axis. Therefore, PCI effects maximize in the projectile-electron velocity matching region [20, 23].
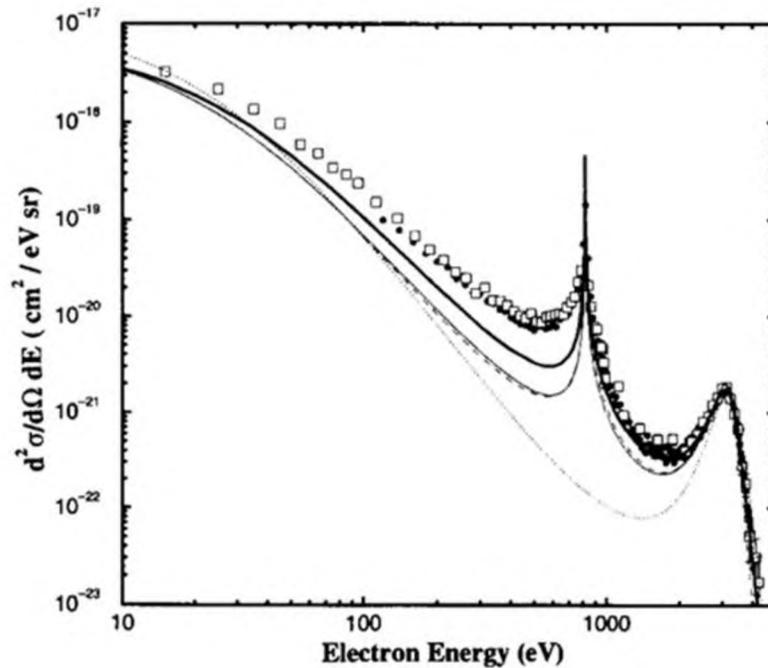
Figure 1.5. DDCS as a function of electron energy for 28.5 MeV F^{9+} + H_2 collisions

At first, this type of focusing effect by PCI in ion-atom collisions was observed in doubly differential electron energy spectra. A sharp peak structure, referred to as the cusp, was observed in the region corresponding to an electron speed equal to that of projectile speed [31]. Figure 1.5 gives a nice example of a double differential electron spectrum showing a cusp at about 800 eV, which corresponds to the velocity matching region, in addition to the binary peak at about 3000eV (corresponding to the momentum transfer region), taken for 28.5 MeV F^{9+} + H_2 collisions [28]. In the Figure, the dotted line

represents the First-Born Approximation (FBA), and the thin line represents a higher-order calculation by Brauner and Macek [29]. The dashed and thick solid lines represent two different versions of the CDW-EIS model, and open squares represent a classical trajectory Monte Carlo (CTMC) simulation by Schultz and Reinhold [30]. One important point to be noted is that the cusp is only predicted by the higher-order calculations and is completely missing in the FBA. This shows that the cusp is indeed due to higher-order mechanisms. Similar focusing structures were also observed in the recoil ion momentum spectra [32] and in the scattered projectile spectra [33]. The average scattering angles of projectiles were observed to be minimized in the cusp region. These studies showed that all of the signatures of PCI were maximized when electrons were ejected with the velocity equal to that of the projectile.

The most sensitive test of the theoretical description of the few-body dynamics is offered by fully differential cross-sections (FDCS). In FDCS, different characteristics of PCI were also observed in different theoretical studies. In the velocity matching region, in the electron ejection angle dependence of calculated FDCS, in addition to the binary peak in the direction of the momentum transfer, another pronounced peak structure, referred to as the forward peak, was observed in the direction of the initial projectile beam direction, i.e. at zero electron ejection angle [26]. Another similar characteristic signature of PCI was found in the electron energy dependence of FDCS [26].

To measure FDCS requires a kinematically complete experiment, which is particularly challenging in the velocity matching region of ionization by ion impact. In single ionization, if all the momentum components of two particles are measured then the momentum components of the third particle can be deduced using momentum conservation

laws. The unique facility at the Laboratory for Atomic, Molecular, and Optical Physics Research (LAMOR), Missouri University of Science and Technology, in combination with COLTRIMS, provided the opportunity to perform a kinematically complete experiment in this kinematic region. For all the experiments reported here, all three momentum vectors of the residual target ion and the scattered projectile in coincidence were directly measured and then those of the ejected electrons were deduced by using conservation laws. Hence, the data is fully differential.

Until a few years ago, kinematically complete experiments for ionization by ion impact were performed only for electrons ejected with much smaller speeds than the projectile speed. The only fully differential measurement in the region of the cusp was performed for 75 keV p+ H_2 in the laboratory at Missouri S&T [24]. However, this study was limited to only one electron energy. Furthermore, the data were compromised by a detector problem, which was only noticed later. Therefore, a systematic experimental study of PCI, covering a broad range of electron energies around the velocity matching region, on a fully differential level was lacking.

For small electron energies, the results from various theoretical approaches and experimental data were at least in qualitative agreement [39]. However, for the cusp region, severe discrepancies between the experiment and the theory, and also within similar theoretical models were observed [24, 25]. Therefore, to have a complete understanding of the reaction dynamics at the cusp region, a systematic study at a fully different level for different targets (atomic and molecular) with several different electron energies above and below the velocity matching region was necessary. This dissertation work filled that gap and provided a very systematic fully differential study in the region near velocity matching.

Kinematically complete experiments for 75 keV p + H_2 and He were performed for different electron-energies around the cusp region. All the measured FDCS in terms of different reaction parameters were compared to the results of the aforementioned two different, but conceptually very similar, theoretical calculations. The results of this dissertation study are published in three papers. The first paper is about the H_2 target with a narrow electron-energy range close to the cusp [16]. The second paper is the same as the first paper, but for a He target [17], and the third paper covers a broad electron-energy range, above and below the cusp, for both targets [18]. Considering these publications, a strong dataset is developed for both atomic and molecular targets with electron energies well above, below, and at the velocity matching region for a systematic study of the PCI on a fully differential level.

PAPER

I. FEW-BODY DYNAMICS UNDERLYING POSTCOLLISION EFFECTS IN THE IONIZATION OF H₂ BY 75-keV PROTON IMPACT

M. Dhital[1], S. Bastola[1], A. Silvus[1], A. Hasan[2], B.R. Lamichhane[1], E. Ali[1], M.F. Ciappina[3], R.A. Lomsadze[4], D. Cikota[1], B. Boggs[1], D.H. Madison[1], and M. Schulz[1]

[1]Dept. of Physics and LAMOR, Missouri University of Science & Technology, Rolla, MO 65409

[2]Dept. of Physics, UAE University, P.O. Box 15551, Al Ain, Abu Dhabi, UAE

[3]Institute of Physics of the ASCR, ELI-Beamlines, 182 21 Prague, Czech Republic

[4]Tbilisi State University, Tbilisi 0179, Georgia

ABSTRACT

We have measured fully differential cross sections (FDCS) for ionization in 75 keV p + H₂ collisions for ejected electron speeds close to the projectile speed. The data were analyzed both in dependence on the electron emission and the projectile scattering angle. Pronounced post-collisional effects between the projectile and the ejected electrons were observed. Significant differences between experiment and theory and between two conceptually very similar theoretical models were found. This shows that in the region of electron-projectile velocity matching the FDCS are very sensitive to the details of the underlying few-body dynamics.

1. INTRODUCTION

One of the most important goals of ion-atom collision research is to advance our understanding of the few-body dynamics in systems consisting of a small number of charged particles [1,2]. To this end, one process which has been studied extensively, and which is also the focus of the present article, is ionization of simple target atoms or molecules by charged particle impact (for reviews see e.g. [2,3]). The major theoretical challenge in this task is that the Schrödinger equation is not analytically solvable for more than two mutually interacting particles even when the underlying forces are precisely known. As a result, theory has to resort to numeric models and the assumptions and approximations entering in these models have to be tested by detailed experimental data.

Such numeric approaches can crudely be grouped into perturbative and non-perturbative models. The latter have the advantage that they tend to be numerically "more complete" in the sense that a large number of basis states can be included so that the influence of reaction channels other than the process of interest on the cross sections can be accounted for. As a result, ionization of simple target atoms (and other processes) by electron impact are often well described by such models (e.g. [4-6]). For ion-atom collisions non-perturbative calculations are much more challenging due to the much larger projectile mass which means that an enormous number of partial waves have to be considered to adequately describe the scattered projectile. Furthermore, the positive charge of the projectile necessitates the inclusion of projectile states in the basis sets if the effect of the capture channel is to be considered. As a result, the literature on non-perturbative calculations for ion impact [e.g. 7-10] is not as extensive as for electron impact.

Perturbative models effectively represent two-state approximations (accounting only for the initial state and the final state observed in the experiment). In one class of perturbative models, the transition amplitude is expanded in powers of the interaction potential (Born series) [11]. One advantage of this approach is that it tends to be more transparent than non-perturbative methods to the physical mechanisms leading to the collision process. Each expansion term can be associated with a specific contribution which classically corresponds to a sequence of interactions between pairs of particles within the collision system. By comparing experimental results with theory, the relative importance of the various interaction sequences in the collision dynamics can be evaluated.

The disadvantage of this expansion series approach is that in practice it has to be truncated after some order to be numerically feasible. Calculations have been carried out to second order for several processes [e.g. 12-14], but we are not aware of any attempts to calculate third- or higher-order terms. For collision systems with relatively small perturbation parameters η (projectile charge to speed ratio) a second- (and in some cases even a first-order) description is often sufficient, however, for large η higher-order terms can be quite important and the expansion series may not even converge at all. An alternative perturbative approach to account for higher-order contributions is offered by distorted wave methods, which treat such contributions in the final state wavefunction [e.g. 15-19]. The advantage compared to the Born series is that any physical effect contained in the wavefunction is automatically included to all orders of perturbation theory so that the convergence problem of the Born series does not occur directly and is significantly reduced. However, it is not completely solved because it is not possible to include all the important physical effects in the wavefunction. Thus, these effects become part of the

perturbation. Nevertheless, perturbative calculations on processes occurring in ion-atom collisions have focused on distorted wave approaches in recent years.

One higher-order mechanism that has been studied extensively is known as the post-collision interaction (PCI) [e.g. 20-26]. Here, the projectile interacts at least twice with a target electron. In the primary interaction the electron is lifted to the continuum and in the second interaction the projectile and the electron "focus" each other leading to a reduction in their relative velocity vector. However, classically either the electron or the projectile needs to be redirected by a collision with the target nucleus before the second projectile-electron interaction can occur. Therefore, the two leading-order interaction sequences leading to PCI are V_{Pe}-V_{Te}-V_{Pe} and V_{Pe}-V_{PT}-V_{Pe} [27,28], where the subscripts P, T, and e stand for projectile, target nucleus, and electron. Of course, contributions of higher order containing these sequences are also possible and are accounted for in distorted wave approaches. Such focusing effects caused by PCI were found in the ejected electron energy spectra [e.g. 20,21], in the projectile scattering angle dependence of double differential cross sections (DDCS) [22,28], as well as in recoil-ion momentum spectra [26]. These signatures maximize when the electron and projectile velocities v_e and v_p are equal to each other (matching velocity). However, especially for highly charged ion impact PCI can alter the momentum distribution of the ejected electrons significantly even far away from the matching velocity [29]. Apart from affecting the velocity vector of electrons ejected in ionization, PCI effects can also distort the line shape of autoionization following inner shell vacancy production by ionization, excitation or capture in ion-atom collisions [30]. Finally, we note that post-collisional effects of the residual target ion on the ejected electron have been observed as well [31].

The most sensitive tests of theoretical calculations are generally offered by fully differential cross sections (FDCS) extracted from kinematically complete experiments. In the fully differential angular distribution of electrons ejected by highly charged ion impact a pronounced peak structure in the direction of the initial projectile velocity (defining $\theta_e = 0$), caused by PCI, was observed even for electron speeds much smaller than the projectile speed [23]. On the other hand, for collisions with protons or moderately charged ions only a shift of structures in the angular distribution towards $\theta_e = 0°$, but no separate peak structure at $\theta_e = 0°$ was found if $v_e \ll v_p$, in accordance with theoretical predictions [24,32]. In contrast, for $v_e = v_p$ calculated FDCS for 75 keV p + H_2 collisions were completely dominated by a sharp peak structure at $\theta_e = 0$ [33]. Surprisingly, this forward peak was nearly completely absent in experimental data [25]. One possible explanation that was considered was that the capture channel, not accounted for by perturbative models, might remove significant flux from the ionization channel, especially near $\theta_e = 0$. The presence of the capture channel could then also make the FDCS for ionization quite sensitive to the ejected electron energy (or equivalently the projectile energy loss) because its impact should sharply maximize at the matching velocity.

In this article we present a joint experimental and theoretical study of FDCS for ionization in 75 keV p + H_2 collisions. Earlier experiments, performed almost at the matching velocity (corresponding to an energy loss of 56.5 eV), were extended to a broader range covering electron speeds from just below to just above the projectile speed (corresponding to energy losses of 50, 53, 57, and 60 eV). In the new data a clear peak structure at $\theta_e = 0$ is now observed in the FDCS. The comparison of the data with two

conceptually very similar theoretical models shows that near the matching velocity the few-body dynamics become very sensitive to the electron speed and ejection angle.

2. EXPERIMENTAL SETUP

The experiment was performed at the medium energy ion accelerator at the Missouri University of Science & Technology. A schematic set-up is shown in Figure 1. A proton beam was generated with a hot cathode ion source and accelerated to an energy of 75 keV. The beam was collimated with horizontal and vertical slits, each with a width of 150 μm, placed at a distance of about 50 cm from the target region. This slit geometry, along with the projectile de Broglie wavelength of 2×10^{-3} a.u., corresponds to a transverse coherence length of about 3.5 a.u. [34]. After passing through the target region, the beam was charge-state analyzed by a switching magnet. The protons which did not undergo charge exchange were then decelerated to an energy of 5 keV and energy – analyzed by an electrostatic parallel plate analyzer [35] with a resolution of 2.5 eV full width at half maximum (FWHM). The energy-analyzed projectiles were then detected by a two-dimensional position-sensitive multi-channel plate detector. From the position information the projectile scattering angle θ_p was determined with a resolution of about 0.1 to 0.15 mrad FWHM. From the energy loss ε and θ_p the Cartesian components of the momentum transfer from the projectile to the target $\mathbf{q} = \mathbf{p_o} - \mathbf{p_f}$ were obtained as $q_x = p_o \tan \theta_p$ and $q_z = \varepsilon/v_p$, where the x- and z-axes are parallel to the analyzer slits and the initial projectile momentum, respectively (see coordinate system in Fig 1). The y-component of $\mathbf{q}$ was fixed at zero due to the very narrow width of the entrance and exit slits of the analyzer (75 μm).

In the target chamber the projectile beam was crossed with a very cold (T ≈ 1- 2 K) molecular hydrogen beam from a supersonic gas jet propagating in the y-direction. The recoiling H_2^+ ions created at the intersection point between both beams were extracted in the x-direction by a weak electric field (≈ 6 V/cm) and guided onto another two-dimensional position-sensitive multi-channel plate detector, which was set in coincidence with the projectile detector. The y-and z-components of the recoil-ion momentum $\mathbf{p_r}$ are determined by the corresponding position components on the detector and the x-component by the time of flight of the recoil ions from the collision region to the detector, which, in turn, is contained in the coincidence time.
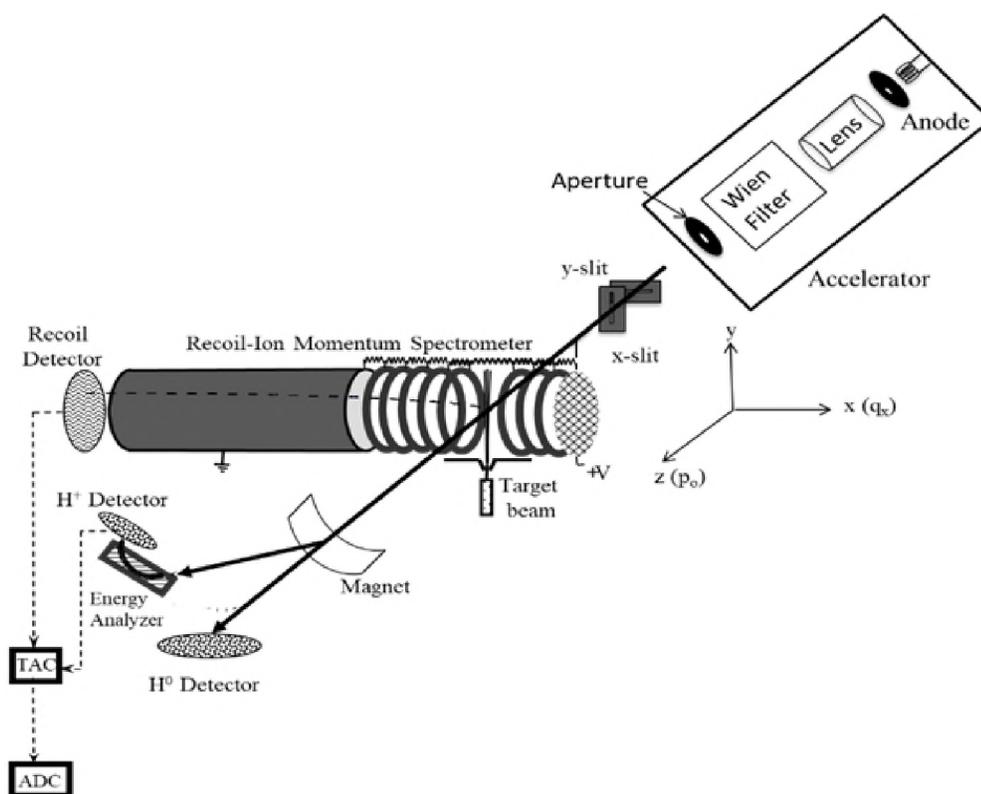
Figure 1. Schematic sketch of the experimental setup

The electron momentum was then deduced from momentum conservation as $\mathbf{p_e}$ = $\mathbf{q}$ - $\mathbf{p_r}$. The azimuthal electron emission angle is given by φ_e = atan (p_{ey}/p_{ex}) and the polar angle by θ_e = asin(p_{ex}/p_e). The magnitude of the electron momentum p_e was calculated from the energy loss (in a.u.) by $p_e = [2(\varepsilon - I)]^{1/2}$, where I is the ionization potential of H_2 (I = 15.4 eV = 0.57 a.u.). The resolution in p_e is thus determined by the energy loss resolution as $\Delta p_e = \Delta\varepsilon/p_e = 0.06$ a.u. The resolution in p_{ex} is dominated by the projectile scattering angle resolution and amounts to about 0.3 a.u. From these numbers a resolution in θ_e of about $10°$ FWHM was estimated for the forward direction and $13°$ to $15°$ (depending on θ_p) in the direction of $\mathbf{q}$, where the so-called binary peak is expected. FDCS were analyzed for electrons of fixed energy ejected into the scattering plane spanned by $\mathbf{p_0}$ and $\mathbf{q}$ (i.e. φ_e was fixed at zero within ± $5°$) and plotted for fixed projectile scattering angles as a function of θ_e.

3. RESULTS AND DISCUSSION

In Figure 2, the FDCS = $d^3\sigma/(dE_e d\Omega_e d\Omega_p)$ are plotted as a function of θ_e for θ_p = 0.1 mrad and for energy losses as indicated by the insets. Here, ε = 57 eV corresponds to the matching speed $v_e = v_p$ (within 1%). For all four energy losses a strong peak structure at $\theta_e = 0$ is found, which becomes increasingly narrow with v_e approaching v_p (the FWHM in order of increasing ε are $30°$, $26°$, $22°$, and $24°$). It should be noted that this width is mostly due to the binary peak, located near the direction of $\mathbf{q}$, which for small θ_p is not resolved from the forward peak. Its intensity relative to the one of the forward peak is

expected to minimize at the matching speed thus resulting in a minimized angular width. The data of our earlier study for $\varepsilon = 57$ eV [25], where this peak structure was shifted to 15°, are thus not reproduced by the present results. The reason for this discrepancy could be related to a crack in the anode of the projectile detector used in [25], which became apparent after the experiment was completed and the data were published. However, it probably started already earlier as a tiny hair crack which went unnoticed because the signals were not yet visibly affected. It nevertheless may have compromised the projectile position resolution in the x-direction and thereby the corresponding component of the electron momentum.
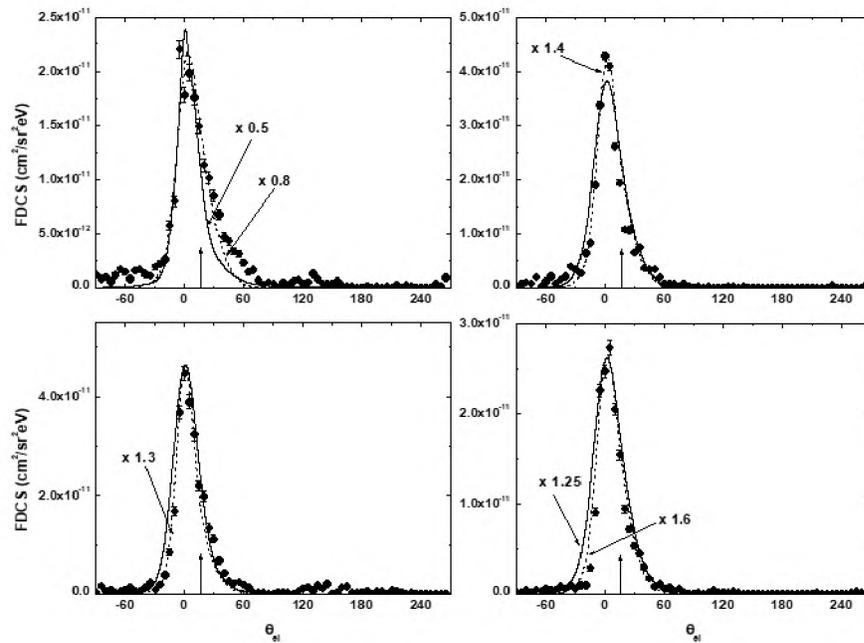
Figure 2. Fully differential cross sections for electrons ejected into the scattering plane for a projectile scattering angle of 0.1 mrad

The dashed and solid curves in Figure 2 show our continuum distorted wave-eikonal initial state (CDW-EIS) [18] and 3-body distorted wave (3DW) calculations [33], respectively. Both models represent perturbative approaches in which higher-order contributions are treated in the final-state wavefunction. Since the natural width of the forward peak in the calculations (varying between $2°$ and $10°$ FWHM, depending on ε) is in most cases smaller than the experimental resolution, theory had to be convoluted with the latter in order to make possible a meaningful comparison to the measured data. However, the resolution estimated in the experimental section yields theoretical peak structures which are too broad. Theory was therefore convoluted with a resolution of $5°$ FWHM, which for the two smaller scattering angles reproduced the half width of the negative angle wing of the peak in the experimental data very well. This suggests that our estimate of the angular resolution is too pessimistic. On the other hand, in the vicinity of the binary peak a resolution of $5°$ FWHM is probably too optimistic. However, the natural width of the binary peak is much larger than the experimental resolution so that here the convolution has no significant impact on the FDCS.

Both models reproduce the qualitative dependence of the measured FDCS on θ_e very well. However, in magnitude there are some differences between experiment and both theories. Furthermore, the two theories differ from each other by as much as about 40%. Since both models are conceptually very similar, this can be taken as a first indication for the FDCS being relatively sensitive to the details of the reaction dynamics in the region of the matching velocity.

In Figure 3, the FDCS are shown for $\theta_p = 0.2$ mrad and for the same energy losses as in Figure 2. The data still maximize near $\theta_e = 0$, but while for $\theta_p = 0.1$ mrad the FDCS

are nearly symmetric around $\theta_e = 0$ (except for $\epsilon = 50$ eV), for $\theta_p = 0.2$ mrad the wing for

positive θ_e is larger than the one for negative θ_e. For $\epsilon = 50$ eV there might even be a

separate peak structure at $\theta_e = 25°$, although the statistical significance of the forward peak

due to a single data point $\theta_e = 0°$ is not clear. This asymmetry is a signature of an increasing

contribution of the binary peak to the FDCS. The binary peak results from events in which

momentum is exchanged predominantly between the projectile and the active electron (i.e.

the residual target ion remains to a large extent passive) and therefore occurs near the

direction of q (indicated in Figs. 2-5 by the vertical arrows). For ejected electron speeds

much less than the projectile speed it is usually the dominant structure in the FDCS. For

$\theta_p = 0.2$ mrad the direction of q is between $26°$ and $31°$ (depending on energy loss) so that

the binary peak is not resolved from the forward peak (with the possible exception of $\epsilon =$

50 eV). Rather, its contribution only leads to the aforementioned asymmetry favoring

positive θ_e.
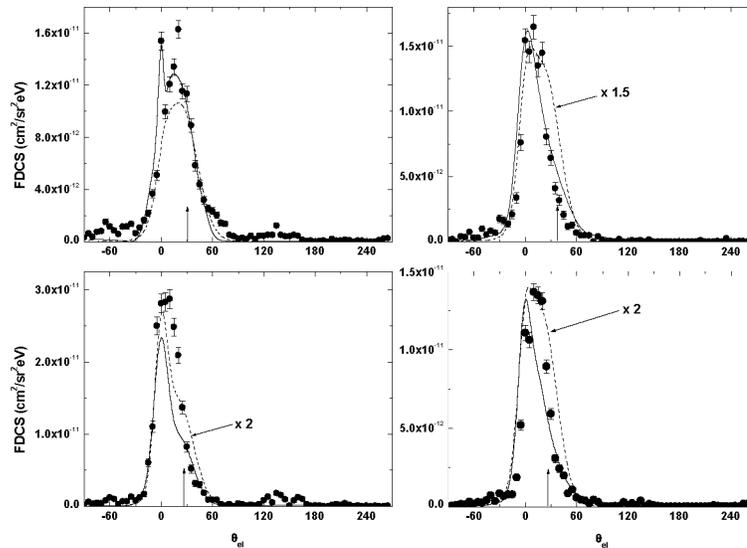
Figure 3. Same as Figure 2 for a projectile scattering angle of 0.2 mrad

The comparison to theory reveals increasing discrepancies with the experimental data, not only in magnitude, but also in shape. Furthermore, the differences between both theories are also increased and are quite noticeable in shape as well. While the centroid of the FDCS calculated with CDW-EIS tends to be shifted to slightly larger angles than in the experimental data, for the 3-DW model the centroid is shifted to smaller angles, at least for the two larger energy losses. In magnitude the differences between both calculations is now increased to as much as a factor of two. Overall, in shape the experimental data fall somewhere between both theories. We note that the 3DW calculation yields separate forward and binary peak structures at $\varepsilon = 50$ eV, lending some credence to the measured data point at $\theta_e = 0°$.
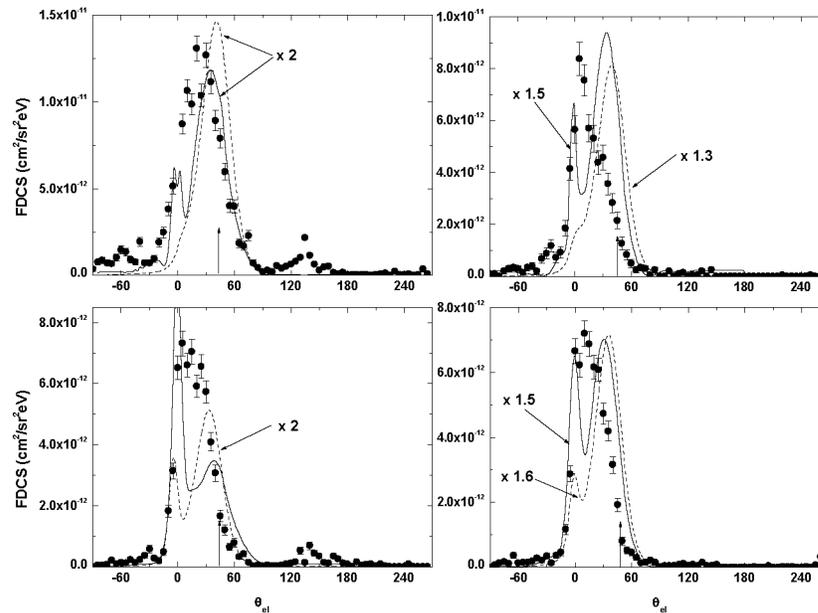
Figure 4. Same as Figure 2 for a projectile scattering angle of 0.325 mrad

At θ_p = 0.325 mrad the contributions to the FDCS (shown in Figure 4) from the

binary peak relative to the forward peak have increased (compared to the smaller θ_p) to the

extent that the data no longer maximize at θ_e = 0, especially for ε = 50 and 60 eV. This

trend is also seen in both theoretical models, where the binary peak is in most cases even

clearly separated from the forward peak. At this scattering angle there are significant and

qualitative discrepancies between both calculations and the measured data as well as

between both models. There is some element of qualitative agreement between the

theoretical results in so far as they both predict the forward to binary peak intensity ratio

to maximize around v_e/v_p =1 (i.e. at ε = 57 eV), as expected. But quantitatively, that ratio

is significantly larger in the 3DW model for all ε.
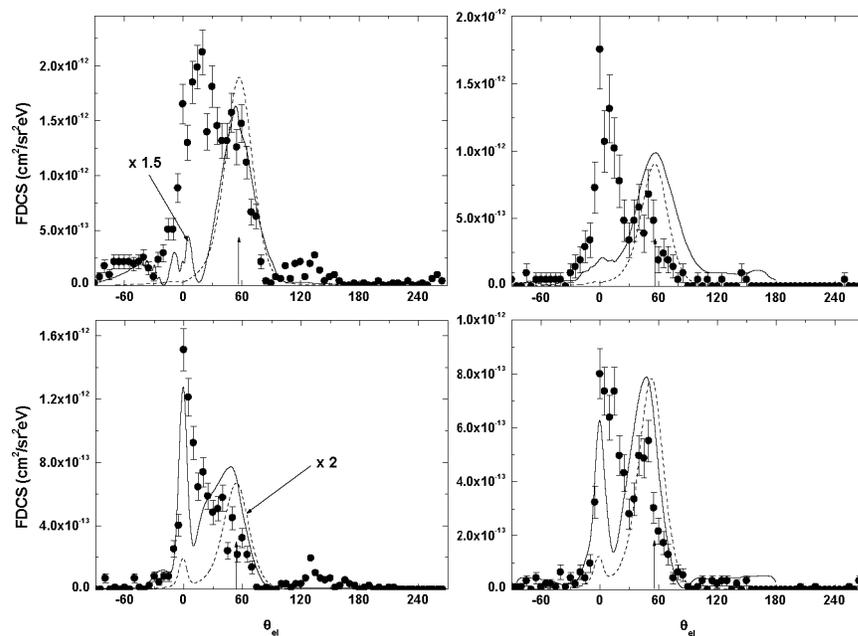
Figure 5. Same as Figure 2 for a projectile scattering angle of 0.55 mrad

The FDCS for $\theta_p = 0.55$ mrad are plotted in Figure 5. At this scattering angle the binary peak in the experimental data is clearly separated from the forward peak, except for $\varepsilon = 57$ eV. Since at this energy loss the momentum transfer occurs at $\theta_e = 55°$ the binary peak should be separated from the forward peak. The observation that the binary peak is not at the direction of the momentum transfer points to another well-known signature of higher-order contributions: they lead to a forward shift of the binary peak relative to the direction of $\mathbf{q}$ [36]. Indeed, for the other energy losses the peak is shifted as well and the shift increases, as expected, with decreasing departure of the electron speed from the projectile speed.

A small forward shift of the binary peak is also observed in the 3DW calculations, at least for the two larger ε, but interestingly not in the CDW-EIS results even at $\varepsilon = 57$ eV (i.e. $v_e = v_p$). On the other hand, a small shift of about 7° is seen in the calculation for $\varepsilon = 57$ eV and $\theta_p = 0.325$ mrad. This trend in the CDW-EIS results is similar to what was measured and calculated for FDCS in 16 MeV O^{7+} + He collisions for electron speeds much smaller than the projectile speed [36]: the forward shift of the binary peak decreased with increasing transverse momentum transfer (q_{tr}) and reached a minimum at $q_{tr} \approx 1.5$ to 2 a.u., which for the present collision system corresponds to $\theta_p \approx 0.55$ mrad, making it even larger than in the 3DW results. In contrast, at $\varepsilon = 57$ eV the 3DW model predicts a larger forward shift for $\theta_p = 0.55$ mrad than for 0.325 mrad.

It seems plausible to associate the forward shift of the binary peak with PCI. However, it should be noted that for 16 MeV O^{7+} + He collisions studied in [36] it could be clearly traced to PCI only for $q_{tr} > 2$ a.u. For $q_{tr} < 1.5$ a.u. this shift was explained by another higher-order mechanism involving the projectile – target nucleus (PT) interaction

and an interaction of the electron, already promoted to the continuum by the projectile, with the target nucleus. On the other hand, it should also be noted that in the present work we study a very different kinematic regime. More specifically, since the electron speed is close to the projectile speed it is quite possible that even for $q_{tr} < 1.5$ a.u. (or $\theta_p < 0.5$ mrad) the forward shift of the binary peak is mostly caused by PCI.

Apart from the forward shift of the binary peak at $\theta_p = 0.55$ mrad there are also large and qualitative differences between the 3DW and CDW-EIS calculations in the binary to forward peak intensity ratio and in the overall magnitude of the FDCS and both calculations show large discrepancies to the measured FDCS. Considering the conceptual similarity of both models this is a very surprising observation which calls for an explanation. To this end, the conclusions obtained from a double differential study of ionization of atomic hydrogen by 75 keV p impact [28] may point in the right direction. There, it was found that in the CDW-EIS model PCI effects are predominantly caused by the V_{Pe}-V_{PT}-V_{Pe} sequence. The description of the PT interaction, occurring in this sequence, represents the perhaps most significant difference between the two models. While in the CDW-EIS approach this interaction is treated semi-classically, assuming a straight-line trajectory for the projectile and using the eikonal approximation, in the 3DW model it is accounted for fully quantum-mechanically in terms of a Coulomb factor in the final-state wavefunction. For a 75 keV proton it may not seem obvious that this difference is important. On the other hand, the increasing discrepancies between experiment and theory and between both calculations with increasing θ_p show that the FDCS become very sensitive to the details of the few-body dynamics, especially at large θ_p.

Another question to be answered is why the disagreement between theory and experiment grow so large at large θ_p. Several factors may contribute to these discrepancies. First, in the case of an atomic hydrogen target it was found that in a hybrid model, referred to as second Born approximation with Coulomb waves (SBA-C), the relative importance of the two interaction sequences contributing to PCI (V_{Pe}-V_{PT}-V_{Pe} and V_{Pe}-V_{eT}-V_{Pe}) is reversed compared to CDW-EIS [28]. In the SBA-C approach the PT interaction is treated in the operator of the transition amplitude, but the higher-order contributions in the projectile – electron interaction is treated in the final-state wavefunction. Generally, the experimental data were in better agreement with the SBA-C than with the CDW-EIS calculations. This can be taken as an indication that the contributions from the V_{Pe}-V_{eT}-V_{Pe} sequence may be underestimated by the CDW-EIS results.

Second, in [28] it was argued that treating higher-order contributions in the projectile – electron interaction in the final state wavefunction (as done in both CDW-EIS and 3DW) should be more accurate than in the Born series truncated after the second-order term. However, contributions involving the PT interaction were believed to be more adequately described in terms of the second Born approximation (as done in the SBA-C model). The reasoning for this assumption was that such higher-order contributions are expected to select events in which all three particles are relatively close together. The projectile needs to approach the electron to a close distance in order to transfer sufficient energy for ionization to occur. But the projectile also needs to approach the target nucleus rather closely for the PT interaction to play an important role. However, the final-state wavefunction in distorted wave approaches is known to be accurate only if at least one particle is far from the other two [37,38]. Therefore, even if the V_{Pe}-V_{PT}-V_{Pe} sequence

provides the dominant contribution to PCI it may not be treated with sufficient accuracy by the CDW-EIS and 3DW models. Close encounters between the projectile and the target nucleus should be particularly important at large θ_p, which would explain the increasing discrepancies with increasing θ_p.

Furthermore, the capture channel, not accounted for in either model, may contribute to the discrepancies [32]. The flux in this channel is erroneously counted as ionization in the calculations. Discrepancies resulting from this factor should maximize at the matching velocity (i.e. for $v_e = v_p$ and $\theta_e = 0$). This seems to be indeed the case in the 3DW results for $\theta_p = 0.325$ and 0.55 mrad, but not for the two smaller scattering angles. On the other hand, the CDW-EIS approach systematically underestimates this structure. Since neither calculation accounts for the capture channel the comparison between experiment and theory does not allow for definite conclusions regarding its importance.

Finally, both theoretical models treat the projectiles as completely coherent, i.e. the transverse coherence length Δr is infinite. On the other hand, it has been demonstrated that measured cross sections can sensitively depend on Δr [39]. If Δr is significantly smaller than the effective dimension of the diffracting object (i.e. the target), any interference term predicted by theory may not be observable. The effective target dimension, in turn, is basically determined by the impact parameter dependence of the reaction probability. At impact parameters larger than 3.5 a.u. (i.e. the coherence length realized in this experiment) the ionization probability is expected to be rather small. Nevertheless, it has been theoretically demonstrated that even at $\Delta r = 3.5$ a.u. the projectiles cannot be regarded as fully coherent and that the cross sections are very sensitive to Δr in this region [40].

As pointed out in the introduction PCI represents a focusing effect between the projectile and the ejected electron in which both particles attract each other towards the initial projectile beam axis. Therefore, it should lead to a narrowing of the angular distribution of the scattered projectiles. This was indeed observed in double differential cross sections (DDCS) (in energy loss and projectile solid angle) for ionization of atomic and molecular hydrogen [28] by proton impact. On the other hand, the DDCS represent an integration of the FDCS over all ejected electron solid angles. Therefore, electrons ejected at large θ_e, i.e. those which are not affected by PCI very strongly, contribute to the width of the projectile angular distribution. An even larger narrowing effect could therefore be expected in the FDCS for θ_e fixed at 0 as a function of θ_p.
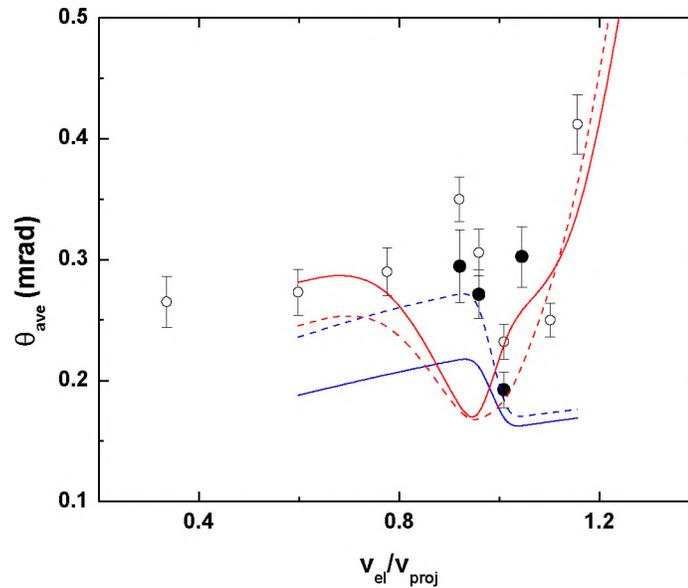
Figure 6. Average projectile scattering angle θ_{ave} for electrons ejeceted at $\theta_e = 0$ as a function of the electron to projectile speed ratio

In Figure 6 we present the average scattering angle,

$$\theta_{avg} = \int (d^3\sigma/d\Omega_p d\Omega_e dE_e)\, \theta_p\, d\Omega_p / \int (d^3\sigma/d\Omega_p d\Omega_e dE_e)\, d\Omega_p \qquad (1)$$

for $\theta_e = 0$ as a function of the electron to projectile speed ratio v_e/v_p as closed symbols. For comparison, the open symbols represent the corresponding average angles obtained from the DDCS reported in [28]. In both data sets a pronounced minimum is observed near $v_e/v_p = 1$, confirming a pronounced focusing effect caused by PCI. Furthermore, this focusing effect indeed appears to be stronger in the FDCS than in the DDCS because the minimum is deeper and narrower. The dashed and solid blue curves in Figure 6 show the CDW-EIS calculations with and without the PT interaction included, respectively, and the dashed and solid red curves the corresponding results of the 3DW model. Remarkably large differences between all four calculations and the experimental data are quite apparent.

First, we analyze the comparison of both CDW-EIS calculations with the experimental data. Both reproduce a minimum at $v_e/v_p = 1$, but in both cases it is not as pronounced as in the measured values because for $v_e/v_p > 1$ the calculated θ_{avg} rise much slower than in the experimental data. Up to the matching speed the calculation without the PT interaction is in much better agreement with experiment, while for $v_e/v_p > 1$ both curves approach each other. This suggests that within the CDW-EIS model the V_{Pe}-V_{PT}-V_{Pe} sequence becomes relatively unimportant for $v_e/v_p > 1$ and that its contribution to PCI may be overestimated for $v_e/v_p < 1$.

The 3DW results exhibit a good qualitative agreement with experiment except for the location of the minimum of the cross section for the velocity matching region. Whereas experiment finds the minimum at unity, the 3DW has a minimum at $v_e/v_p = 0.95$ and the width is much broader than in experiment. In the 3DW model the effect of including the

PT interaction is significantly smaller than in the CDW-EIS model, suggesting that in the former the V_{Pe}-V_{PT}-V_{Pe} sequence plays a much less important role. Overall, the 3DW model is in satisfactory agreement with the experimental data. On the other hand, the CDW-EIS yields reasonable agreement up to, but not above the matching speed and the inclusion of the PT interaction does not lead to improved agreement. The comparison between the experimental data and both models thus reinforces the conclusion drawn from the analysis of the fully differential angular electron distributions that near the matching speed the FDCS are very sensitive to the details of the collision dynamics.

At the matching speed, PCI seems to have a much stronger effect for H_2 (even in θ_{ave} obtained from the DDCS, open symbols in Figure 6) than for helium. This was not necessarily expected because of the larger ionization potential I of helium. By considering the asymptotic case of I approaching zero one would expect PCI effects to become more important with increasing I. This scenario of an unbound electron is equivalent to the target nucleus not even being present so that neither of the two interaction sequences leading to PCI is present. The dependence of PCI effects on the target ionization potential was further investigated in a separate study for heavy targets (Neon and Argon), which will be reported in a forthcoming publication of the most important goal

4. CONCLUSIONS

We have measured and calculated fully differential cross sections for ionization of H_2 by 75 keV proton impact for ejected electron speeds close to the projectile speed. The data confirm a very pronounced peak structure for electrons ejected in the forward direction

which was predicted by theory earlier [33]. This feature was not observed in a previous experiment for the same collision system and for similar kinematic conditions, probably due to a hair crack in the anode of the projectile detector resulting in a compromised electron angular resolution.

The comparison between the experimental data and two conceptually very similar perturbative models show that near the electron – projectile matching speed the fully differential cross sections are very sensitive to the few-body dynamics. Large differences are found both in the angular distributions of the ejected electrons and of the scattered projectiles. The most important difference between the 3DW and CDW-EIS models is the description of the projectile - target nucleus interaction, which is treated fully quantum-mechanically in the former and semi-classically in the latter model. It seems likely that the discrepancies between the experimental data and the CDW-EIS calculations can to a large extent be related to the description of the PT interaction. However, there are also significant discrepancies between the measured data and the 3DW calculation. This shows that either the PT interaction is not treated with sufficient accuracy in the 3DW model either or that other factors, such as the finite projectile coherence length or the capture channel not accounted for in theory, contribute to these discrepancies. One potential problem concerning the PT interaction, and which could affect both models, is that higher-order mechanisms involving the PT interaction could be quite selective on events in which all three particles approach each other to a relatively small distance. However, the 3-body final-state wavefunction is only accurate if at least one particle is far away from the other two. To test a potential influence from this factor calculations based on the second Born approximation and on non-perturbative approaches could be very helpful.

ACKNOWLEDGEMENTS

REFERENCES

[1] M. Schulz, R. Moshammer, D. Fischer, H. Kollmus, D.H. Madison, S. Jones, and J. Ullrich, Nature $\underline{422}$, 48 (2003)

[2] M. Schulz and D.H. Madison, International Journal of Modern Physics A $\underline{21}$, 3649 (2006)

[3] H. Ehrhardt, K. Jung, G. Knoth, and P. Schlemmer, Z. Phys. D $\underline{1}$, 3 (1986)

[4] T.N. Resigno, M. Baertschy, W.A. Isaacs, and C.W. McCurdy, Science $\underline{286}$, 2474 (1999)

[5] X. Ren, I. Bray, D.V. Fursa, J. Colgan, M.S. Pindzola, T. Pflüger, A. Senftleben, S. Xu, A. Dorn, and J. Ullrich, Phys. Rev. A $\underline{83}$, 052711 (2011)

[6] J. Colgan, M. Foster, M.S. Pindzola, I. Bray, A.T. Stelbovis, and D.V. Fursa, J. Phys. B $\underline{42}$, 145002 (2009)

[7] M. McGovern, D. Assafrao, J.R. Mohallem, C.T. Whelan, H.R.J. Walters, Phys. Rev. A $\underline{81}$, 042704 (2010)

[8] M.S. Pindzola, J. Colgan, Robicheaux, T.G. Lee, M.F. Ciappina, M. Foster, J.A. Ludlow, S.A. Abdel-Naby, Ad. At. Mol. Opt. Phys. $\underline{65}$, 291 (2016)

[9] M. Baxter, T. Kirchner, and E. Engel, Phys. Rev. A $\underline{96}$, 032708 (2017)

[10]   I.B. Abdurakhmanov, J.J. Bailey, A.S. Kadyrov, and I. Bray, Phys. Rev. A 97, 032707 (2018)

[11]   J.R. Taylor, Scattering Theory: The Quantum Theory of Nonrelativistic Collisions (Wiley, New York, 1972)

[12]   O. Chuluunbaatar, S.A. Zaytsev, K.A. Kouzakov, A. Galstyan, V.L. Shablov, and Yu.V. Popov, Phys. Rev. A 96, 042716 (2017)

[13]   A.L. Godunov, C.T. Whelan, and H.R.J. Walters, Phys. Rev. A 78, 012714 (2008)

[14]   D. Belkić, Phys. Rev. A 43, 4770 (1991)

[15]   J. Fiol, V.D. Rodríguez, and R.O. Barrachina J. Phys. B 34, 933 (2001)

[16]   D. H. Madison, D. Fischer, M. Foster, M. Schulz, R. Moshammer, S. Jones, and J. Ullrich, Phys. Rev. Lett. 91, 253201 (2003)

[17]   R.T. Pedlow, S.F.C. O'Rourke, and D.S.F. Crothers, Phys. Rev. A 72, 062719 (2005)

[18]   M.F. Ciappina and R.D. Rivarola, J. Phys. B 41, 015203 (2008)

[19]   A.B. Voitkiv, Phys. Rev. A 95, 032708 (2017)

[20]   G. B. Crooks and M. E. Rudd, Phys. Rev. Lett. 25, 1599 (1970)

[21]   L. Sarkadi, J. Palinkas, A. Köver, D. Berenyi, and T. Vajnai, Phys. Rev. Lett. 62, 527 (1989)

[22]   T. Vajnai, A. D. Gaus, J. A. Brand, W. Htwe, D. H. Madison, R. E. Olson, J. L. Peacher, and M. Schulz, Phys. Rev. Lett. 74, 3588 (1995)

[23]   M. Schulz, R. Moshammer, A.N. Perumal, and J. Ullrich, J. Phys. B 35, L161 (2002)

[24]   M. Schulz, B. Najjari, A.B. Voitkiv, K. Schneider, X. Wang, A.C. Laforge, R. Hubele, J. Goullon, N. Ferreira, A. Kelkar, M. Grieser, R. Moshammer, J. Ullrich, and D. Fischer, Phys. Rev. A 88, 022704 (2013)

[25]   A. Hasan, T. Arthanayaka, B.R. Lamichhane, S. Sharma, S. Gurung, J. Remolina, S. Akula, D.H. Madison, M.F. Ciappina, R.D. Rivarola, and M. Schulz, J. Phys. B 49, 04LT01 (2016)

[26]   Th. Weber, Diploma Thesis, University Frankfurt, 1998, unpublished

[27]   L. Sarkadi, L. Gulyas, and L. Lugosi, Phys. Rev A 65, 052715 (2002)

[28]   M. Schulz, A.C. Laforge, K.N. Egodapitiya, J.S. Alexander, A. Hasan, M.F. Ciappina, A.C. Roy, R. Dey, A. Samolov, and A.L. Godunov, Phys. Rev. A 81, 052705 (2010)

[29]   R.E. Olson, C.J. Wood, H. Schmidt-Böcking, R. Moshammer, and J. Ullrich, Phys. Rev. A 58, 270 (1998)

[30]   S. Ricz, I. Kádár, J. Végh, Journal de Physique Colloques, 50, C1-199 (1989)

[31]   W. Schmitt, R. Moshammer, F.S.C. O'Rourke, H. Kollmus, L. Sarkadi, R. Mann, S. Hagmann, R.E. Olson, and J. Ullrich, Phys. Rev. Lett. 81, 4337 (1998)

[32]   A. Hasan, S. Sharma, T.P. Arthanayaka, B.R. Lamichhane, J. Remolina, S. Akula, D.H. Madison, and M. Schulz, J. Phys. B 47, 215201 (2014)

[33]   U. Chowdhury, M. Schulz, and D. H. Madison, Phys. Rev. A 83, 032712 (2011)

[34]   M. Schulz, Ad. At. Mol. Opt. Phys. 66, 508 (2017)

[35]   A.D. Gaus, W. Htwe, J.A. Brand, T.J. Gay, and M. Schulz, Rev. Sci. Instrum. 65, 3739 (1994)

[36]   Y.E. Kim and A.L. Zubarev, Phys. Rev. A 56, 521 (1997)

[37]   S. Jones and D.H. Madison, Phys. Rev. A 62 042701 (2000)

[38]   K.N. Egodapitiya, S. Sharma, A. Hasan, A.C. Laforge, D.H. Madison, R. Moshammer, and M. Schulz, Phys. Rev. Lett. 106, 153202 (2011)

[39]   L. Nagy, F. Jarai-Szabo, S. Borbely, T. Arthanayaka, B.R. Lamichhane, A. Hasan and M. Schulz, accepted for publication in "Interdisciplinary Research on Particle Collisions and Quantitative Spectroscopy", Dz. Belkic (editor), World Scientific Publishing, Singapore (2019)Bucki, L. (2013). *Microsoft Word 2013 bible* (4th ed.). Indianapolis, Ind: John Wiley & Sons, Inc.

[40]   A. Silvus, M. Dhital, S. Bastola, J. Buxton, Z. Klok, E. Ali, M.F. Ciappina, B. Boggs, D. Cikota, D.H. Madison, and M. Schulz, J. Phys. B 52, 125202 (2019)

II. TARGET DEPENDENCE OF POSTCOLLISION INTERACTION EFFECTS ON FULLY DIFFERENTIAL IONIZATION CROSS SECTIONS

M. Dhital[1], S. Bastola[1], A. Silvus[1], B.R. Lamichhane[1], E. Ali[1], M.F. Ciappina[2], R. Lomsadze[3], A. Hasan[4], D.H. Madison[1], and M. Schulz[1]

[1]Dept. of Physics and LAMOR, Missouri University of Science & Technology, Rolla, MO 65409

[2]Institute of Physics of the ASCR, ELI-Beamlines, 182 21 Prague, Czech Republic

[3]Tbilisi State University, Tbilisi 0179, Georgia

[4]Dept. of Physics, UAE University, P.O. Box 15551, Al Ain, Abu Dhabi, UAE

ABSTRACT

We have measured and calculated fully differential cross sections (FDCS) for ionization of helium by 75 keV proton impact. Ejected electron with a speed close to and above the projectile speed were investigated. This range of kinematics represents a largely unexplored regime. A high sensitivity of the FDCS to the details of the description of the few-body dynamics, reported earlier for ionization of H_2, was confirmed. A new, so far unexplained peak structure was found in an electron angular range between the regions where the so-called binary and recoil peaks are usually observed. The need for nonperturbative calculations using a two-center basis set is demonstrated.

1. INTRODUCTION

Ionization of atoms and molecules by ion impact has been studied extensively for several decades (for reviews see e.g. [1-4]). Early experiments focused on measuring absolute total cross sections [e.g. 5-9]. Later, with the development of high-resolution electron spectrometers, double differential cross section measurements became feasible [e.g. 10-12]. However, cross sections differential in projectile parameters were very challenging to measure because of the large mass of ions compared to electrons. Direct detection of fast heavy projectiles with sufficient resolution was restricted to scattering angles larger than approximately 0.1 mrad and energy losses larger than approximately 100 eV [13,14]. But for ionization from the target valence shell the largest contributions to the cross section often come from much smaller scattering angles (of the order of μrad or even smaller) and energy losses (close to the target ionization potential). Until about 20 years ago projectile differential cross sections for valence-shell ionization, in the kinematic regime which mostly contributes to the total cross section, could only be measured for light-ion impact [e.g. 15]. Double differential measurements (as a function of scattering angle and energy loss) were further limited to relatively small projectile energies [e.g. 16]. Fully differential cross sections (FDCS) were only measured [4,17-21] after recoil-ion momentum spectroscopy was developed [22,23]. For fast heavy-ion impact this made possible measuring the momentum vectors of the ejected electron and the recoil-ion in coincidence and to determine the scattered projectile momentum from the kinematic conservation laws.

So far, FDCS measurements were focused on electrons ejected with a speed much smaller than the projectile speed [e.g. 4,17-21]. Fully differential data for ejected electron speeds close to the projectile speed were only reported for 75 keV p + H_2 collisions [24], and such data for electrons considerably faster than the projectile are completely lacking. The projectile – electron velocity-matching regime has attracted considerable interest [e.g. 10,16,25,26] because here a specific higher-order mechanism, known as post-collision interaction (PCI), plays a particularly important role, especially for low- and intermediate-energy projectiles. In this process, the projectile interacts at least twice with the active electron. In the primary interaction the projectile transfers sufficient energy to the electron for the latter to be lifted to the continuum, and subsequently the two particles interact with each other for a second time, in which they attract each other towards the initial projectile beam axis and to similar velocities. Furthermore, because of momentum conservation, an interaction between the residual target ion and either the projectile or the active electron needs to be involved in PCI [27]. As a result, the leading - order interaction sequences leading to PCI are V_{pe}-V_{te}-V_{pe} and V_{pe}-V_{pt}-V_{pe}, where the subscripts p, t, and e refer to projectile, target ion, and electron, respectively. As pointed out by Sarkadi et al. [28] PCI is therefore a two-center process.

One important manifestation of the focusing due to PCI predicted by theory [29,30] is a strong peak structure in the fully differential electron angular distribution in the velocity matching regime occurring in the forward direction. This forward peak was recently confirmed experimentally for the case of an H_2 target [24]. Nevertheless, large discrepancies between experiment and theory and between two conceptually very similar theoretical models were found. In contrast, for electron energies well below the velocity-

matching regime discrepancies between experiment and theory are much smaller and various theoretical models are usually in reasonable agreement with each other [31,32]. This illustrates that, in the velocity-matching regime, the FDCS are very sensitive to the details of the few-body dynamics. Therefore, this regime is particularly important to test theoretical models.

Further signatures of PCI, which are not fully understood, were found in double differential cross sections (DDCS) as a function of scattering angle, which were measured for a broad range of ejected electron energies and for several target species [33]. For ejected electron energies below the velocity matching regime focusing effects due to PCI appeared to become increasingly pronounced with increasing target ionization potential I, which is the expected and theoretically predicted trend [24]. However, at the velocity matching the trend was not clear. On the one hand, the width of the scattering angle dependence of the DDCS increased with increasing I, suggesting a decreasing focusing due to PCI. On the other hand, a broadening of the DDCS could be caused by another higher-order mechanism, involving the projectile – target nucleus (PT) interaction, but only a single projectile-electron interaction. Such a process should become increasingly important with increasing I. It is thus possible that PCI increases with increasing I even at the velocity matching, but that it is masked by the higher-order mechanism involving the PT interaction. The results of [24] and [33] show that our understanding of the few-body dynamics in this regime is much less complete than it is for electron energies well below the velocity-matching regime. Furthermore, for electrons much faster than the projectiles no experimental FDCS have been reported at all yet.

In this paper we present measured FDCS for ionization in 75 keV p + He collisions. Two main goals were pursued in this project: first, we wanted to investigate the target dependence of PCI effects on the FDCS by comparing data for a target with a relatively large I (24.6 eV for He) to previously reported data for a target with a relatively small I (15.4 eV for H_2). Second, we wanted to study the role of PCI for ejected electron energies well above the velocity-matching regime. We will show that a clear dependence of PCI effects on the target could not be identified in the electron angular distribution of the FDCS, however, fully differential electron energy spectra show a stronger role of PCI for He compared to H_2 at large projectile scattering angles. Furthermore, PCI effects remain surprisingly strong at electron energies well above the velocity-matching regime.

2. EXPERIMENTAL SETUP

The experiment was performed at the ion-accelerator of the Missouri University of Science & Technology. The set-up is identical to the one used previously to study ionization of H_2 [24]. A proton beam was generated with a hot cathode ion source and extracted at an energy of 5 keV and then accelerated to 75 keV. The beam, propagating in the z-direction, was collimated by a pair of slits with a width of 150 μm placed at a distance of 50 cm from the target region. With a projectile deBroglie wavelength of 2×10^{-3} a.u. this slit geometry corresponds to a transverse coherence length of about 3.5 a.u. [34]. After passing through the target region, the projectiles were charge-analyzed by a switching magnet. The projectiles which were not charge-exchanged were decelerated by 70 keV, energy analyzed using an electrostatic parallel plate analyzer [35] and detected by a two-

dimensional position-sensitive multi-channel plate detector. From the position information and the energy loss ε the complete three-dimensional momentum vector was obtained in the data analysis. The resolution in ε was about 2.5 eV full width at half maximum (FWHM) and the scattering angle resolution 0.12 mrad FWHM.

In the collision chamber the projectile beam was crossed with a very cold helium beam (T $\approx$ 1-2 K), propagating in the y-direction, from a supersonic jet. The recoil ions produced in the collision were extracted by a weak and uniform electric field of 6 V/cm and detected by a second two-dimensional position-sensitive detector, which was set in coincidence with the projectile detector. The coincidence time contains the time-of-flight information of the recoil ions from the collision region to the detector (the spread in the time-of-flight of the projectiles due to the energy loss is negligible), from which the momentum component in the direction of the extraction field (x-direction) was determined. The y- and z-components of the recoil-ion momentum were extracted from the position information. The momentum resolution was about 0.15 a.u. FWHM for the x- and z-components and, due to the target temperature, 0.35 a.u. FWHM in the y-direction.

The ejected electron momentum was deduced from momentum conservation as $\mathbf{p_e}$ = $\mathbf{q}$ - $\mathbf{p_r}$, where $\mathbf{q}$ is the momentum transfer from the projectile to the target. The FDCS will be presented for electrons ejected with various fixed energies E_e into the scattering plane (spanned by the initial and final projectile momenta) and various fixed projectile scattering angles θ_p as a function of the electron emission angle θ_e. Since $E_e = \varepsilon - I$ (I = 24.6 eV = 0.904 a.u.), the electron energy resolution is the same as the resolution in ε. The angular resolution depends on θ_e itself and ranges from $8°$ in the forward direction to about

12° FWHM in the direction of $\mathbf{q}$, where the so-called binary peak (see Results and Discussion section) is usually observed.

3. THEORY

The data were compared to two different, but conceptually very similar distorted wave calculations. Our continuum distorted wave – eikonal initial state (CDW-EIS) model is a single active electron approach where we assume that in the final state the ejected electron moves in the combined Coulomb field of the incident ion and the residual target core. Partial screening of the active electron-target interaction due to the 'passive' helium electron is modelled by means of a Hartree-Fock scheme. Distortion of the final electronic state by the projectile is represented by a pure Coulomb function, and by an eikonal phase in the entrance channel. In an extension of the CDW-EIS model, the projectile – residual target ion (PT) interaction is accounted for in terms of a pure Coulomb interaction between the projectile and the target core (CDW-EIS-PT model). This interaction is then included in the transition amplitude, by invoking the eikonal approximation, through its multiplication by a phase factor. For more details see [36].

Whereas the CDW-EIS-PT approach is a semi-classical approximation which treats the projectile motion as straight lines, the 3-body distorted wave-eikonal initial state (3DW-EIS) model is a fully quantum mechanical treatment. The incident projectile is treated as a plane wave with an eikonal phase approximating the initial state PT interaction. The final state wave function for the projectile is a Coulomb wave for a net charge of +1, so the final state PT interaction is approximated as the projectile moving in the field of the ion. The

ejected electron wave function is a distorted wave which is a solution of the Schrödinger

equation using a numerical potential whose radial dependence contains the screening of

the nucleus by the electron cloud. For small radii, this potential has a net charge equal to

that of the nucleus. For increasing radii, the net charge reduces to that of the ion for radii

larger than the size of the ion. For a more complete description, see [37] and references

therein.

4. RESULTS AND DISCUSSION

In Figures 1 – 4, we present FDCS for energy losses of $\varepsilon = 62.5$, 65.5, 68.5, and 85

eV (corresponding to electron to projectile speed ratios of 0.965, 1, 1.04, and 1.22,

respectively), and for fixed scattering angles (from top to bottom panels) of $\theta_p = 0.1$, 0.2,

0.3, and 0.5 mrad as a function of the polar electron emission angle θ_e. In each case

electrons ejected into the scattering plane were selected, i.e. the azimuthal electron angle

was fixed at $\varphi_e = 0° \pm 5°$. Here, $\theta_e = 0°$ coincides with the initial projectile beam direction,

$\theta_e = 90°$, with the direction of the transverse component of $\mathbf{q}$, and $\theta_e = 270°$ with the

direction of the transverse component of $-\mathbf{q}$. The direction of $\mathbf{q}$ ($\theta_q = \arctan(q_{tr}/q_z)$) is

indicated by the arrow in each panel.

Qualitatively, the electron angular dependences of the FDCS are quite similar to

those we recently reported for ionization of H_2. For He, too, in most cases a strong forward

peak is observed, which dominates the FDCS at small θ_p (except for $\varepsilon = 85$ eV). This

structure is due to the mutual focusing of the projectile and the electron towards the beam

axis caused by PCI. Furthermore, the binary peak, which is expected near the direction of

q, at small θ_p manifests itself in terms of a "shoulder" on the large angle wing of the forward peak, and with increasing θ_p becomes increasingly visible as a separate peak structure. In a first-order approximation the binary peak can be described as being caused by a single interaction between the projectile and the electron, where the target nucleus remains essentially passive. Momentum conservation then demands that the binary peak occurs exactly in the direction of **q**. However, the binary peak can be shifted by contributions from higher-order mechanisms. More specifically, PCI effects tend to move the binary peak in the forward direction relative to **q** [e.g. 18,19,21,24,30]. Such a shift is also seen in the present data for those cases where the binary peak is resolved from the forward peak. Thus, signatures of strong PCI effects manifest themselves both in the forward and in the binary peak.
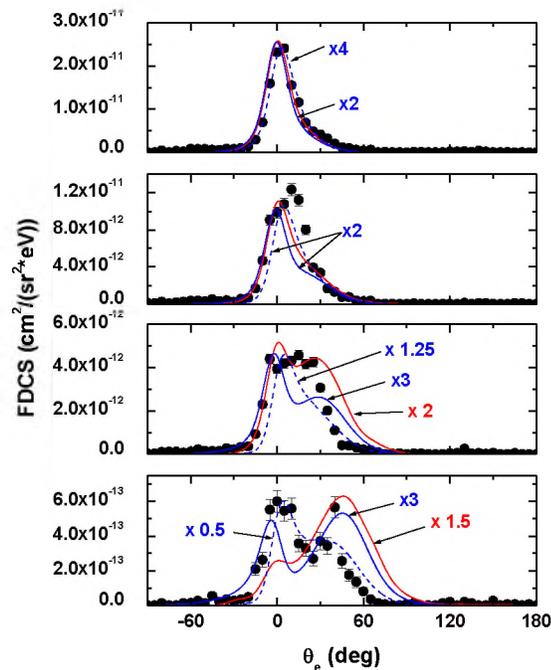
Figure 1. Fully differential cross sections for electrons ejected into the scattering plane for a projectile energy loss of 62.5 eV as a function of electron ejection angle
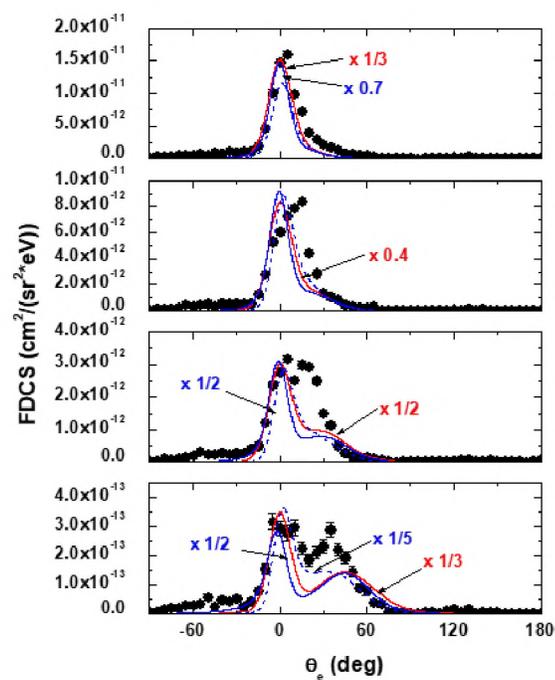
Figure 2. Same as Figure 1 for a projectile energy loss of 65.5 eV
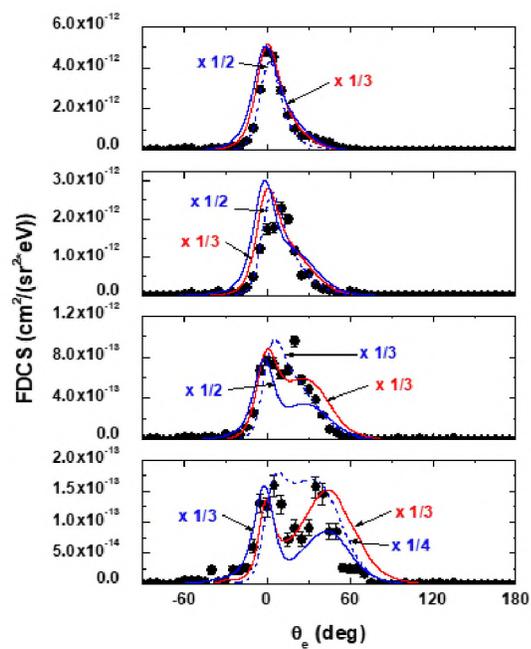
Figure 3. Same as Figure 1 for a projectile energy loss of 68.5 eV
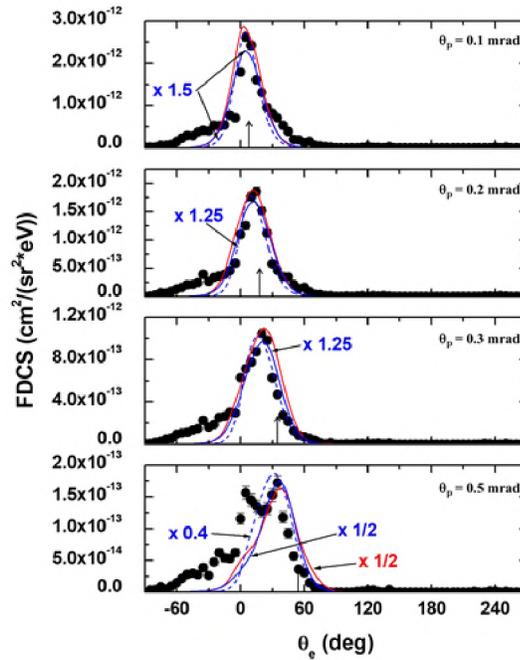
Figure 4. Same as Figure 1 for a projectile energy loss of 85 eV

A surprising behavior is seen in the FDCS for $\varepsilon = 85$ eV. This energy loss corresponds to an electron to projectile speed ratio of $v_e/v_p = 1.22$, which cannot be regarded as falling within the velocity matching regime. Therefore, one would expect the forward peak to be much less important relative to the binary peak than for the smaller energy losses. Indeed, the peak structure observed in the data for $\theta_p = 0.1$ mrad does not occur at $\theta_e = 0^o$, but rather close to the direction of $\mathbf{q}$ ($\theta_q = 10^o$). Here, the forward peak is not resolved from the binary peak so that a quantitative evaluation of the contribution from the forward peak is difficult. Nevertheless, the observation that the peak structure occurs very close to θ_q shows that the binary peak must be dominant. At $\theta_p = 0.2$ mrad the maximum has moved to even larger θ_e, and at 0° the FDCS is further reduced. However, at larger θ_p a sudden increase of the FDCS at 0° (relative to the value at θ_q) is seen. At $\theta_p = 0.3$ mrad

a "shoulder" on the small-angle wing of the maximum is found and at $\theta_p = 0.5$ mrad a peak structure close to $0°$ clearly separated from the binary peak is observed. In fact, at this scattering angle the peak height ratio between the forward and binary peaks is quite similar to the corresponding values for the smaller energy losses. These data suggest that with increasing departure of the ejected electron speed from the projectile speed the relative importance of PCI tends to increase with increasing scattering angle, while for electron speeds equal to the projectile speed, within approximately 5 to 10 %, the opposite trend is observed. A similar conclusion was drawn for electrons well below the velocity matching regime ejected in 16 MeV O^{7+} + He collisions. There, an increasing forward shift of the binary peak with increasing q was found [38]. Later, such a trend was also theoretically predicted for fast proton-helium collisions [39]. However, at present we do not have a conceptual explanation for these trends.

The presence of separate forward and forward-shifted binary peak structures at θ_p = 0.5 mrad may at first glance seem plausible. However, here, we point out that, in a classical picture, it is not straight forward to explain this phenomenon (and a classical explanation may not be possible at all). Both the existence of the forward peak and the forward shift of the binary peak are caused by the same mechanism, namely by the attraction of the ejected electron towards the beam axis by the projectile. In both cases this attraction results in a shift of the corresponding peak relative to the direction of $\mathbf{q}$. The difference is merely of a quantitative nature: In the case of the forward peak this shift is equal to θ_q, while in the case of the binary peak it is only about 20 to 30% of θ_q. This raises the question why a shift of say 50% of θ_q is significantly less likely than a shift of 20 to 30% and 100% of θ_q, i.e. why there is a minimum separating the forward and binary peaks.

A resolution of this apparent dilemma is probably only possible within a quantum-mechanical treatment. There, the minimum can probably be interpreted as destructive interference between different transition amplitudes leading to the same final state.

The dashed blue curves in Figs. 1-4 represent our CDW-EIS calculations, which do not account for the PT interaction. The solid blue curves in Figs. 1-4 represent our CDW-EIS-PT calculations, which do account for the PT interaction [36]. The red curves show our 3DW-EIS calculations, which also account for the PT interaction [37]. As mentioned in the introduction, CDW-EIS-PT and 3DW-EIS are conceptually very similar. The most important difference lies in the treatment of the PT interaction. While the CDW-EIS-PT model assumes straight-line trajectories, in the 3DW-EIS model the PT interaction is treated fully quantum-mechanically.
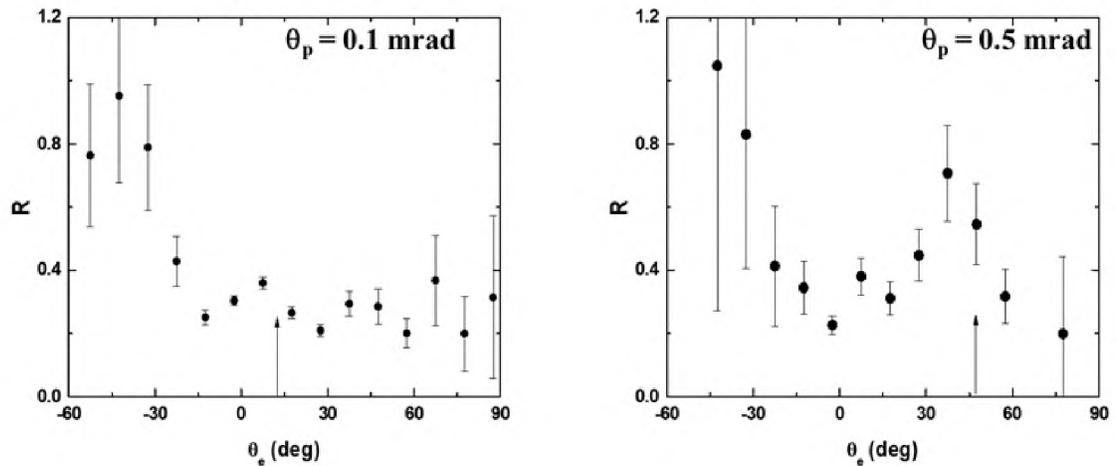
Figure 5. Ratios between the fully differential cross sections for ionization of He and H_2 as a function of the electron ejection angle

The comparison between experiment and theory and between both theoretical models also reveals some similarities to the FDCS reported earlier for ionization of H_2 [24]. For the smallest and the largest energy losses, which are furthest from the electron-projectile velocity matching, and at small θ_p, the 3DW-EIS calculations are in very good agreement with the experimental data. The CDW-EIS-PT calculations also reproduce the qualitative electron angular dependence of the measured FDCS very well, but there are considerable discrepancies in absolute magnitude. However, at large θ_p, especially for the other two energy losses close to the velocity matching, theory does not even reproduce the experimental data qualitatively. Furthermore, in spite of the conceptual similarities the two models differ substantially from each other in this regime. This reconfirms the conclusion, drawn from the fully differential study of ionization of H_2, that the FDCS in the velocity matching regime are particularly sensitive to the details of the few-body dynamics.

One important question is how PCI effects depend on the target ionization potential. By considering the asymptotic case of $I = 0$ one would expect such effects to become increasingly important with increasing I. This scenario is equivalent to the target nucleus not even being present. On the other hand, as mentioned in the introduction, the interaction of the nucleus with either the ejected electron or the scattered projectile plays an essential role in PCI. One could argue that I approaching to zero is not necessarily a signature of a vanishing nuclear charge, but that it can also signify an increasing screening of the nuclear charge by the passive electrons. However, the total unscreened charge of the nuclei is the same for H_2 and He. One would therefore expect the larger screened effective nuclear charge (which to a large extent determines I) of He, to lead to larger PCI effects than in H_2. Instead, measured DDCS as a function of projectile energy loss and scattering angle

seemed to suggest that PCI actually becomes stronger with decreasing *I* [16,27]. On the other hand, as mentioned in the introduction, a follow-up study on DDCS for heavier targets [33] suggested that effects due to PCI could be masked by those due to another higher-order mechanism, involving the PT interaction, but only a single projectile-electron interaction (for simplicity, we refer to this process as the second-order PT process). Therefore, the dependence of PCI effects on *I* could not be conclusively determined from DDCS measurements.
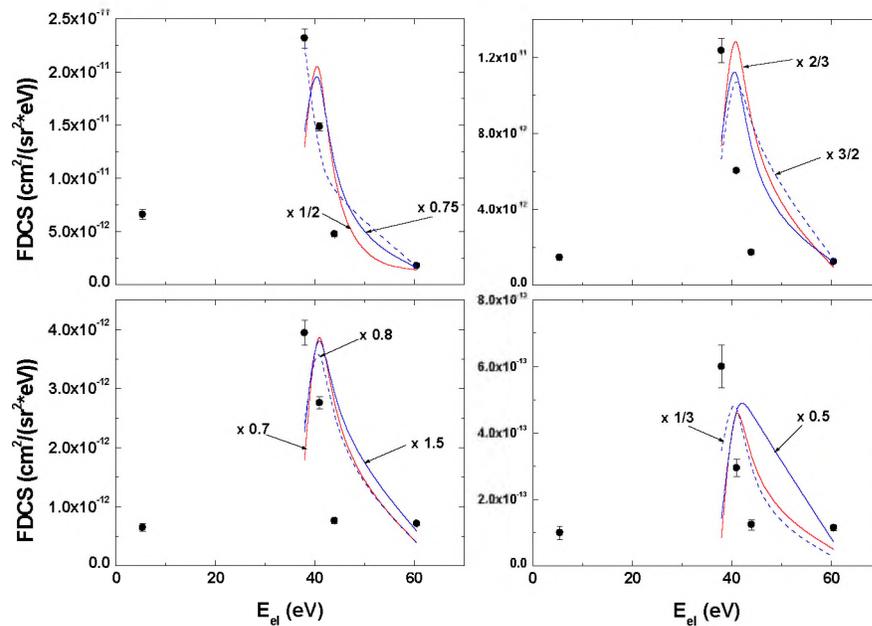
Figure 6. Fully differential cross sections for electrons ejected into the scattering plane for a fixed electron ejection angle of 0° as a function of electron energy

Further insight should be obtainable from the FDCS measurements, especially by analyzing the forward peak. The second-order PT process is not expected to significantly

contribute at $\theta_e = 0^\circ$ because there the last step in PCI, leading to the focusing towards 0°, is missing. Therefore, in contrast to DDCS, PCI effects to a large extent can be separated in the θ_e – dependence of the FDCS from the second-order PT process. Considering the asymptotic case of I approaching 0 one would not only expect PCI to become weaker, but at the same time the binary peak in the FDCS to become stronger and narrower. Therefore, if PCI effects indeed increase with increasing I, the ratio between the FDCS for ionization of He and H_2 should exhibit a strong maximum at $\theta_e = 0^\circ$. These ratios are shown in Figure 5 for electrons emitted with the projectile speed (corresponding to $\varepsilon = 65.5$ eV for He and $\varepsilon = 57$ eV for H_2) and for $\theta_p = 0.1$ mrad (upper panel) and $\theta_p = 0.5$ mrad (lower panel) as a function of θ_e. At $\theta_p = 0.1$ mrad the ratios are essentially flat for $\theta_e > -30^\circ$. At $\theta_p = 0.5$ mrad, there appears to be a weak structure near $\theta_e = 45^\circ$, which is close to the direction of $\mathbf{q}$. Therefore, if there is any statistically significant departure from a flat dependence of R on θ_e at all it would indicate a preference of the binary peak, rather than the forward peak, at larger I.

Apart from the forward peak in the electron angular distribution another prominent signature of PCI is a strong peak structure, the so-called cusp peak, in the electron energy spectrum at $E_e \approx \frac{1}{2} v_p^2$ (in a.u.) for θ_e fixed at 0° [e.g. 10,25,26]. If very small θ_p in addition to $\theta_e = 0^\circ$ are selected one would expect the cusp peak to become even more pronounced. In Figure 6 the FDCS for $\theta_e = 0^\circ$ and for the same θ_p as in Figs. 1 – 4 (from upper left to lower right) are plotted as a function of E_e. Two remarkable features are seen in this Figure: first, from the data the exact location of the cusp peak cannot be determined because of a large gap in the data between 5 and 38 eV, nevertheless it is clear that it occurs very close
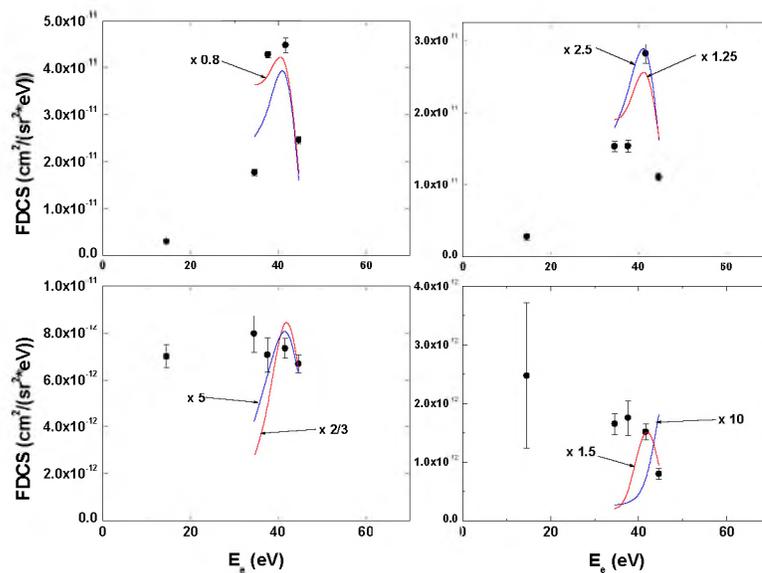
Figure 7. Same as Figure 6 for H_2 target; data and calculations from [24]
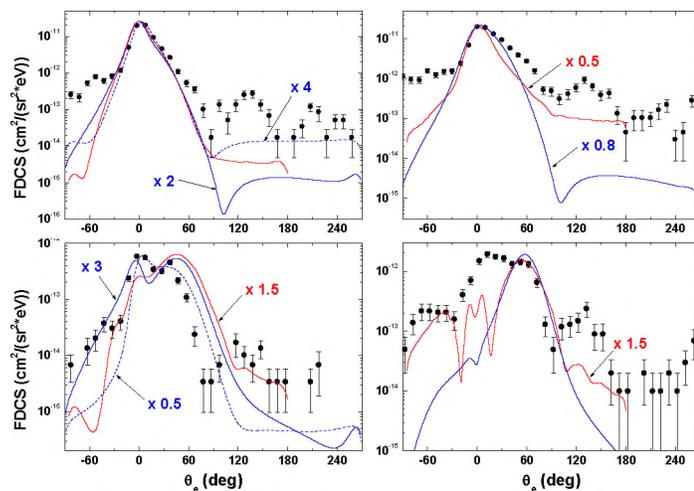
Figure 8. Fully differential cross sections for electrons ejected from He (left panels) and H_2 (right panels) into the scattering plane for a projectile energy loss of 62.5 eV (He target) and 50 eV (H_2 target) as a function of the electron ejection angle

to, but slightly below $E_e = \frac{1}{2} v_p^2$ (indicated by the arrows). Second, a very steep high-energy wing of the cusp peak can even be seen at the largest scattering angle of 0.5 mrad. For comparison, in Figure 7 the corresponding data are shown for ionization of H_2. There, the cusp peak occurs exactly at $\frac{1}{2} v_p^2$ and it is only seen at the two smaller θ_p.

Both models accounting for the PT interaction predict the cusp peak very close to $E_e = \frac{1}{2} v_p^2$ for both targets (except for the CDW-EIS-PT calculations at the largest scattering angle). However, interestingly the CDW-EIS calculation (not accounting for the PT interaction) agrees rather well with the experimental data for the He target at $\theta_p = 0.1$ mrad. Furthermore, at $\theta_p = 0.5$ mrad the cusp peak is shifted to smaller E_e compared to the CDW-EIS-PT calculation. This can be taken as a hint that the shift of the cusp peak is characteristic to the V_{pe}-V_{te}-V_{pe} interaction sequence. If this is indeed the case one would have to conclude that near the cusp energy PCI proceeds mostly through the V_{pe}-V_{te}-V_{pe} sequence and that the V_{pe}-V_{pt}-V_{pe} sequence is overestimated in the CDW-EIS-PT and 3DW-EIS models. Indications for such an overestimation were also found in the FDCS for ionization of H_2 [24] and in the DDCS for ionization of Ne and Ar [33].

The presence of a strong cusp peak even at large θ_p for He, but not for H_2, shows that the dependence of PCI effects on I changes with scattering angle. At small θ_p neither the electron angular distribution nor the electron energy dependence of the FDCS give any indication of an increasing role of PCI with increasing I, while at large θ_p PCI is clearly much more important for He than it is for H_2. In contrast, the CDW-EIS-PT and 3DW-EIS calculations yield strong cusp peaks for the H_2 target even at $\theta_p = 0.3$ mrad and the 3DW-EIS calculation also at $\theta_p = 0.5$ mrad. Furthermore, both calculations exhibit large differences to each other, especially at the largest θ_p. Therefore, the energy dependence of

the FDCS, too, illustrates the high sensitivity of the cross sections to the few-body dynamics.

The ratios between the FDCS for ionization of He and H_2 plotted in Figure 5 show a significant increase at negative electron emission angles. This suggests that apart from the forward and binary peaks additional structures may be present in the FDCS. To investigate this possibility further, we present the FDCS in Figure 8 on a logarithmic scale for He at $\varepsilon = 62.5$ eV (left panels) and for H_2 at $\varepsilon = 50$ eV (right panels). The scattering angle was fixed at $\theta_p = 0.1$ mrad (top panels) and $\theta_p = 0.5$ mrad (bottom panels). In order to reduce the statistical error bars, here the bin size in the electron angle was increased by a factor of two. Indeed, especially at $\theta_p = 0.1$ mrad, a shoulder on the small-angle wing of the forward peak is visible for both targets. In addition, maxima are found near $\theta_e = 135°$ and, in the case of the He target for $\theta_p = 0.1$ mrad, a weak peak near $\theta_e = 210°$. The latter structure is not observed for larger θ_p and for the H_2 target at any θ_p.

The location of the structure around $\theta_e = 210°$ coincides quite well with the direction of $-\mathbf{q}$ ($\theta_{-q} \approx 195°$), where in a first-order treatment the recoil peak is expected. It is due to a direct hit between the projectile and the electron followed by a backscattering of the electron by its parent nucleus at 180°. Just like the binary peak, the recoil peak, too, is usually forward-shifted relative to $-\mathbf{q}$ by PCI so that the location of the maximum in the data at 210° is consistent with the recoil peak. Furthermore, the absence of this structure for H_2 and at large θ_p is in accord with the expectation that the importance of the recoil peak (relative to the binary peak) decreases with increasing θ_p and decreasing I.

A structure at electron angles between 0 and -90° was also observed for ionization of He leading to $\varepsilon = 30$ eV [19]. It was interpreted within a classical picture as a two-step process, involving the PT interaction, in which the projectile passes the target atom between the nucleus and the active electron [40]. The interaction of the projectile with the electron leads to a forward component of the longitudinal momentum transfer. The interaction with the nucleus, in contrast, only transfers momentum in the transverse direction (because the inelasticity in this interaction is practically zero). This interaction is on average stronger than the projectile-electron interaction so that the direction of the total transverse momentum transfer is opposite to the transverse electron momentum. This combination of a positive longitudinal and a negative transverse (relative to **q**) electron momentum leads to an angle between 0 and -90°. The electrons emitted in this region were labelled "swing by electrons" [40].

In contrast to the recoil peak and swing by electron "shoulder", a structure analogous to the one found in the present data around $\theta_e \approx 135°$ was never observed in previous FDCS measurements, which were all performed for electron energies well below the velocity matching regime. It seems plausible to attempt to understand the origin of this peak by comparing to theoretical models. However, the sensitivity of the FDCS to the details of the few-body dynamics, which is normally regarded as a benefit, could become a problem if it is too high and if the primary goal is to identify the mechanism leading to a specific feature in the data. In this case, it can be very difficult to identify any systematic trend in the agreement (or lack thereof) with the data depending on the theoretical description of certain physical effects. This is illustrated in the following comparison

between the data and the CDW-EIS-PT and 3DW-EIS models in the region of the structures which are too small to be visible on a linear scale.

Overall, the agreement between experiment and theory outside the regions of the forward and binary peaks is not good. On the other hand, there is an element of qualitative agreement in so far as under certain kinematic conditions one or both theoretical models show the features seen in the data approximately in the same region. For example, at θ_p = 0.1 mrad the CDW-EIS-PT calculations shows a minimum at about $\theta_e = 100°$ for both targets, which in the experimental data separates the binary peak (not resolved from the forward peak) from the structure around 135°. Furthermore, in the 3DW-EIS calculations a maximum can be seen in the region of the swing by electrons, which is even in reasonably good quantitative agreement with the data at θ_p = 0.5 mrad in the case of the H_2 target. Furthermore, some structures are visible in the same calculation in the region of the maximum around 135°. However, given the large overall discrepancies it is not clear how significant this qualitative agreement is. Furthermore, it is difficult to discern a systematic pattern under which condition a particular model reproduces the data better or worse than the others. For example, in the swing by electron region at θ_p = 0.5 mrad the 3DW-EIS model reproduces the data for the H_2 fairly well, while the CDW-EIS-PT model is in poor agreement. But for the He target the roles are reversed and the CDW-EIS-PT model reproduces the data much better than the 3DW-EIS model. At θ_p = 0.1 mrad both models are in poor agreement with the data for both targets. Furthermore, it is difficult to evaluate the role of the PT interaction. Comparing the CDW-EIS, CDW-EIS-PT, and 3DW-EIS calculations to the data for the He target at θ_p = 0.5 mrad, one might be tempted to conclude that the 135^0 structure is caused by a mechanism involving the PT interaction because both

models including this interaction are significantly closer to the experimental data. But at $\theta_p = 0.1$ mrad for the same target, the CDW-EIS results are in much better agreement.

The discussion above suggests that identifying the mechanisms underlying the various structures in the FDCS requires having theoretical models which yield better overall agreement with the experimental data. Both approaches presented here are perturbative distorted wave methods, for which the range of validity is crudely given by the condition $Q_p/v_p^2 \ll 1$ [41], which is marginally satisfied for the collision system studied here ($Q_p/v_p^2 = 0.33$). A perhaps even bigger problem is that the capture channel is not included. This channel is expected to have a particularly large effect on FDCS for ionization in the velocity matching regime because of the energetic proximity of the final electron continuum state to the bound states in the projectile. In spite of these constraints the CDW-EIS-PT and 3DW-EIS models were quite successful in reproducing experimental data for electron energies well below the velocity matching regime [19,32]. The present data show the limitations of perturbative approaches and demonstrate that calculating FDCS for electrons in the cusp peak is one of the biggest remaining challenges in advancing our understanding of the few-body dynamics underlying ionization.

Non-perturbative approaches for ion impact are much more challenging to implement than for electron impact, because the much larger projectile mass means that a much larger number of angular momentum states have to be considered for the scattered projectiles. Nevertheless, in recent years such models were developed to describe ionization by ion impact [e.g. 30,42,43]. They use basis sets including projectile states so that the capture channel is accounted for. Two of these models [30,42] were used to calculate DDCS and one [30] to calculate FDCS for ionization of atomic hydrogen. There,

the FDCS at the matching velocity look qualitatively quite similar to the present data for ionization of He. Furthermore, the DDCS are in good agreement with experimental data [27,44]. More recently, one model [42] was applied to calculate FDCS for ionization of He for electron energies well below the velocity matching regime [45]. Improved agreement with the experimental data, compared to perturbative approaches, was achieved. These are promising indicators that comparison of measured FDCS in the velocity matching regime to non-perturbative calculations will result in a major advancement in the understanding of the few-body dynamics underlying ionization

5. CONCLUSIONS

We have measured and calculated fully differential cross sections (FDCS) for ionization of helium by 75 keV proton impact for electrons ejected with a speed close to the projectile speed. Apart from the binary peak, occurring near the direction of the momentum transfer $\mathbf{q}$, which usually dominates the FDCS for relatively small electron energies, we also observe a strong peak structure in the forward direction. This forward peak is a manifestation of a higher-order process, known as post-collision interaction (PCI), which involves two (or more) interactions between the projectile and the active electron and an additional interaction of the target nucleus with either the projectile or the electron.

The data were compared to those previously published for ionization of H_2. In the electron angle dependence of the FDCS for fixed projectile scattering angle and electron energy we did not find any signatures suggesting that PCI was more important for one target than for the other. However, in the electron energy dependence of the FDCS for an

electron ejection angle fixed at $\theta_e = 0$ and projectile scattering angles fixed at large values, PCI leads to a much more pronounced cusp peak for He than it does for H_2. This trend is not reproduced by theory.

While for small electron energies perturbative distorted wave approaches often yield satisfactory agreement with experimental data, major discrepancies are found in the present data taken in the velocity matching regime. Furthermore, two conceptually very similar versions of such distorted wave approaches differ significantly from each other. This confirms a very high sensitivity of the FDCS to the details of the underlying few-body dynamics in the velocity matching regime found earlier for ionization of H_2. In fact, the level of sensitivity is so high that it actually turns into a detriment: the resulting discrepancies among different theories and with experimental data seem to lack any systematic pattern that could be used to track the physics underlying the observed features in the FDCS or which is missing (or not sufficiently accounted for) in theory.

A further complication for perturbative methods is presented by the sensitivity of FDCS to the projectile coherence properties [46,47]. Along with the other constraints discussed in this article this suggests that a time-dependent, non-perturbative calculation, using a large two-center basis set and describing the projectiles by a wave packet with a width reflecting the coherence length, would have a high potential for providing important insight into the understanding of the measured FDCS even in the velocity matching regime.

ACKNOWLEDGEMENTS

REFERENCES

[1] M.E. Rudd, Y.-K. Kim, D.H. Madison, and J.W. Gallagher, Rev. Mod. Phys. 57, No. 4, 965 (1985)

[2] N. Stolterfoht, R.D. DuBois, R.D. Rivarola, Electron Emission in Heavy Ion-Atom Collisions, Springer Verlag, Heidelberg (1997)

[3] M.E. Rudd, Y.-K. Kim, D.H. Madison, and T.J. Gay, Rev. Mod. Phys. 64, No. 2, 441 (1992)

[4] M. Schulz and D.H. Madison, International Journal of Modern Physics A 21, 3649 (2006)

[5] M.E. Rudd and T. Jorgensen, Phys. Rev. 131, 666 (1963)

[6] V.V. Afrosimov, Yu. A. Mamaev, M.N. Panov, and V. Uroshevich, Zh. Tekh. Fiz. 37, 717 (1967)

[7] J.T. Park, J.E. Aldag, J.M. George, J.L. Peacher, and J.H. McGuire, Phys. Rev. A 15, 508 (1977)

[8] M.B. Shah and H.B. Gilbody, J. Phys. B 14, 2361 (1981)

[9] M.E. Rudd, R.D. Dubois, L.H. Toburen, C.A. Ratcliffe, and T.V. Goffe, Phys. Rev. A 28, 3244 (1983)

[10] G.B. Crooks and M.E. Rudd, Phys. Rev. Lett. 25, 1599 (1970)

[11] D.H. Lee, P. Richard, T.J.M. Zouros, J.M. Sanders, J.L. Shinpaugh, and H. Hidmi, Phys. Rev. A 41, 4816 (1990)

[12] L.C. Tribedi, P. Richard, D. Ling, Y. D. Wang, C. D. Lin, R. Moshammer, G. W. Kerby, M. W. Gealy, and M. E. Rudd, Phys. Rev. A 54, 2154 (1996)

[13] R. Schuch, H. Schöne, P.D. Miller, H.F. Krause, P.F. Dittner, S. Datz, and R.E. Olson, Phys. Rev. Lett. 60, 925 (1988)

[14] H. Schöne, R. Schuch, S. Datz, M. Schulz, P.F. Dittner, J.P. Giese, Q.C. Kessel, H.F. Krause, P.D. Miller, and C.R. Vane, Phys. Rev. A 51, 324 (1995)

[15] E. Y. Kamber, C. L. Cocke, S. Cheng, and S. L. Varghese, Phys. Rev. Lett. 60, 2026 (1988)

[16] T. Vajnai, A.D. Gaus, J.A. Brand, W. Htwe, D.H. Madison, R.E. Olson, J.L. Peacher, and M. Schulz, Phys. Rev. Lett. 74, 3588 (1995)

[17] M. Schulz, R. Moshammer, D. Fischer, H. Kollmus, D.H. Madison, S. Jones, and J. Ullrich, Nature 422, 48 (2003)

[18] D. Fischer, R. Moshammer, M. Schulz, A. Voitkiv, and J. Ullrich, J. Phys. B 36, 3555 (2003)

[19] N.V. Maydanyuk, A. Hasan, M. Foster, B. Tooke, E. Nanni, D.H. Madison, and M. Schulz, Phys. Rev. Lett. 94, 243201 (2005)

[20] H. Gassert, O. Chuluunbaatar, M. Waitz, F. Trinter, H.-K. Kim, T. Bauer, A. Laucke, Ch. Müller, J. Voigtsberger, M. Weller, J. Rist, M. Pitzer, S. Zeller, T. Jahnke, L. Ph. H. Schmidt, J. B. Williams, S. A. Zaytsev, A. A. Bulychev, K. A. Kouzakov, H. Schmidt-Böcking, R. Dörner, Yu. V. Popov, and M. S. Schöffler, Phys. Rev. Lett. 116, 073201 (2016)

[21] O. Chuluunbaatar, K.A. Kouzakov, S.A. Zaytsev, A.S. Zaytsev, V.L. Shablov, Yu.V. Popov, H. Gassert, M. Waitz, H.-K. Kim, T. Bauer, A. Laucke, C. Müller, J. Voigtsberger, M. Weller, J. Rist, K. Pahl, M. Honig, M. Pitzer, S. Zeller, T. Jahnke, L.Ph.H. Schmidt, H. Schmidt-Böcking, R. Dörner, and M.S. Schöffler, Phys. Rev. A 99, 062711 (2019)

[22] R. Dörner, V. Mergel, O. Jagutzski, L. Spielberger, J. Ullrich, R. Moshammer, and H. Schmidt-Böcking, Phys. Rep. 330, 95 (2000)

[23] J. Ullrich, R. Moshammer, A. Dorn, R. Dörner, L. Schmidt, and H. Schmidt-Böcking, Rep. Prog. Phys. 66, 1463 (2003)

[24] M. Dhital, S. Bastola, A. Silvus, A. Hasan, B.R. Lamichhane, E. Ali, M.F. Ciappina, R.A. Lomsadze, D. Cikota, B. Boggs, D.H. Madison, and M. Schulz, Phys. Rev. A 99, 062710 (2019)

[25] L. Sarkadi, J. Palinkas, A. Köver, D. Berenyi, and T. Vajnai, Phys. Rev. Lett. 62, 527 (1989)

[26] L.C. Tribedi, P. Richard, W. Dehaven, L. Gulyás, M.W. Gealy, M.E. Rudd, Phys. Rev. A 58, 3619 (1998)

[27] M. Schulz, A.C. Laforge, K.N. Egodapitiya, J.S. Alexander, A. Hasan, M.F. Ciappina, A.C. Roy, R. Dey, A. Samolov, and A.L. Godunov, Phys. Rev. A 81, 052705 (2010)

[28] L. Sarkadi, L. Gulyas, and L. Lugosi, Phys. Rev. A 65, 052715 (2002)

[29] U. Chowdhury, M. Schulz, and D. H. Madison, Phys. Rev. A 83, 032712 (2011)

[30] H.R.J. Walters and C.T. Whelan, Phys Rev. A 92, 062712 (2015)

[31] A. Hasan, S. Sharma, T.P. Arthanayaka, B.R. Lamichhane, J. Remolina, S. Akula, D.H. Madison, and M. Schulz, J. Phys. B 47, 215201 (2014)

[32] M.F. Ciappina, C.A. Tachino, R.D. Rivarola, S. Sharma, and M, Schulz, J. Phys. B 48, 115204 (2015)

[33] A. Silvus, M. Dhital, S. Bastola, J. Buxton, Z. Klok, E. Ali, M.F. Ciappina, B. Boggs, D. Cikota, D.H. Madison, and M. Schulz, J. Phys. B 52, 125202 (2019)

[34] M. Schulz, in "Advances in Atomic, Molecular, and Optical Physics", Vol. 66, 508-543, edited by E. Arimondo, C.C. Lin, and S. Yelin, Elsevier (2017)

[35] A.D. Gaus, W. Htwe, J.A. Brand, T.J. Gay, and M. Schulz, Rev. Sci. Instrum. 65, 3739 (1994)

[36] M.F. Ciappina, W.R. Cravero and M. Schulz, J. Phys. B 40, 2577 (2007)

[37] M. Foster, J. L. Peacher, M. Schulz, A. Hasan, and D. H. Madison, Phs. Rev. A 72, 062708 (2005)

[38] M. Schulz, B. Najjari, A.B. Voitkiv, K. Schneider, X. Wang, A.C. Laforge, R. Hubele, J. Goullon, N. Ferreira, A. Kelkar, M. Grieser, R. Moshammer, J. Ullrich, and D. Fischer, Phys. Rev. A 88, 022704 (2013)

[39]   O. Chuluunbaatar, S.A. Zaytsev, K.A. Kouzakov, A. Galstyan, V.L. Shablov, and Yu.V. Popov, Phys. Rev. A 96, 042716 (2017)

[40]   J. Fiol and R. E. Olson, J. Phys. B 35, 1759 (2002)

[41]   D.S.F. Crothers and J.F. McCann, J. Phys. B 16, 3229 (1983)

[42]   I.B. Abdurakhmanov, J.J. Bailey, A.S. Kadyrov, and I. Bray, Phys. Rev. A 97, 032707 (2018)

[43]   M.S. Pindzola, J. Colgan, Robicheaux, T.G. Lee, M.F. Ciappina, M. Foster, J.A. Ludlow, S.A. Abdel-Naby, Ad. At. Mol. Opt. Phys. 65, 291 (2016)

[44]   A.C. Laforge, K.N. Egodapitiya, J.S. Alexander, A. Hasan, M.F. Ciappina, M.A. Khakoo, and M. Schulz, Phys. Rev. Lett. 103, 053201 (2009)

[45]   S.U. Alladustov, I.B. Abdurakhmanov, A.S. Kadyrov, I. Bray, and K. Bartschat, J. of Physics Conf. Proc., in press (2019)

[46]   K.N. Egodapitiya, S. Sharma, A. Hasan, A.C. Laforge, D.H. Madison, R. Moshammer, and M. Schulz, Phys. Rev. Lett. 106, 153202 (2011)

[47]   L. Nagy, F. Jarai-Szabo, S. Borbely, T. Arthanayaka, B.R. Lamichhane, A. Hasan and M. Schulz, in "Interdisciplinary Research on Particle Collisions and Quantitative Spectroscopy", Dz. Belkic (editor), World Scientific Publishing, Singapore, in press (2019)Bucki, L. (2013). *Microsoft Word 2013 bible* (4th ed.). Indianapolis, Ind: John Wiley & Sons, Inc.

III. EJECTED-ELECTRON-ENERGY AND ANGULAR DEPENDENCE OF FULLY DIFFERENTIAL IONIZATION CROSS SECTIONS IN MEDIUM-VELOCITY PROTON COLLISIONS WITH He AND H2

M. Dhital[1], S. Bastola[1], A. Silvus[1], J. Davis[1], B.R. Lamichhane[1], E. Ali[2], M.F. Ciappina[3,4], R.A. Lomsadze[5], A. Hasan[6], D.H. Madison[1], and M. Schulz[1]

[1]Dept. of Physics and LAMOR, Missouri University of Science & Technology, Rolla, MO 65409

[2]Dept. of Natural Sciences, Northwest Missouri State University, Maryville, MO 64468

[3]ICFO-Institut de Ciencies Fotoniques, The Barcelona Institute of Science and Technology, 08860 Castelldefels, Barcelona, Spain

[4]Institute of Physics of the ASCR, ELI-Beamlines, 182 21 Prague, Czech Republic

[5]Tbilisi State University, Tbilisi 0179, Georgia

[6]Dept. of Physics, UAE University, P.O. Box 15551, Al Ain, Abu Dhabi, UAE

ABSTRACT

We have measured fully momentum-analyzed recoiling target ions and scattered projectiles, produced in ionization of He and H_2 by 75 keV proton impact, in coincidence. The momentum of the ejected electrons was deduced from momentum conservation. From the data we extracted fully differential ionization cross sections as a function of the polar electron emission angle (for fixed electron energies) and as a function of the electron energy (for fixed electron emission angles). Comparison between experiment and various distorted wave calculations confirms that under kinematic conditions where the post-collision interaction plays an important role, the few-body dynamics underlying the ionization process are still poorly understood.

1. INTRODUCTION

One of the most important goals of research in atomic physics is to advance our understanding of the few-body dynamics in simple systems (e.g., [1,2]). Theoretically, this is a problem, which cannot be solved analytically for more than two mutually interacting particles even if the underlying forces are precisely known. Therefore, sophisticated numer- ical methods need to be developed. The assumptions and approximations entering in these models need to be tested by detailed experimental data. The most sensitive tests of theory are offered by experiments, in which the complete kinematic information of every single particle in the system (kinemati- cally complete experiments) is obtained (for reviews see, e.g., [3-7]).

One process that has attracted particularly strong interest is ionization of simple atoms or molecules by charged particle impact. In the case of electron projectiles, the first kinematically complete experiment was performed already some 50 years ago [8]. Since then, a rich literature on mea- sured fully differential cross sections (FDCS) has emerged covering just about every kinematic configuration conceivable (e.g., [9–19]). Initially, ionization by electron impact was a particularly suitable test case to develop theoretical models. There, the collision system consists of two light particles (the projectile electron and the active target electron) and only one heavy particle (the residual target ion including the passive electrons), where the heavy particle is practically identical with the center of mass of the system. Under such circum- stances, the scattered projectiles can be accurately described in terms of just a few angular momentum states, which is a favorable condition for nonperturbative approaches. Indeed, numerous such methods have been developed over

the last two decades and good agreement with measured FDCS for ionization of simple targets is routinely achieved (e.g., [2,19– 22]).

For ion impact, fully differential studies of ionization, both experimental and theoretical, are much more challenging. Experimentally, the difficulty is that the large projectile mass results in typical scattering angles of only a fraction of a mrad (for fast heavy ions a fraction of a μrad). Furthermore, the projectile energy loss is usually only a tiny fraction of the initial energy, especially for fast heavy ions. As a result, kine- matically complete experiments on ionization by ion impact directly momentum analyzing the projectiles (along with the recoil ions) so far have only been performed for 75 keV proton impact (e.g., [7,23–27]). For heavier and faster ions FDCS were measured by momentum analyzing the recoil ions and the ejected electrons in coincidence and deducing the projec- tile momentum transfer from the kinematic conservation laws (e.g., [1,7,28–35]).

Theoretically, the challenges to nonperturbative ap- proaches also stem from the much larger projectile masses in case of ion-impact compared to electron collisions. As a result, an enormous number of angular momentum states has to be considered to accurately describe the scattered projectiles. Nevertheless, several nonperturbative methods on ionization have been developed in recent years [36–39]. How- ever, comparison of FDCS calculated with these approaches with experimental data is still rather limited and the agreement is not as satisfactory as it is for electron impact [37,38]. Research on ion-atom collisions thus still has to rely to a large extent on perturbative models.

One major limitation with the recoil-electron coincidence technique is that fast ejected electrons cannot be measured with sufficiently large effective solid angle. Slow electrons can be confined to the solid angle subtended by the detector by a combination of

the electric extraction field and a magnetic field. However, to accomplish this for fast electrons both fields would have to be so large that they would significantly compromise the momentum resolution for both the recoil-ions and the electrons. As a result, FDCS for ionization measured using the recoil-electron coincidence technique so far have only been obtained for electron speeds much smaller than the projectile speed.

Using the scattered projectile-recoil coincidence technique for moderate-energy light-ion impact, it was possible to cover a larger kinematic regime. In the first kinematically complete experiment performed with this method FDCS were obtained for an electron energy around 5 eV [23]. However, later, FDCS were measured for electron speeds close to the pro- jectile speed corresponding to an energy of 40.8 eV, known as the cusp energy (note that in projectile energy loss the cusp energy differs for different targets) [26,27]. For small electron energy the agreement between experiment and perturbative calculations was not very good, but qualitatively satisfactory (e.g., [23,24]). In contrast, near the cusp energy, major discrepancies between experiment and theory were found, especially at large scattering angles [26,27]. Moreover, two conceptually very similar perturbative models did not even qualitatively agree with each other. In this kinematic regime, the collision dynamics are believed to be dominated by a higher-order mechanism known as post-collision interaction (PCI). Apart from the primary interaction lifting the electron to the continuum, it involves a second projectile-electron in- teraction in the outgoing part of the collision, where they attract each other towards the initial projectile beam axis. The observations of [23,24,26,27] suggest that the kinematic regime around the cusp energy represents a severe limitation to perturbative methods in accurately describing the few-body dynamics. However, so far FDCS were only measured for a few electron

energies very close to the cusp energy and for only one energy well below the cusp energy. In between, and at energies well above the cusp energy, fully differential data are lacking. Therefore, systematic conclusions regarding the limitations of perturbative approaches cannot be reached yet. In this article, we present measured and calculated FDCS for an extended kinematic regime, filling the gap between a very small ejected electron energy and the cusp energy region. The data confirm the severe difficulties of perturbative approaches accurately describing FDCS in the region where PCI is dominant. However, they also demonstrate that, even in regimes where PCI was not expected to be dominant, perturbative approaches do not always lead to accurate results either.

2. EXPERIMENT

The experiment was performed at the medium-energy ion accelerator of the Missouri University of Science and Tech- nology (S&T). Protons were generated with a hot cathode ion source and extracted with an energy of 5 keV. They were then further accelerated to 75 keV by a high-voltage platform. Af- ter passing through a pair of collimating slits, the proton beam intersected with very cold target beams (He and H_2) froma su- personic jet (T=1–2 K in the direction of expansion, a frac- tion of 1 K in the plane perpendicular to the expansion). The collimating slits had a width of 150 μm and were placed at a distance of 50 cm from the target region. This slit geometry corresponds to a transverse coherence length of about 3.3 a.u. [40,41]. This is larger than the internuclear separation in H_2 (1.4 a.u.) and larger than the impact parameter range mostly contributing to ionization. Therefore, the coherence requirement for observable

interference is satisfied for molecular two-center as well as for single-center interference [42]. How- ever, it should be noted that a theoretical study demonstrated that even at this relatively large coherence length, the FDCS change very sensitively with the coherence length and the projectiles therefore cannot be regarded as fully coherent [43]. After the collision, the projectiles were charge-state an- alyzed by a switching magnet. The beam component that did not charge exchange was decelerated by 70 keV, energy analyzed by an electrostatic parallel-plate analyzer [44], and detected by a two-dimensional position sensitive multichannel plate (MCP) detector. The analyzer slits were oriented in the horizontal direction (x direction) and had a width of 75 μm, resulting in an energy resolution of 2.5 eV full width at half maximum (FWHM), and a length of about 2.5 cm. Since the direction of dispersion of the analyzer is in the y direction, the narrow-slit width means that only one energy loss (i.e., only one ejected electron energy) could be recorded at a time, i.e., for each energy loss a separate experiment was performed. From the energy, the longitudinal projectile momentum com- ponent was determined with a resolution of 0.03 a.u. The x component was obtained from the position information with a resolution of 0.35 a.u. Due to the narrow analyzer slits, the y component was kept fixed at 0 within the resolution of about 0.1 a.u. FWHM.

The recoiling target ions were extracted with a weak elec- tric field of about 6 V/cm in the x direction, momentum analyzed by a COLTRIMS (cold target recoil-ion momentum spectroscopy) apparatus and detected by another position- sensitive MCP detector. The recoil-ion and projectile detectors were set in coincidence. From the time of flight of the re- coil ions from the collision to the detector, contained in the coincidence time, the x component of the recoil momentum was obtained with a resolution of 0.1 a.u. FWHM. The

other two components were deduced from the recoil position in- formation. In the z direction, defined by the initial projectile beam direction, the resolution was 0.12 a.u. FWHM. In the y direction, the resolution (0.35 a.u. FWHM) is limited by the temperature of the target gas in the direction of the expansion. The electron momentum is determined through momentum conservation through the relation $\mathbf{k} = \mathbf{q}\text{-}\mathbf{p}_{rec}$, where $\mathbf{q}$ is the momentum transfer from the projectile to the target and it is the negative of the momentum change vector of the projectile. FDCS were obtained for electrons ejected into the scattering plane spanned by $\mathbf{q}$ and the initial projectile momentum $\mathbf{K}_i$, which in our coordinate system is the xz plane. For fixed projectile scattering angle θ_p the FDCS were analyzed as a function of projectile energy loss ε (or equivalently electronenergy $E_{el} = \varepsilon - I$, where I is the target ionization potential) for fixed polar electron ejection angles θ_{el} (measured relative to the projectile beam axis) and as a function of θ_{el} for fixed ε. The y component of the electron momentum is only needed to select the scattering plane; however, it does not enter in the determination of θ_{el}. Therefore, the resolution in θ_{el} is nearly unaffected by the resolution in the y components of the measured momenta, which is worse than for the other two components.

In the case of the He target, FDCS were measured for en- ergy losses corresponding to $E_{el} = \varepsilon - I = 15.4, 25.4, 32.4,$ and 35.4 eV, where I is the ionization potential of the ground state of He, and analyzed together with previously published data for E_{el} 5.4, 37.9, 40.9, 43.9, and 60.4 eV [27]. Here, E_{el} 40.7 eV corresponds to the cusp energy. For the H_2 target new data were obtained for $E_{el} = 24.6$ and 54.6 eV in addition to previously published data for $E_{el} = 14.6, 34.6, 37.6, 41.6,$ and 44.6 eV [26]. The FDCS were put on an abso- lute scale by integrating them over the electron solid angle and normalizing for each energy

loss to double differential cross sections in projectile solid angle and electron energy, which were measured previously for He [45] and H_2 [46].

In the case of the He target, ionization plus excitation of the second electron could contribute to the data. The threshold for this process in ε is 65.2 eV so that it cannot contribute   to the data for ε up to 62.5 eV (E_{el} 37.9 eV). Due to the proximity to the threshold, the cross section for ionization excitation at ε 65.5 eV is entirely negligible compared to single ionization. For the larger energy losses (68.5 and 85 eV or E_{el} 43.9 and 60.4 eV) the contributions from this process are only significant for θ_p much larger than 0.5 mrad. In the angular range for which we present data here, these contributions do not exceed 5% relative to single ionization and become smaller with decreasing θ_p. In the case of the H_2 target, ionization-excitation results in dissociation of the molecule and thus cannot contribute at all to true coincidences with the recoiling H2+ ions.

3. THEORY

Calculations were carried out for He and H_2 using CDW- EIS (continuum distorted-wave eikonal initial-state) and 3DW-EIS (three-body distorted-wave eikonal initial-state) theories as base models. First, we consider ionization of He using the CDW-EIS method. We treat helium single ionization as a single active electron process and assume that in the final state the ejected electron moves in the combined Coulomb field of both the incident ion and the residual target core. Partial screening of the active electron-target interactiondue to the "passive" bound helium electron is modeled by effective charges as considered within the usual prior CDW-EIS approach (see below for more details).

In the center-of-mass (CM) frame, fully differential cross sections (FDCS) as a function of the energy and ejection angle of the electron, and direction of the outgoing projectile, can be written as

$$\frac{d^3\sigma}{dE_{el}d\Omega_{el}\,d\Omega_k} = N_e(2\pi)^4\mu^2 k\frac{K_f}{K_i}|T_{fi}|^2\,\delta(E_f - E_i), \tag{1}$$

where Ne is the number of electrons in the atomic shell, μ is the reduced mass of the projectile-target subsystem, K_i (K_f) is the magnitude of the initial (final) projectile momentum, and E_i (E_f) is the total initial (final) energy of the system in the CM frame. The ejected electron's energy is given by $E_{el} = k^2/2$, where k is the magnitude of the electron momentum. The solid angles Ω_K and Ω_{el} represent the direction of scattering of the projectile and the ionized electron, respectively. The projectile solid angle $d\Omega_K = \sin\theta_K d\theta_K d\varphi_K$ can be expressed in terms of the transversal component magnitude of the momentum transfer $q_\perp$ via the relationship $q_\perp \approx K_i \sin\theta_K \approx K_i\,\theta_K$ and $K_i \approx K_f$, fulfilled for heavy ions projectiles and small scattering angles. Finally, let us note that the projectile momentum transfer $\mathbf{q} = (\mathbf{q}\perp, q_z) = \mathbf{K}_i - \mathbf{K}_f$, where $\mathbf{K}_i$ ($\mathbf{K}_f$) is the initial (final) momentum of the incoming particle. In our context $\mathbf{q}\perp \cdot \bar{\upsilon} = 0$, where $\bar{\upsilon}$ is a unit vector that defines the direction of the projectile velocity vector $\mathbf{v}$ and $q_z = \varepsilon/v$.

Let us note that when differential cross sections depend on the projectile scattering angle, for example, the interaction between the projectile and the residual target ion (dubbed PT interaction) may play an important role and is therefore considered in our theoretical analysis. On the other hand, when differential cross sections are functions only of the electron energy and/or angular coordinates, this interaction is not included since their influence in the transition amplitude is reduced to a complex phase factor that gives no

contribution to the cross sections values (for details see, e.g., [47,48]). Invoking the eikonal approximation, the PT interaction can be included in the transition amplitude $A_{if}(\rho)$ as a phase factor, which for a pure Coulomb PT interaction yield

$$A_{if}(\rho) = i(\rho v)^{2iv} A_{if}(\rho) \qquad (2)$$

with $v = Z_P Z_T / v$, Z_P, and Z_T being the projectile and residual-target ion charges, respectively, and where ρ defines the impact parameter ($\rho \cdot v = 0$). We consider the PT interaction as a pure Coulomb one between a projectile with charge Z_P and the "bare" target core charge, $Z_T = 1$. Other values for Z_T have been used, to partially account for the screening of the remaining bound electron. However, this choice has little influence on the calculated FDCS. $A_{if}(\rho)$ $(A'_{if}(\rho))$ is the transition amplitude with (without) the PT interaction. Using a two-dimensional Fourier transform it is possible to find a relation between $A_{if}(\rho)$ and $T^{(-)}_{fi}(\mathbf{q}\perp)$, i.e., the transition matrices as a function of the impact parameter ρ or the transverse component of the momentum transfer $\mathbf{q}\perp$. Consequently, the transition matrices with and without the PT interaction can be written as

$$T_{fi}'^{(-)}(\mathbf{q}\perp) = \frac{1}{2\pi} \int d\rho \, e^{i\mathbf{q}\perp \cdot \rho} A'_{if}(\rho), \qquad (3)$$

$$T_{fi}^{(-)}(\mathbf{q}\perp) = \frac{iv^{2iv}}{2\pi} \int d\rho \, \rho^{2iv} e^{i\mathbf{q}\perp \cdot \rho} \rho A'_{if}(\rho), \qquad (4)$$

respectively. Applying the inverse Fourier transform in Eq. (3) and replacing $A_{if}(\rho)$ in Eq. (4), results in

$$T_{fi}^{(-)}(\mathbf{q}\perp) = \frac{iv^{2iv}}{(2\pi)^2} \int d\mathbf{q}'_\perp \, T_{fi}^{(-)}(\mathbf{q}\perp) \int d\rho \, \rho^{2iv} e^{i(\mathbf{q}\perp - \mathbf{q'}\perp) \cdot \rho} \rho A'_{if}(\rho), \qquad (5)$$

The two-dimensional integral over the impact parameter can be done analytically to finally obtain [49,50]

$$T_{fi}^{(-)}(\mathbf{q}\perp) = \frac{iv^{2iv}(2\pi)^{-iv}}{2^4\pi^3} \int d\mathbf{q}'_\perp \, T'^{(-)}_{fi}(\mathbf{q}'_\perp) \, | \mathbf{q}\perp - \mathbf{q}'_\perp |^{-2(1+iv)} \qquad (6)$$

The last multidimensional integral in Eq. (6) is evaluated numerically using quadratures. As is well known, the eikonal approximation is valid as long as (i) the projectile suffers very small deflections in the collision (the so-called straight line approximation) and (ii) the velocity of the recoil ion remains small compared to that of the emitted electron. In the present work we only consider scattering angles of up to 0.5 mrad so that condition (i) is fulfilled. Additionally, because of the large recoil-ion to electron mass ratio, condition (ii) is satisfied as well.

In the computation of the transition amplitude $T^{(-)}{}_{fi}$ $(\mathbf{q}\perp)$, we use nonorthogonal Jacobi coordinates $(\mathbf{r}_P, \mathbf{r}_T)$ to describe the ionization process [51]. These coordinates represent the position of the active electron with respect to the incoming projectile $(\mathbf{r}P)$ and the target ion $(\mathbf{r}_T)$, respectively. $\mathbf{R}_T$ is also considered, representing the position of the heavy projectile with respect to the center of mass (CM) of the electron-target subsystem. If we neglect terms of orders $1/M_T$ and $1/M_P$, where M_T and M_P are the masses of the target ion nucleus and incident heavy ion, respectively, we can write $\mathbf{R}_T \approx \mathbf{r}_T - \mathbf{r}_P$. Within the prior CDW-EIS model, the transition amplitude can then be computed as

$$T_{fi}{}^{(-)} (\mathbf{q}\perp) = <\chi_f^{-CDW} \mid W_i \mid \chi_i^{-EIS} >, \tag{7}$$

where the initial (final) state distorted wave $\chi+i$ $(\chi-f)$ is an approximation to the initial (final) state satisfying outgoingwave (+) (incoming-wave (−)) asymptotic conditions. For the initial state the asymptotic form of the Coulomb distortion, the so-called eikonal phase, is used in the electron-projectile interaction together with a semianalytical Rothan-Hartree-Fock description for the initial bound-state wave function [52]:

$$\chi_i^{-EIS} = (2\pi)^{-3/2}\exp (i\mathbf{K}_i \cdot \mathbf{R}_T)\ \psi_{RHF} (\mathbf{r}_T)\ \mathcal{E}^+{}_v (\mathbf{r}_P), \tag{8}$$

where $\mathcal{E}^+_v(\mathbf{r_P})$ is

$$\mathcal{E}^+_v(\mathbf{r_P}) = \exp\left[-i\frac{Z_P}{v}\ln(vr_P - \mathbf{v} \cdot \mathbf{r_P})\right], \tag{9}$$

and $\psi_{RHF}(\mathbf{r_T})$

$$\psi_{RHF}(\mathbf{r_T}) = \sum_{i=0}^{5} x^k a^{n-k} N_i e^{-\zeta_{ir}T} \tag{10}$$

The normalization factors N_i and effective charges ζ_i are obtained from Ref. [52].

The final-state wave function is cast into the form

$$\chi_f^{-CDW} = (2\pi)^{-3/2}\exp(i\mathbf{K_f} \cdot \mathbf{R_T})\chi_T^-(\mathbf{r_T})C_{Pe}^-(\mathbf{r_P}), \tag{11}$$

where $C_{Pe}^-(\mathbf{r_P})$ represents the Coulomb distortion of the ejected electron wave function due

to the projectile, i.e.,

$$C_{Pe}^-(\mathbf{r_P}) = N(v_P)\ {}_1F_1(-i\ v_P, 1, ik_P r_P - ik_P.r_P) \tag{12}$$

$v_P = Z_P/k_P$ is the Sommerfeld parameter, $\mathbf{k}_P$ is the relative momentum of the electron-

projectile subsystem, and $N(v_P)$ the Coulomb factor, defined as

$$N(v_P) = \Gamma(1 - iv_P)\exp(\pi v_P/2) \tag{13}$$

Additionally, the wave function of the ejected electron in the field of the target

residual ion $\chi_T^-(\mathbf{r}_T)$ can be written as

$$\chi_T^-(\mathbf{r_T}) = (2\pi)^{-3/2}\exp(i\mathbf{K_T} \cdot \mathbf{r_T})N(v_T)\ {}_1F_1(-i\ v_T, 1, ik_T r_T - ik_T.r_T) \tag{14}$$

Here, $v_T = Z_{eff}/k_T$, $\mathbf{k}_T$ and Z_{eff} being the relative momentum and the effective charge of the

electron-target subsystem, respectively, and $N(v_T)$ the Coulomb factor, defined now as

$$N(v_T) = \Gamma(1 - iv_T)\exp(\pi v_T/2) \tag{15}$$

We use a variational calculated $Z_{eff} = 1.6875$ for the final ion state, to partially account the

influence of the remaining passive electron [53]. Small variations in the FDCS can be

observed for other values of Z_{eff}. Finally, the perturbation potential W_i in Eq. (7) is defined by

$$(H_i - E_i) \chi_i^+ = W_i \chi_i^+, \tag{16}$$

where H_i is the full electronic initial Hamiltonian, neglecting the total CM motion. Particularly, W_i is composed of two differential operators [54], i.e.,

$$W_i = \frac{1}{2} \nabla_{rp}^2 - \nabla_{rP} \cdot \nabla_{rT}, \tag{17}$$

The details on extending the CDW-EIS approach to the H2 molecule were reported in [55]. Here, we only summarize the main differences to the treatment of the He target. The molecular transition amplitude $T^{(-)}{}_{fi}$ ($\mathbf{q}\perp$, $\mathbf{R}$) can be written as

$$|T_{fi}{}^{(-)} (\mathbf{q}\perp, R)|^2 = 2\{1+\cos [P_{rec}.R]\} \, ||^2 \, |T_{fi}{}^{eff(-)} (\mathbf{q}\perp)|^2 \tag{18}$$

where $\mathbf{p}_{rec} = \mathbf{q} - \mathbf{k}$ and $\mathbf{R}$ is the vector that identifies the relative position of the nuclei in the molecule.

In Eq. (18) $T^{eff(-)}{}_{fi}$ ($\mathbf{q}\perp$) is the CDW-EIS transition amplitude corresponding to effective atomic centers located at the position of each H atom. The pure ionization of the H2 molecule is modeled using an equilibrium distance $R = 1.4$ a.u. and the initial electronic state in each center is given by a hydrogenic function with a variational charge $Z = 1.19$ and the corresponding normalization factor N_i $(R) = 0.5459$. For the final electronic state, continuum wave functions centered on each target nucleus are used with an effective charge $Z_{eff} = \sqrt{(2\varepsilon_i)}$, being $\varepsilon_i = 0.566$ a.u. being the H2 binding energy.

An average over all the molecular orientations should be performed in Eq. (18) for the case of randomly oriented molecules. Consequently, we obtain the molecular transition amplitude $T^{(-)}{}_{fi}$ ($\mathbf{q}\perp$, $\mathbf{R}$) as

$$|T_{fi}^{(-)} (\mathbf{q}\perp, R)|^2 = 2 \{1+\frac{sin\chi}{\chi}\} |T_{fi}^{eff(-)} (\mathbf{q}\perp)|^2 \tag{19}$$

where $T^{eff, (-)}_{fi} (\mathbf{q}\perp)$ is the same atomic transition amplitude as in the case of oriented

molecules and $\chi = p_{rec}R$. The H_2 FDCS can then be computed by inserting the molecular

transition amplitude $T^{(-)}_{fi} (\mathbf{q}\perp, \mathbf{R})$ [Eq (19)] in Eq. (1). The PT interaction is included in

the same way as in the case of the He atom. In both the He atom and H2 molecule cases,

when comparing with the experimental data, we use CDW-EIS-PT (CDW-EIS) to label the

calculations with (without) the PT interaction included.

The 3DW-EIS is a fully quantum mechanical model which is described in Refs.

[56,57], and here we provide only a short overview to show the similarities and differences

with the CDW-EIS. Using the two-potential formulation, Foster *et al.* [56] showed that an

exact transition matrix T_{fi} for Eq. (1) can be written as

$$T_{fi} = <\chi_f^-| V_i | \beta_i> + <\chi_f^-| W_i^f | \psi_i^+ - \beta_i> \tag{20}$$

where χ_f^- is an approximate final-state wave function, W^+_f is the final-state perturbation,

ψ^+_i is the exact initial-state wave function that must be approximated, and β_i is the

asymptotic initial-state wave function, defined by

$$\beta_i = \Phi_{pw}^+(K_i, R_T) \psi_t(r_T), \tag{21}$$

where $\varphi^+_{PW} (\mathbf{K}_i, \mathbf{R}_T)$ is a plane wave for the incident proton and $\psi_t (\mathbf{r}_T)$ is the bound-state

wave function for the target. For helium, this wave function is approximated as an

analytical fit to the Hartree-Fock (HF) ground state wave function of helium [58] and, for

the H2 molecule, as the Dyson molecular orbital for the active electron $\psi_t (\mathbf{r}_T) = \varphi^{Dy}_{1s}$

[59,60]. The final-state wave function χ_f^- is cast into the form

$$\chi_f^- = \Phi_{pw}^-(K_f, R_T) C_{PT}^-(R_T) \Phi_{DW}^-(k, r_T) C_{Pe}^-(r_P) \tag{22}$$

Here the factor $\varphi_{PW}(\mathbf{K}_f, \mathbf{R}_T)C_{PT}(\mathbf{R}_T)$ is a Coulomb wave for the scattered proton in the field of the target ion which is composed of a plane wave times the Coulomb distortion factor $C_{PT}(\mathbf{R}_T)$ for a target charge of $+1$, $\varphi_{DW}(\mathbf{k}, \mathbf{r}_T)$ is a distorted wave for the ejected electron in the field of the target, and $C_{Pe}(\mathbf{r}_P)$ is the Coulomb distortion factor for the interaction between the ejected electron and the proton. Compared to the final-state wave function for the CDW-EIS of Eq. (11), it is seen that the CDW-EIS approximates the final-state projectile wave function as a plane wave while the 3DW-EIS approximates this wave function as a Coulomb wave; the ejected electron wave function in the CDW is a Coulomb wave for an effective charge while it is a distorted wave in the 3DW; and the final-state ejected-electron-proton interaction is the same in both cases (with the exception of some approximations made in the CDW approach which should be valid for this case).

The exact scattering wave function ψ^+_i in the entrance channel can be approximated by the eikonal initial state (EIS) introduced by Crothers and McCann [61], which is composed of the asymptotic initial-state wave function β_i times the eikonal phase which approximates the long range Coulomb initial-state interaction between the projectile and the target. We thus can write

$$\psi_i^+ = \beta_i \, \mathcal{E}_v^+(r_p, R_T), \tag{23}$$

where $\mathcal{E}_v^+ (r_p, R_T)$ is

$$\mathcal{E}_v^+(r_p, R_T) = \exp[\, i\frac{Z_p}{v} \ln\left(\frac{vR_T - v.R_T}{vr_p - v.r_p}\right)] \tag{24}$$

Comparing Eq. (23) with Eq. (8), it is seen that the CDW-EIS contains the asymptotic form of the proton-electron interaction only while the 3DW-EIS has this interaction plus the asymptotic form of the projectile-nucleus interaction as well. Different

approximations are made for the initial bound state wave function as well, but this is probably not important.

In summary, the primary differences between the CDWEIS and 3DW-EIS are (1) for the initial state, the CDW contains the asymptotic form of the initial state interaction between the projectile and target active electron while the 3DW has this interaction plus the asymptotic interaction with the target ion; (2) for the final state, the CDW approximates the final-state projectile wave function as a plane wave while the 3DW approximates this wave function as a Coulomb wave; and (3) for the final state, the ejected electron wave function in the CDWis a Coulomb wave while it is a distorted wave in the 3DW. From a numerical viewpoint, the biggest difference between the two calculations is the way in which the T matrix is evaluated. The CDW-EIS makes a straight-line approximation for the projectile which allows the integrals over the projectile coordinates to be evaluated analytically. The 3DW-EIS is a fully quantum mechanical calculation that makes no additional approximations, which means that a full six-dimensional (6D) integral over all projectile and electron coordinates must be performed for each fully differential cross section calculation.With the straight-line approximation made in the CDW-EIS, the PT interaction becomes an overall phase factor which can be factored out of the scattering amplitude, while in the 3DW-EIS this interaction is embedded in the 6D T-matrix integral and does not factor out of the integral.

4. RESULTS AND DISCUSSION

Amet venenatis urna cursus eget nunc. In the θ_{el} dependence of the FDCS in the velocity-matching region, which we published previously, we observed a double peak structure for large θ_p [27]. The second peak, at larger E_{el}, known as the binary peak, occurs close to the direction of $\mathbf{q}$. Qualitatively, it can be viewed as a manifestation of first- order contributions, although, especially at small projectile velocities, higher-order contributions need to be considered for an accurate quantitative description. The first peak located near $\theta_{el} = 0°$, to which we refer as the forward peak, is a manifestation of PCI and it is dominated by higher-order contributions. At small θ_p, $\mathbf{q}$ moves closer to θ_{el} 0° and the FDCS are dominated by the forward peak. As a result, only a single peak near θ_{el} 0° was observed. Since PCI is believed to maximize at the velocity matching, it was expected that the forward peak would be most pronounced at the cusp energy (E_{el} 40.8 eV). Instead, for the He target it was found to keep increasing going from E_{el} 40.9 to 37.9 eV (while for the H_2 target it maximized exactly at the cusp energy). However, it was not clear at which electron energy the forward peak max- imizes because at that time no data were available between E_{el} 5.4 and 37.9 eV. We therefore start our analysis of the new data by discussing the θ_{el} dependence of the FDCS for $E_{el}= 35.4\,\text{eV}$.

These data are plotted in Figure 1 for the He target as a function of θel for fixed θp of (from top to bottom) 0.1, 0.2, 0.3, and 0.5 mrad. Qualitatively, the data look very similar to those for $E el = 37.9$ eV. Here, too, at large θp partly resolved forward and binary peaks are visible and at the smallest θp the FDCS are dominated by the forward peak. Another similarity is that the ratio between the FDCS at $\theta el = 0°$ and in the direction of $\mathbf{q}$ minimizes

somewhere between $\theta p = 0.2$ and 0.3 mrad, suggesting that the relative importance of PCI minimizes in this angular range. These θp correspond to a magnitude of $\mathbf{q}$ of about 1.4 to 1.6 a.u. A similar effect was observed earlier in the FDCS for ionization of He by fast heavy ion impact: there, a shift of the binary peak in the forward direction relative to $\mathbf{q}$, caused by PCI, also minimized at similar q [32]. In contrast, for Eel = 15.4 eV the FDCS, shown for the same θp in Figure 2, exhibit a rather different dependence on θel; here, the forward peak is completely absent, as expected, and the data maximize, except for $\theta p = 0.5$ mrad, near the direction of $\mathbf{q}$.

The comparison of the FDCS for Eel = 15.4, 35.4, and 37.9 eV demonstrates that PCI is much less prominent well below the velocity matching and that it plays a similarly important role for Eel = 35.4 and 37.9 eV. However, it does not provide quantitative information as to where exactly the FDCS for θel = 0° maximize. To address this question, in Figure 3 we plot the FDCS for θel fixed at 0° as a function of Eel for fixed θp as indicated by the insets. In all cases, a very sharp peak structure, with a width of about 5 eV FWHM, is observed at around E_{el} = 38 eV, i.e., it is shifted relative to the cusp energy by about 2 to 3 eV. A second, smaller and broader, maximum appears to be present near E_{el} = 15 eV. Although this is manifested by only one data point, it is nevertheless significant as it occurs systematically for all θ_p, except for 0.5 mrad, where no data are available for $E_{el} < 15$ eV.

The blue curves in Figures 1–3 represent the continuum distorted-wave eikonal initial-state (CDW-EIS) calculations with (CDW-EIS-PT, solid curves) and without the PT interaction (CDW-EIS, dashed curves). The red curves show the three-body distorted-wave eikonal initial-state (3DW-EIS) calculations, which also account for the PT interaction. We
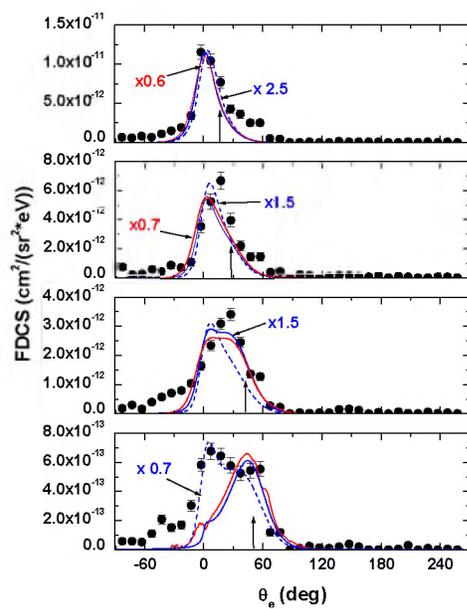
Figure 1. Fully differential cross sections for electrons ejected from He into the scattering plane for an electron energy of 35.4 eV as a function of electron ejection angle
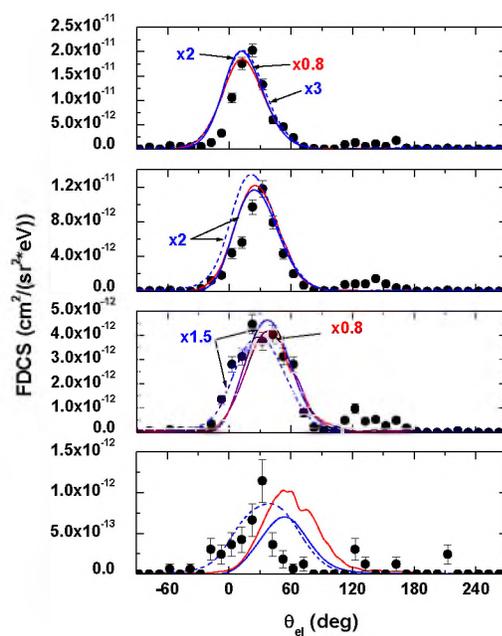
Figure 2. Same as Figure 1, but the electron energy is fixed at 15.4 eV
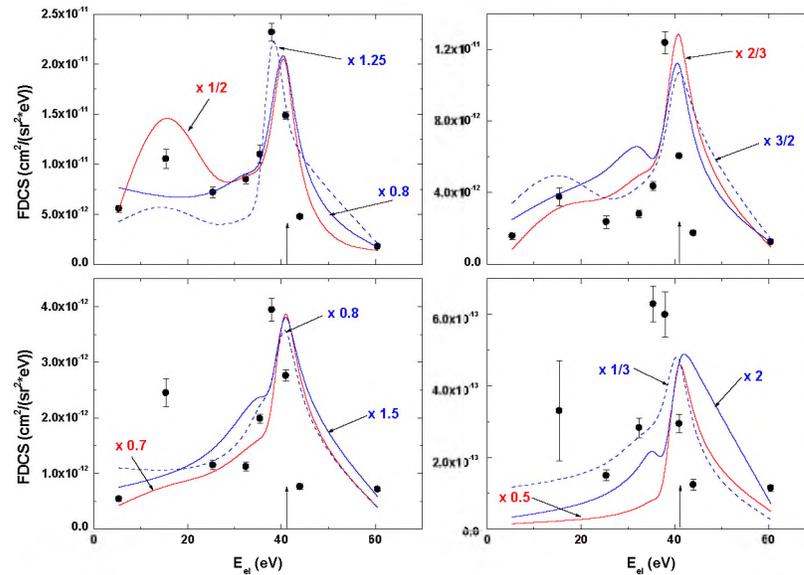
Figure 3. Fully differential cross sections for electrons ejected from He in the forward direction ($\theta_{el} = 0°$) as a function of the electron energy

emphasize that the 3DW-EIS and CDW-EIS-PT models are conceptually very similar and should essentially catch the same physics of the collision process.

The comparison between experiment and theory for the θ_{el} dependence of the FDCS at $E_{el} = 35.4$ eV is quite similar to what we reported previously for other electron energies in the velocity-matching regime: for the smallest θ_p all calculations reproduce the shape of the θel dependence very well. Only in magnitude are there some discrepancies in the CDW-EIS results and to a lesser extent in the 3DW-EIS results. However, with increasing θ_p the disagreement with the experimental data grows larger and the various theoretical models increasingly differ from each other. Surprisingly, the CDW-EIS calculation, which conceptually is the "least complete" model, yields by far the best agreement with the measured FDCS for $\theta p = 0.5$ mrad. For $E el = 15.4$ eV, on the other hand, in the shape of

the θel dependence of the FDCS the agreement between theory and experiment is satisfactory up to θp = 0.3 mrad. Furthermore, for these θp the 3DW-EIS model even reproduces the magnitude of the measured FDCS within less than 20%. In contrast, the agreement of all calculations with the data at θp = 0.5 mrad is rather poor. Here again, the CDW-EIS model gives overall significantly better results than the calculations including the PT interaction. This comparison between theory and experiment near the matching velocity (Eel = 35.4 eV) and well below the matching velocity (Eel = 15.4 eV) reinforces our earlier conclusion that kinematic regions, for which PCI is very strong, are outside the regime of validity of distorted-wave approaches.

In the energy dependence of the FDCS for θel fixed at 0°, shown in Figure 3, the agreement between experiment and theory is mixed. All calculations reproduce a very sharp cusp peak in the velocity-matching regime. However, both calculations including the PT interaction do not reproduce the shift of the centroid of 2 to 3 eV to smaller energies seen in the data. On the other hand, the CDW-EIS model reproduces the cusp peak in the experimental data at θp = 0.1 mrad almost perfectly. At θp = 0.5 mrad, the cusp peak in this calculation is also shifted, but only by 1 eV. At the other two scattering angles the CDW-EIS results exhibit a similar shape and location of the cusp peak as the calculations including the PT interaction. At present, we cannot offer any explanation for this shift observed in the data and in the CDW-EIS calculations.

The smaller peak structure seen in the experimental data at about 15 eV is qualitatively reproduced by the CDW-EIS and the 3DW-EIS calculations. However, the former model underestimates its height (relative to the cusp peak) and the latter overestimates it for θp = 0.1 mrad, while these trends are reversed for θp = 0.2 mrad.

Interestingly, in the CDWEIS approach this maximum is completely removed by the inclusion of the PT interaction. An additional structure is seen in the CDW-EIS-PT calculation at about Eel = 30 eV at all θp, except for 0.1 mrad, which is present neither in the experimental data nor in the other two calculations.

It should be noted that fixing θel at 0° in the energy dependence of the FDCS is about as selective on a strong role of PCI as fixing Eel near the cusp energy in the angular dependence of the FDCS. Indeed, in the energy dependence for θel = 0° the discrepancies between theory and experiment are similarly severe as in the angular dependence of the FDCS, especially at large θp. In addition, conceptually very similar theoretical models yield qualitatively different results. Once again, these observations reinforce our earlier conclusion [27] that kinematic regimes for which PCI plays an important role are particularly challenging to distorted wave approaches. One might expect the agreement between experiment and theory to be significantly improved in the energy dependence of the FDCS for θel fixed at a value closer to the direction of $\mathbf{q}$. This is closer to the region of the binary peak and one might expect PCI effects to be rather insignificant.

In Figure 4, such data are shown for θel = 30° for the same θp as in Figure 3. For θp = 0.1 and 0.2 mrad, indeed the cusp peak has nearly completely disappeared, signifying a strongly reduced role of PCI. Furthermore, the agreement between theory and experiment at θp = 0.1 mrad is significantly improved compared to θel = 0° and the various calculations do not differ as much from each other, at least up to the cusp peak region. However, for θp > 0.2 mrad, an increasingly pronounced cusp peak emerges, which shows that there the FDCS are substantially affected by PCI. At first glance, this may look like a surprising observation because in double differential energy spectra (i.e., FDCS integrated over all

projectile solid angles) the cusp peak tends to disappear rapidly for θel larger than just a few degrees (e.g., [62–64]). However, it should be noted that the presence of a cusp peak at large θp in the data of Figure 4 is not in conflict with the double differential electron spectra. The integral of the FDCS over the projectile solid angle is dominated by θ_p smaller than 0.2 mrad so that the cusp peak observed at larger θp is not visible in the double differential cross sections (DDCS). On the other hand, even if the DDCS are further integrated over all electron solid angles, a weak "shoulder structure" near the cusp energy, of similar shape to that seen in Figure 4 for $\theta p = 0.1$ and 0.2 mrad, is found in the resulting single differential energy-loss spectrum (see also [65]). Furthermore, strong PCI effects for θel significantly larger than 0° are also routinely observed for fast highly charged ion impact, where they manifest themselves by a forward shift of the binary peak relative to **q** (see, e.g., [28,29,32]).

The experimental data of Figure 4 are to some extent qualitatively reproduced by theory insofar as in some cases the calculations also exhibit a cusp peak. Furthermore, the 3DWEIS model correctly predicts that the cusp peak becomes increasingly pronounced with increasing θp. However, the height of the cusp peak is systematically underestimated. In contrast, the CDW-EIS-PT model only shows a clear cusp peak at $\theta p = 0.5$ mrad and generally tends to be in worse agreement with the data than the 3DW-EIS results. Furthermore, the inclusion of the PT interaction in this model does not lead to a systematic improvement in the agreement with the data. In fact, the shape of the cusp peak at $\theta p = 0.5$ mrad is better reproduced by the CDW-EIS model.
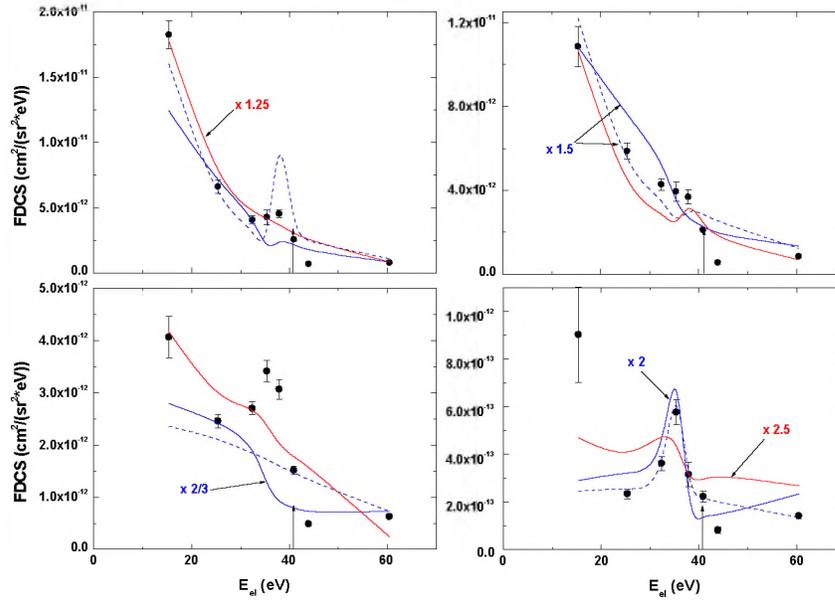
Figure 4. Fully differential cross sections for electrons ejected from He into the scattering plane at a fixed ejection angle of θel = 30∘ as a function of the electron energy

Furthermore, this latter calculation shows a rather pronounced cusp peak at θp = 0.1 mrad, while in the CDW-EISPT results a small minimum is seen near the cusp energy. Two different interaction sequences (in a classical description) have been identified as mostly contributing to PCI [26,27,66,67]. Both start with the primary projectile-electron interaction, lifting the electron to the continuum, and both end with a second projectile-electron interaction, leading to both particles attracting each other towards the projectile beam axis. In between, either the electron (Vep-Vet-Vep sequence) or the projectile (Vep-Vpt-Vep sequence) is redirected by an interaction with the residual-target ion. The pronounced cusp peak in the CDW-EIS calculation at θp = 0.1 mrad shows that the Vep-Vet-Vep sequence plays an important role in PCI at small θp. However, the fact that the

inclusion of the PT interaction in this model results in a minimum strongly suggests that the other sequence is very important as well. The minimum can probably only be explained by destructive interference (e.g., between both sequences). The absence of a minimum in the experimental data suggests that the Vep-Vpt-Vep sequence is overestimated in the CDW-EIS-PT approach. Better agreement with the data in the cusp region is achieved with the 3DW-EIS model.

The behavior of the CDW-EIS calculations, with or without PT interaction, is somewhat erratic. For example, going from $\theta p = 0.3$ to 0.5 mrad the energy dependence of the FDCS in the cusp region rapidly changes from a smooth decline (CDWEIS) or a step (CDW-EIS-PT) to a pronounced peak structure. This is consistent with the presence of strong interference effects, which tend to be quite sensitive to kinematic parameters, such as the scattering angle, determining the phase angle. It is also consistent with the sensitivity of the FDCS to the projectile coherence length found in theoretical calculations [43].

The important observations in the measured FDCS for ionization of He and in the comparison with theory can be summarized as follows: first, there are large discrepancies between experiment and theory and large differences between conceptually very similar models under kinematic conditions where PCI plays an important role. Second, the inclusion of the PT interaction does not lead to significant overall improved agreement with the measured data. In fact, for several kinematic settings the best agreement is achieved with the model not including the PT interaction. Third, PCI can be rather strong at relatively large electron ejection angles. Finally, in some cases the theoretical calculations exhibit a somewhat erratic behavior, which we take as an indication for strong interference effects.
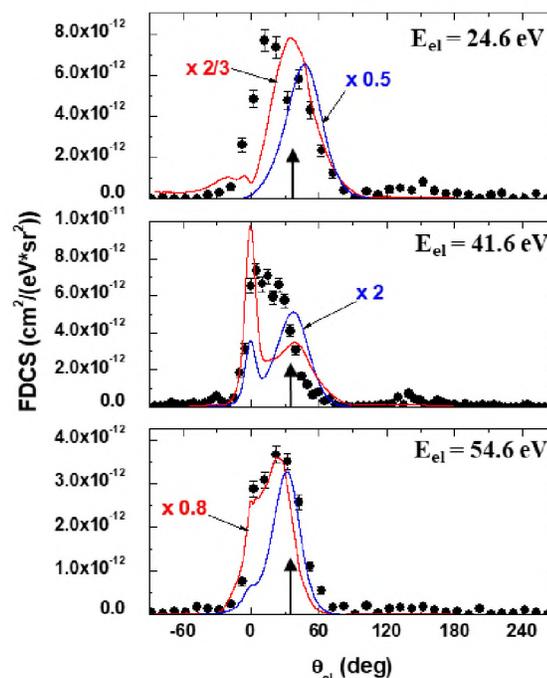
Figure 5. Fully differential cross sections for electrons ejected from H_2 into the scattering plane for a fixed projectile scattering angle of 0.325 mrad and for electron energies as indicated, as a function of electron ejection angle

In Figure 5 we compare the angular dependence of the FDCS for ionization of H2 for an electron energy below the velocity match (top panel, Eel = 14.6 eV or $v$el$/vp$ = 0.77), nearly at the velocity match (center panel, Eel = 41.6 eV or $v$el$/vp$ = 1.01), and above the velocity match (bottom panel, Eel = 54.6 eV or $v$el$/vp$ = 1.16). In all cases, θp is fixed at 0.325 mrad. The curves represent the same calculations as in Figs. 1–4. Like for the He target, here too, the discrepancies between experiment and theory and between the theoretical models are particularly large at the cusp energy. However, one important difference is that for H2 even well outside the velocity-matching regime the discrepancies between the CDW-EIS-PT calculations and the experimental data are quite severe. The

3DW-EIS approach yields significantly better agreement in this kinematic region, but it is nevertheless somewhat worse than for He.
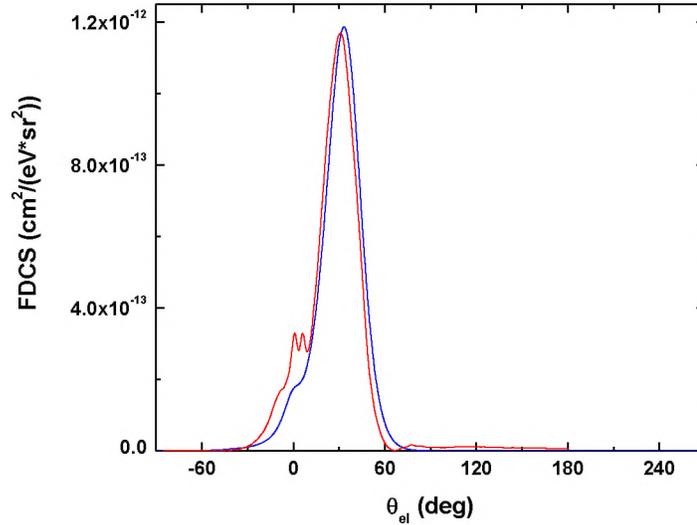
Figure 6. Calculated fully differential cross sections for electrons ejected from atomic H into the scattering plane for projectile scattering angle of 0.325mrad and electron energy of 54.6 eV as a function of electron ejection angle

One important difference between H2 and He is the presence of molecular two-center interference for the former target [68]. The description of this interference probably represents the largest difference between the CDW-EIS-PT and 3DW-EIS models. In the former, it is accounted for in an *ad hoc* manner by multiplying the FDCS for ionization of atomic H with a model interference factor of the form $f = 1 + \sin(precR)/(precR)$, where $prec$ is the recoil-ion momentum and R is the internuclear distance of the molecule at equilibrium (see Sec. III for more details). In the latter model, in contrast, the interference
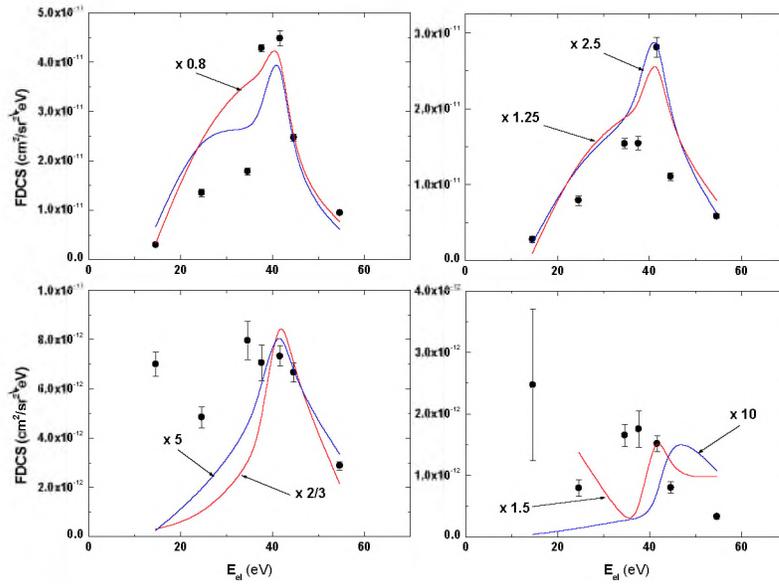
Figure 7. Same as Figure 3, but for electron ejection from H2

is included from first principles in the transition amplitude. In the case of electron impact the interference pattern calculated with the 3DW-EIS model was found to be phase shifted by π relative to the model interference term [69]. This could explain the large differences between the 3DW-EIS and CDW-EIS-PT calculations even well outside the velocity-matching regime. Indeed, for ionization of atomic hydrogen, which is not afflicted with molecular two-center interference, both calculations, shown for Eel = 54.6 eV and θp = 0.325 mrad in Figure 6, give similar results.

In Figure 7, the ejected-electron-energy dependence of the FDCS for H2 is shown for θel = 0° and for the scattering angles as indicated in the insets. As for the He target, here too a sharp cusp peak is found for θp = 0.1 and 0.2 mrad. However, in contrast to He, the cusp peak is not shifted relative to the energy corresponding to the velocity match.

Previously published data only covered electron energies close to the cusp energy and 14.6 eV [27]. For these energies the FDCS seemed to exhibit a rather flat behavior for $\theta_p = 0.325$ and 0.55 mrad. With the new data points there actually appears to be a maximum for the two larger θ_p as well, although it is significantly broader than at small θ_p.

Regarding the comparison between theory and experiment, an important advantage of analyzing the energy dependence of the FDCS is that the molecular two-center interference term hardly varies at all over the energy range plotted in Figure 7. Therefore, if the differences between the CDW-EIS-PT and 3DW-EIS calculations of the angular dependence were mostly due to the different treatment of this interference then both models should yield results that are more similar in the energy dependence. Indeed, for $\theta_p = 0.325$ mrad, for which the angular dependence of the FDCS is plotted in Figure 5, both calculations are much closer to each other in shape, although there are large differences in magnitude. In contrast, large and qualitative differences are visible at $\theta_p = 0.55$ mrad, illustrating that, in spite of their conceptual similarity, both models significantly depart from each other in the description of the fewbody dynamics beyond molecular two-center interference.

5. CONCLUSIONS

We extended previous measurements of fully differential cross sections on ionization of He and H2 by 75 keV proton impact in the region of the ejected electron-projectile velocity matching to a broad energy range covering electronto-projectile speed ratios from 0.36 to 1.22. The data were compared to various conceptually similar distorted-

wave calculations, with and without inclusion of the interaction between projectile and residual target ion (PT interaction). For the He target, qualitatively good agreement between experiment and theory is found for relatively small projectile scattering angles and ejected electron energies well outside the velocity-matching regime. However, with increasing scattering angle and approaching the velocity matching, increasing discrepancies between experiment and theory are observed. At the same time, the various calculations increasingly depart from each other. Especially at the largest scattering angle (0.5 mrad) the experimental data and the various calculations do not even resemble each other qualitatively. Another important observation is that the overall agreement between experiment and theory is not improved with the inclusion of the PT interaction. In fact, in some cases significantly better agreement is obtained using the calculation without the PT interaction.

Higher-order mechanisms including the post-collision interaction (PCI) are known to be particularly important near the velocity-matching regime. Therefore, the severe discrepancies between the data and the various calculations in this region demonstrate that kinematic conditions for which PCI is strong fall outside the regime of validity of distortedwave models. The observation that the inclusion of the PT interaction does not lead to overall improved agreement suggests that higher-order mechanisms leading to PCI which include this interaction represent a particularly large challenge to theory. However, this does not necessarily mean that such mechanisms are generally underestimated. Features characteristic of PCI could also be suppressed through destructive interference even if the role of the PT interaction is overestimated.

In the case of the H2 target discrepancies between experiment and theory and differences between the calculations are already quite significant well outside the velocity-matching regime and at small scattering angles. Here, in addition to the difficulties in accurately describing the few-body dynamics under kinematic conditions were PCI is strong, another challenge is represented by molecular two-center interference. The description of this interference represents the largest difference between the CDW-EIS and 3DW-EIS approaches. For electron impact, it was shown already that this difference can result in a phase shift in the interference pattern calculated with both methods. It would thus not be surprising if for proton impact the FDCS calculated with the same approaches were also afflicted by large differences in the two-center interference term.

ACKNOWLEDGMENTS

REFERENCES

[1]   M. Schulz, R. Moshammer, D. Fischer, H. Kollmus, D. Madison, S. Jones, and J. Ullrich, Nature (London) **422**, 48 (2003).

[2]   T. N. Rescigno, M. Baertschy, W. Isaacs, and C. McCurdy, Science **286**, 2474 (1999).

[3]   H. Ehrhardt, K. Jung, G. Knoth, and P. Schlemmer, Z. Phys. D**1**, 3 (1986).

[4]   A. Lahmam-Bennani, J. Phys. B **24**, 2401 (1991).

[5]   R. Dörner, V. Mergel, O. Jagutzski, L. Spielberger, J. Ullrich, R. Moshammer, and H. Schmidt-Böcking, Phys. Rep. **330**, 95 (2000).

[6]   J. Ullrich, R. Moshammer, A. Dorn, R. Dörner, L. Schmidt, and H. Schmidt-Böcking, Rep. Prog. Phys. **66**, 1463 (2003).

[7]   M. Schulz and D. Madison, Int. J. Mod. Phys. A **21**, 3649 (2006).

[8]   H. Ehrhardt, M. Schulz, T. Tekaat, and K. Willmann, Phys. Rev. Lett. **22**, 89 (1969).

[9]   G. Stefani, L. Avaldi, and R. Camilloni, J. Phys. B **23**, L227 (1990). Wempen, F. (2015). *Word 2016 in depth* (1st ed.). Indianapolis, Indiana: Que. Wempen, F., & John Wiley & Sons. (2015). *Microsoft Office 2016 at work for dummies*. Hoboken, NJ: John Wiley & Sons.

[10]   A. Murray, M. Woolf, and F. Read, J. Phys. B **25**, 3021(1992).

[11]   J. Röder, H. Ehrhardt, I. Bray, D. Fursa, and I. McCarthy, J.Phys. B **29**, 2103 (1996).

[12]   R. W. van Boeyen, N. Watanabe, J. W. Cooper, J. P. Doering, J. H. Moore, and M. A. Coplan, Phys. Rev. A **73**, 032703 (2006).

[13]   M. Dürr, C. Dimopoulou, B. Najjari, A. Dorn, K. Bartschat, I.Bray, D. V. Fursa, Z. Chen, D. H. Madison, and J. Ullrich, Phys.Rev. A **77**, 032717 (2008).

[14]   X. Ren, A. Senftleben, T. Pflüger, A. Dorn, J. Colgan, M. S. Pindzola, O. Al-Hagan, D. H. Madison, I. Bray, D. V. Fursa, and J. Ullrich, Phys. Rev. A **82**, 032712 (2010).

[15] E. S. Casagrande, A. Naja, F. Mezdari, A. Lahmam-Bennani, P. Bolognesi, B. Joulakian, O. Chuluunbaatar, O. Al-Hagan, D. Madison, D. Fursa, and I. Bray, J. Phys. B **41**, 025204 (2008).

[16] S. M. Bellm, C. J. Colyer, B. Lohmann, and C. Champion, Phys. Rev. A **85**, 022710 (2012).

[17] B. A. de Harak, K. Bartschat, and N. L. S. Martin, Phys. Rev. Lett. **100**, 063201 (2008).

[18] J. Williams, P. Bartlett, and A. Stelbovics, Phys. Rev. Lett. **96**, 123201 (2006).

[19] X. Ren, A. Senftleben, T. Pflüger, K. Bartschat, O. Zatsarinny, J. Berakdar, J. Colgan, M. Pindzola, I. Bray, D. V. Fursa, and A. Dorn, Phys. Rev. A **92**, 052707 (2015).

[20] I. Bray and D. V. Fursa, Phys. Rev. A **54**, 2991 (1996).

[21] J. Colgan, M. S. Pindzola, G. Childers, and M. A. Khakoo, Phys. Rev. A **73**, 042710 (2006).

[22] A. T. Stelbovics, I. Bray, D. V. Fursa, and K. Bartschat, Phys. Rev. A **71**, 052716 (2005).

[23] N. V. Maydanyuk, A. Hasan, M. Foster, B. Tooke, E. Nanni, D. H. Madison, and M. Schulz, Phys. Rev. Lett. **94**, 243201 (2005).

[24] S. Sharma, T. P. Arthanayaka, A. Hasan, B. R. Lamichhane, J. Remolina, A. Smith, and M. Schulz, Phys. Rev. A **90**, 052710 (2014).

[25] A. Hasan, S. Sharma, T. Arthanayaka, B. Lamichhane, J. Remolina, S. Akula, D. Madison, and M. Schulz, J. Phys. B **47**, 215201 (2014).

[26] M. Dhital, S. Bastola, A. Silvus, A. Hasan, B. R. Lamichhane, E. Ali, M. F. Ciappina, R. A. Lomsadze, D. Cikota, B. Boggs, D. H. Madison, andM. Schulz, Phys. Rev. A **99**, 062710 (2019).

[27] M. Dhital, S. Bastola, A. Silvus, B. R. Lamichhane, E. Ali, M. F. Ciappina, R. Lomsadze, A. Hasan, D. H. Madison, and M. Schulz, Phys. Rev. A **100**, 032707 (2019).

[28] M. Schulz, R. Moshammer, A. Perumal, and J. Ullrich, J. Phys. B **35**, L161 (2002).

[29]   D. Fischer, R. Moshammer, M. Schulz, A. Voitkiv, and J. Ullrich, J. Phys. B **36**, 3555 (2003).

[30]   M. Schulz, R. Moshammer, A. Voitkiv, B. Najjari, and J. Ullrich, Nucl. Instrum. Methods B **235**, 296 (2005).

[31]   R. Hubele, A. LaForge, M. Schulz, J. Goullon, X. Wang, B. Najjari, N. Ferreira, M. Grieser, V. L. B. de Jesus, R. Moshammer, K. Schneider, A. B. Voitkiv, and D. Fischer, Phys. Rev. Lett. **110**, 133201 (2013).

[32]   M. Schulz, B. Najjari, A. B. Voitkiv, K. Schneider, X. Wang, A. C. Laforge, R. Hubele, J. Goullon, N. Ferreira, A. Kelkar, M. Grieser, R. Moshammer, J. Ullrich, and D. Fischer, Phys. Rev. A **88**, 022704 (2013).

[33]   K. Schneider, M. Schulz, X. Wang, A. Kelkar, M. Grieser, C. Krantz, J. Ullrich, R. Moshammer, and D. Fischer, Phys. Rev. Lett. **110**, 113201 (2013).

[34]   H. Gassert, O. Chuluunbaatar, M. Waitz, F. Trinter, H.-K. Kim, T. Bauer, A. Laucke, C. Müller, J. Voigtsberger, M. Weller, J. Rist, M. Pitzer, S. Zeller, T. Jahnke, L. P. H. Schmidt, J. Williams, S. A. Zaytsev, A. A. Bulychev, K. A. Kouzakov, H. Schmidt-Böcking, R. Dörner, Y. V. Popov, and M. S. Schöffler, Phys. Rev. Lett. **116**, 073201 (2016).

[35]   O. Chuluunbaatar, K. A. Kouzakov, S. A. Zaytsev, A. S. Zaytsev, V. L. Shablov, Y. V. Popov, H. Gassert, M. Waitz, H.-K. Kim, T. Bauer, A. Laucke, C. Müller, J. Voigtsberger, M. Weller, J. Rist, K. Pahl, M. Honig, M. Pitzer, S. Zeller, T. Jahnke, L. P. H. Schmidt, H. Schmidt-Böcking, R. Dörner, and M. S. Schöffler, Phys. Rev. A **99**, 062711 (2019).

[36]   H. R. J. Walters and C. T. Whelan, Phys. Rev. A **92**, 062712 (2015).

[37]   M. McGovern, D. Assafrão, J. R. Mohallem, C. T. Whelan, and H. R. J. Walters, Phys. Rev. A **81**, 042704 (2010).

[38]   I. B. Abdurakhmanov, A. S. Kadyrov, S. U. Alladustov, I. Bray, and K. Bartschat, Phys. Rev. A **100**, 062708 (2019).

[39]   M. F. Ciappina, M. S. Pindzola, and J. Colgan, Phys. Rev. A **87**, 042706 (2013).

[40]   M. Schulz, in *Advances in Atomic, Molecular, and Optical Physics*, edited by E. Arimondo, C. Lin, and S. Yelin, Vol. 66 (Elsevier, Amsterdam, 2017), p. 508.

[41]   K. N. Egodapitiya, S. Sharma, A. Hasan, A. C. Laforge, D. H. Madison, R. Moshammer, and M. Schulz, Phys. Rev. Lett. **106**, 153202 (2011).

[42] T. Arthanayaka, S. Sharma, B. Lamichhane, A. Hasan, J. Remolina, S. Gurung, and M. Schulz, J. Phys. B **48**, 071001 (2015).

[43] L. Nagy, F. Járai-Szabó, S. Borbély, T. Arthanayaka, B. Lamichhane, A. Hasan, and M. Schulz, in *The State-of-The-Art-Reviews on Energetic Ion-Atom and Ion-Molecule Collisions*, edited by D. Belki´c, I. Bray, and A. Kadyrov, Vol. 2 (World Scientific, Singapore, 2019) p. 129.

[44] A. Gaus, W. T. Htwe, J. Brand, T. Gay, and M. Schulz, Rev. Sci. Instrum. **65**, 3739 (1994).

[45] M. Schulz, T. Vajnai, A. D. Gaus, W. Htwe, D. H. Madison, and R. E. Olson, Phys. Rev. A **54**, 2951 (1996).

[46] J. S. Alexander, A. C. Laforge, A. Hasan, Z. S. Machavariani, M. F. Ciappina, R. D. Rivarola, D. H. Madison, and M. Schulz, Phys. Rev. A **78**, 060701(R) (2008).

[47] M. F. Ciappina, O. A. Fojón, and R. D. Rivarola, J. Phys. B **47**, 042001 (2014).

[48] P. D. Fainstein, V. H. Ponce, and R. D. Rivarola, J. Phys. B **24**, 3091 (1991).

[49] G. Gasaneo, W. Cravero, M. D. Sánchez, and C. R. Garibotti, Phys. Rev. A **54**, 439 (1996).

[50] M. D. Sánchez, W. R. Cravero, and C. R. Garibotti, Phys. Rev. A **61**, 062709 (2000).

[51] N. Stolterfoht, R. D. DuBois, and R. D. Rivarola, *ElectronEmission in Heavy Ion-Atom Collisions* (Springer, Berlin, 1997).

[52] E. Clemente and C. Roetti, At. Data Nucl. Data Tables **14**, 177 (1974).

[53] B. H. Brandsen and C. J. Joachain, *Physics of Atoms and Molecules* (John Wiley & Sons, New York, 1990).

[54] D. S. F. Crothers and L. J. Dubé, Adv. At. Mol. Opt. Phys. **30**, 287 (1992).

[55] M. E. Galassi, R. D. Rivarola, P. D. Fainstein, and N. Stolterfoht, Phys. Rev. A **66**, 052705 (2002).

[56] M. Foster, D. H. Madison, J. L. Peacher, and J. Ullrich, J. Phys. B **37**, 3797 (2004).

[57] M. Foster, D. H. Madison, J. L. Peacher, M. Schulz, S. Jones, D. Fischer, R. Moshammer, and J. Ullrich, J. Phys. B **37**, 1565 (2004).

[58] F. W. Byron and C. J. Joachain, Phys. Rev **146**, 1 (1966).

[59] J. Gao, D. H. Madison, and J. L. Peacher, J. Phys. B **39**, 1275 (2006).

[60] U. Chowdhury, M. Schulz, and D. H. Madison, Phys. Rev **83**, 032712 (2011).

[61] D. S. F. Crothers and J. F. McCann, J. Phys. B **16**, 3229 (1983).

[62] G. Bernardi, P. Focke, and W. Meckbach, Phys. Rev. A **55**, R3983 (1997).

[63] L. Sarkadi, U. Brinkmann, A. Báder, R. Hippler, K. Tökési, and L. Gulyás, Phys. Rev. A **58**, 296 (1998).

[64] D. R. Schultz and C. O. Reinhold, Phys. Rev. A **50**, 2390 (1994).

[65] J. Park and F. D. Schowengerdt, Phys. Rev. **185**, 152 (1969).

[66] L. Sarkadi, L. Gulyás, and L. Lugosi, Phys. Rev. A **65**, 052715 (2002).

[67] M. Schulz, A. C. Laforge, K. N. Egodapitiya, J. S. Alexander, A. Hasan, M. F. Ciappina, A. C. Roy, R. Dey, A. Samolov, and A. L. Godunov, Phys. Rev. A **81**, 052705 (2010).

[68] N. Stolterfoht, B. Sulik, V. Hoffmann, B. Skogvall, J. Y. Chesnel, J. Ragnama, F. Frèmont, D. Hennecart, A. Cassimi, X. Husson, A. L. Landers, J. A. Tanis, M. E. Galassi, and R. D. Rivarola, Phys. Rev. Lett. **87**, 023201 (2001).

[69] A. Senftleben, T. Pflüger, X. Ren, O. Al-Hagan, B. Najjari, D. Madison, A. Dorn, and J. Ullrich, J. Phys. B **43**, 081002 (2010). Bucki, L. (2013). *Microsoft Word 2013 bible* (4th ed.). Indianapolis, Ind: John Wiley & Sons, Inc.

SECTION

2. CONCLUSIONS AND OUTLOOK

2.1. CONCLUSIONS

A vast literature can be found on both experimental and theoretical studies on the few-body dynamics in ionization of simple targets by a charged-particle impact [6, 7]. In recent years, good agreement between experiment and theory has been routinely observed in the case of electron impact [34, 35]. However, for ionization by ion impact, fully differential studies were much more challenging, both experimentally and theoretically. From a theoretical point of view, one major problem is that due to the large projectile mass an enormous number of angular momentum states of the scattered projectile have to be considered. From an experimental point of view, it is extremely difficult to measure the scattering angle and the energy loss with sufficient resolution. As a result, until recently fully differential data were only available for relatively small electron energies. More specifically, such data were lacking in a kinematic regime, where the electrons are ejected with speeds close to that of the projectiles. In this regime, the relative speed between the electron and the projectile is small; therefore, they interact with each other for a long time. As a result, multiple interactions can happen with considerable probability, i.e. higher-order contributions are quite significant in this region. In this dissertation, a systematic fully differential study of higher-order contributions in ionization of simple targets by ion impact was performed for a broad spectrum of ejected electron energies below, close to,

and above the projectile-electron velocity matching region with two different targets He and H_2.

For all the data collected, FDCS were analyzed for electrons ejected into the scattering plane and different fixed projectile scattering angles as a function of electron ejection angle that were measured relative to the initial projectile beam direction (for fixed electron energy) and as a function of the ejected electron energy (for fixed electron ejection angle). For the first-order processes, momentum conservation demands that electrons must be ejected near the direction of the momentum transfer (q). In the electron ejection angle dependence of FDCS, a peak structure was observed close to q, which is called the binary peak, and which is often associated with a first-order process. However, this peak was shifted towards $\theta_{el} = 0°$ (away from q), for electron energies approaching the velocity-match, suggesting that the binary peak cannot be explained as a pure first-order process. In addition to the binary peak, another structure was observed close to zero degrees. We refer to this peak as the forward peak. As the PCI has the property to focus the electrons toward the original beam direction, the forward peak and the shifting of the binary peak towards zero degrees are both signatures of PCI. The forward peak became stronger relative to the binary peak with a decreasing projectile scattering angle (θ_p). As a result, for smaller θ_p, a single-peaked structure was observed in the velocity-matching region, where the binary peak was weak compared to the forward peak. However, well outside the velocity-matching region, the binary peak always dominated the forward peak [16-18].

In addition to the forward peak and the shifting of the binary peak in the electron ejection angle dependence, another signature of PCI was observed in the ejected electron energy dependence of FDCS. For collisions in which electrons were ejected in the direction

of the projectile beam (and for some data for an electron emission angle of 30° in the scattering plane), FDCS were analyzed as a function of electron energy for different fixed projectile scattering angles. For all projectile scattering angles, a strong peak (called cusp peak) close to the velocity-matching region was observed. When the particles have similar velocities, the projectile (proton) and the electron attract each other more effectively and tend to travel alongside each other with equal speeds. Therefore, the cusp peak is another prominent signature of PCI [16-18].

Moreover, the average projectile scattering angles were analyzed as a function of the projectile to ejected electron speed ratio. A sharp minimum was observed in the velocity-matching region (speed ratio close to 1). In a recent study, such behavior was also observed in the DDCS of heavier targets as well [19]. Hence, PCI not only has the property to focus the ejected electrons but also the scattered projectiles towards the original beam direction.

To look for a possible target dependence of PCI, data were taken with two different targets (atomic He and molecular H_2) with significantly different ionization potentials. Comparative studies of FDCS with these targets were made. Only a surprisingly weak target dependence of the PCI was observed at a fully differential level [18]. However, in a DDCS study for heavier targets, significant target dependence of PCI was observed [19].

The experimental data were compared to the results of two different perturbative calculations. Both models are based on different versions of distorted wave approximations. Therefore, they should carry essentially the same physics. Quite significant discrepancies not only between experiment and theory but also within these conceptually very similar theories were observed for vel $\approx$ vp. These discrepancies

increased with increasing scattering angle and approaching the velocity matching. At the largest scattering angle (0.55 mrad), they do not resemble each other qualitatively. However, from the results of previous data from our group, at smaller projectile energy loss, 30eV [36], these theories were in much better agreement with each other, and the discrepancy with the experiment was also much smaller for all scattering angles [16-18]. This showed that in the velocity matching region, especially with larger projectile scattering angles, the FDCS are very sensitive to the details of the underlying few-body dynamics.

Several factors may contribute to these discrepancies. One possible cause is that the description of the projectile-target (PT) interaction may not be accurate in theory. The 3C wavefunction is a product of three two-body Coulomb interactions representing each pair of particles. This model is only accurate if at least one particle is far from the other two. For the PE-PT-PE sequence to happen all three particles must be close to each other. The projectile must be close to the electron, so it can transfer enough energy to be lifted to the continuum. At the same time, the projectile must be close to the target, so it can transfer a significant amount of momentum to the target nucleus. This is necessary because the direction of the electron momentum is far from q i.e. momentum cannot be conserved without the involvement of the recoil-ion. Hence, all three particles the electron, the projectile, and the target ion must be close to each other. On the other hand, distorted wave methods are remarkably successful in describing double differential ejected electron spectra, which are not sensitive to the PT interaction. This suggests that the inaccuracies in the 3C wave functions caused by the proximity of all three particles mostly affect the description of the PT interaction. In a recent calculation of DDCS for ionization of atomic

hydrogen, correlations between particle pairs were accounted for by summing over several 3C wave functions [27]. This significantly improved the agreement with experimental data.

Another possible cause is that perturbation theories effectively represent two state approximations with a well-defined initial state and final state. The final state in the calculation is designed to account for the state observed in the experiment. Other target states or bound projectile states contribute only in so far as the final state is not necessarily orthogonal to these states. Nevertheless, other processes like e.g. capture are not fully and not in a controlled manner accounted for. As a result, because of unitarity, these processes are erroneously counted as ionization in the transition amplitude. The third possible reason relates to possible coherence effects of the projectile beam, which is something not discussed in detail in this dissertation. It has been observed in several studies that due to the intrinsic momentum spread, projectiles have some finite coherence length [36, 40, 41]. However, projectiles are treated as fully coherent waves in these theories.

This discussion leads to the question, what type of theory is needed? Experimental results indicated that perturbative models do not work well for the projectile-electron velocity-matching region. In this region, the relative velocity between the ejected electron and the projectile is very small. As a result, they interact with each other for a long time and the projectile can thus not be regarded as a small perturbation to the target Hamiltonian. Therefore, we need to look for non-perturbative approaches. The next point is that instead of taking the continuum eigenstate of the target only in the final state, theory should include a large two-center basis set including projectile bound states to account for the capture channel. It is also very crucial that the projectile beam is described by a wave packet with a width reflecting the coherence length.

Non-perturbative models with two-center basis sets for ion impact have been developed recently independently by different groups, for example, Kadyrov et al., Walters et al., and Pindzola et al. First results for the velocity matching regime on the FDCS for H_2 and He can be expected soon. However, because of the larger projectile mass, a very large number of angular momentum states are required to completely describe the reaction. This makes it hard to treat the coherence property of the projectile accurately. Therefore, incorporating wave packets in such models is challenging.

In conclusion, experimental data provided a sensitive test to different theoretical models in one of the important and unexplored regimes of ionization. This will help to determine the most appropriate approaches to account for the higher-order contributions. The data indicated the limitation of perturbative models and the need for non-perturbative approaches, at least, in the velocity matching region of the ionization of simple targets by ion impact. Nevertheless, it may be challenging to include a larger projectile mass, non-perturbative approaches could describe this region well.

2.2. OUTLOOK

One aspect of FDCS in the velocity matching regime, which should be addressed in future studies, relates to the electron angular dependence for large projectile scattering angles and near the velocity matching. An example is shown in Figure 2.1 for ionization of H_2 for a projectile energy loss of 60eV and a scattering angle of $\theta_P = 0.55$mrad [16]. Here, a pronounced double-peak structure is observed. For electron energies far from the velocity-matching, the binary peak is a signature of a first-order process, while the forward peak is a signature of PCI. In a pure first-order process, the binary peak should be in the

direction of the momentum transfer. The forward shift of the binary peak in the velocity matching regime shows that it is not purely a first-order process, but PCI plays an important role too. Why is a shift of approximately 55° (forward peak) and about 15° (binary peak) much more likely than a shift of about 25° (minimum, $\theta_{el} \approx 30°$)?
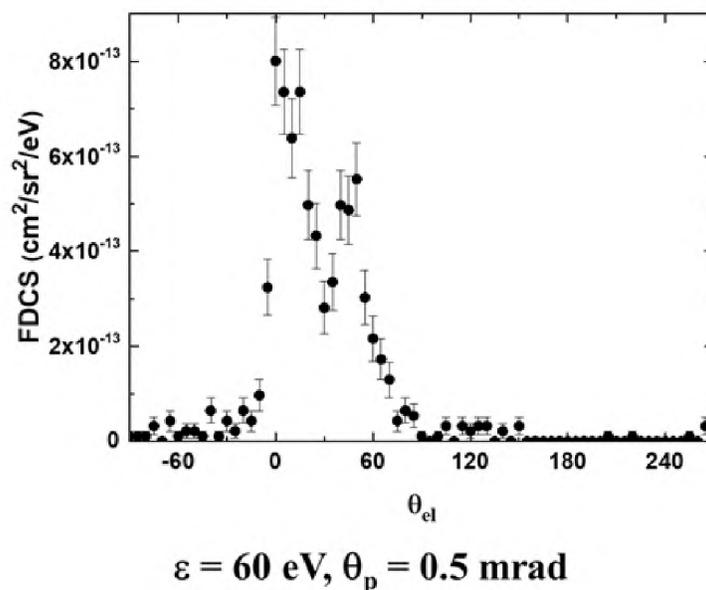
Figure. 2.1. FDCS as a function of electron ejection angle for H_2 target with 60eV projectile energy loss and 0.55 mrad scattering angle

This cannot be explained in a classical picture. In the light of quantum mechanics, this minimum could be due to destructive interference. However, interference is only observable for a coherent beam. Therefore, it is important to repeat the experiment with an incoherent beam. If this interpretation is correct, then this minimum should disappear. Such an experiment is currently in progress as the research project of another Ph.D. student.

BIBLIOGRAPHY

[1] Artur Beiser, Concepts of Modern Physics, 6th Edition. Mc Graw Hill. ISBN 0-07-244848-2

[2] M. Schulz, R. Moshammer, D. Fischer, H. Kollmus, D.H. Madison, S. Jones, and J. Ulrich, Nature 422, 48 (2003)

[3] C. Froese-Fischer, T. Brage, and P. Johnson, Computational atomic structure: An MCHF Approach, CRC press (1997)

[4] E. Rutherford, Philos. Mag.21, 669 (1911)

[5] M. Schulz, Ad. At. Mol. Opt. Phys. 66, 508 (2017)

[6] M. Schulz and D.H. Madison, International Journal of Modern Physics A 21, 3649 (2006)

[7] M. Schulz, Ion-Atom Collisions: The Few-Body Problem in Dynamic Systems, De Gruyter; 1st edition

[8] T.N. Rescigo, M. Baertschy, W. Isaacs, and C. McCurdy, Science 286, 2474 (1999)

[9] B.A. de Harak, K. Bartschant, and N.L.S. Martin, Phys. Rev. Lett. 100, 063201 (2008)

[10] A.L. Godunov, C.T. Whelan, and H.R.J. Walters, Phys. Rev. A 78, 012714 (2008)

[11] Knolyrov et al

[12] J.R. Taylor, Scattering Theory: The Quantum Theory of Nonrelativistic Collisions (Wiley, New York, 1972)

[13] O. Chuluunbaatar, S.A. Zaytsev, K.A. Kouzakov, A. Galstyan, V.L. Shablov, and Yu.V. Popov, Phys. Rev. A 96, 042716 (2017)

[14] J. Fiol, V.D. Rodríguez, and R.O. Barrachina J. Phys. B 34, 933 (2001)

[15] D. H. Madison, D. Fischer, M. Foster, M. Schulz, R. Moshammer, S. Jones, and J. Ullrich, Phys. Rev. Lett. 91, 253201 (2003)

[16] M. Dhital, S. Bastola, A. Silvus, A. Hasan, B.R. Lamichhane, E. Ali, M.F. Ciappina, R.A. Lomsadze, D. Cikota, B. Boggs, D.H. Madison, and M. Schulz, Phys. Rev. A 99, 062710 (2019)

[17] M. Dhital, S. Bastola, A. Silvus, A. Hasan, B.R. Lamichhane, E. Ali, M.F. Ciappina, R.A. Lomsadze, D. Cikota, B. Boggs, D.H. Madison, and M. Schulz, Phys. Rev. A 99, 062710 (2019)

[18] M. Dhital, S. Bastola, A. Silvus, J. Davis, B.R. Lamichhane, E. Ali, M.F. Ciappina, R. Lomsadze, A. Hasan, D.H. Madison, and M. Schulz, Phys. Rev. A 102, 032818 (2020)

[19] A. Silvus, M. Dhital, S. Bastola, J. Buxton, Z. Klok, E. Ali, M.F. Ciappina, B. Boggs, D. Cikota, D.H. Madison, and M. Schulz, J. Phys. B 52, 125202 (2019)

[20] G. B. Crooks and M. E. Rudd, Phys. Rev. Lett. 25, 1599 (1970)

[21] L. Sarkadi, J. Palinkas, A. Köver, D. Berenyi, and T. Vajnai, Phys. Rev. Lett. 62, 527 (1989)

[22] L. Sarkadi, L. Gulyas, and L. Lugosi, Phys. Rev A 65, 052715 (2002)

[23] T. Vajnai, A. D. Gaus, J. A. Brand, W. Htwe, D. H. Madison, R. E. Olson, J. L. Peacher, and M. Schulz, Phys. Rev. Lett. 74, 3588 (1995)

[24] T.P. Arthanayaka, S. Sharma, B.R. Lamichhane, A. Hasan, J. Remolina, S. Gurung, L. Sarkadi, and M. Schulz, J. Phys. B, 48, 175204 (2015)

[25] A. Hasan, T. Arthanayaka, B.R. Lamichhane, S. Sharma, S. Gurung, J. Remolina, S. Akula, D.H. Madison, M.F. Ciappina, R.D. Rivarola, and M. Schulz, J. Phys. B 49, 04LT01 (2016)

[26] U. Chowdhury, M. Schulz, and D. H. Madison, Phys. Rev. A 83, 032712 (2011)

[27] J. Fan, X. Miao, and X. Jia, Chinese Physics B, accepted for publication (2020)

[28] D.H. Lee, P. Richard, T.J.M. Zouros, J.M. Sanders, J.L. Shinpaugh, and H. Hidmi, Phys. Rev. A 41, 4816 (1990)

[29] M. Brauner and J.H. Macek, Phys. Rev. A 46, 2519 (1992)

[30] D.R. Schultz and C.O. Reinhold, Phys. Rev. A 50, 2390 (1994)

[31] A. Salin, J. Phys. B 8: Proc. Phys. Soc., London 2, 631 (1969)

[32] T. Weber, Diploma Thesis, University Frankfurt, (1998)

[33] D. Belkić, Phys. Rev. A 43, 4770 (1991)

[34] T.N. Resigno, M. Baertschy, W.A. Isaacs, and C.W. McCurdy, Science 286, 2474 (1999)

[35] X. Ren, I. Bray, D.V. Fursa, J. Colgan, M.S. Pindzola, T. Pflüger, A. Senftleben, S. Xu, A. Dorn, and J. Ullrich, Phys. Rev. A 83, 052711 (2011)

[36] S. Sharma, T.P. Arthanayaka, A. Hasan, B.R. Lamichhane, J. Remolina, A. Smith, and M. Schulz, Phys. Rev. A 90, 052710 (2014)

[37] A.C. Laforge, Ph.D. thesis, Missouri University of Science and Technology (2010)

[38] R. Dörner, V. Mergel, O. Jagutzski, L. Spielberger, J. Ullrich, R. Moshammer, and H. Schmidt-Böcking, Phys. Rep. 330, 95 (2000)

[39] M.F. Ciappina, C.A. Tachino, R.D. Rivarola, S. Sharma, and M, Schulz, J. Phys. B 48, 115204 (2015)

[40] K.N. Egodapitiya, S. Sharma, A. Hasan, A.C. Laforge, D.H. Madison, R. Moshammer, and M. Schulz, Phys. Rev. Lett. 106, 153202 (2011)

[41] M Schulz, A Hasan, B Lamichhane, T Arthanayaka, M Dhital, S Bastola, L Nagy, S Borbély, F Járai-Szabó, Journal of Physics: Conference Series 1412 (6), 062007 (2020)

VITA

Madhav Dhital was born and raised in Dudhpokhari-1, Lamjung, Nepal. After finishing high school in his remote village, Madhav went to Kathmandu, the capital city of Nepal, to pursue higher education. He got his bachelor's degree in science majoring in physics and minoring in mathematics and statistics in December 2010 from Trichandra college, Tribhuvan University. Then, he earned a Master of Science in Physics in May 2013 from Tribhuvan University, Kirtipur, Nepal.

Madhav joined the Missouri University of Science and Technology, Rolla, Missouri in Fall 2014. He received a Master of Science in Physics in May 2017 and a graduate certificate in 'Big Data Management and Analysis' in December 2019 from Missouri S&T. To do research in experimental atomic, molecular, and optical physics, Madhav joined Dr. Schulz's lab. He has contributed to seven peer-reviewed publications in different prestigious journals including three first-author papers in Physical Review A. He presented his research work in three different Gaseous Electronics Conferences (GEC) in 2018, 2019, and 2020. In GEC 2020, he presented as a finalist of the Student Excellence Award. Madhav received his Doctor of Philosophy in Physics from Missouri University of Science and Technology, Rolla, Missouri, USA in December 2020 under the supervision of Dr. Michael Schulz.